NASA Contractor Report 172598

DELAMINATION MICROMECHANICS ANALYSIS

Donald F. Adams and Jayant M. Mahishi

UNIVERSITY OF WYOMING
Laramie, Wyoming

Grant NAG1-454
May 1985

National Aeronautics and
Space Administration

Langley Research Center
Hampton, Virginia 23665

PREFACE

This technical report presents the development of a three-dimensional finite element fracture mechanics analysis of composite materials, sponsored in part by NASA-Langley Research Center under Research Grant NAG-1-454. This grant was initiated in March 1984, preliminary development work having been underway as an in-house effort at the University of Wyoming for some time prior to that date. The NASA-Langley Technical Monitor was Dr. John H. Crews, Jr.

All work was performed by the Composite Materials Research Group (CMRG) within the Department of Mechanical Engineering at the University of Wyoming. The Principal Investigator was Dr. Donald F. Adams, Professor of Mechanical Engineering. He was assisted by Mr. Jayant M. Mahishi, Ph.D. graduate student in Mechanical Engineering.

Use of names of manufacturers in this report does not constitute official endorsement of such manufacturers, either expressed or implied, by the National Aeronautics and Space Administration.

TABLE OF CONTENTS

TABLE OF CONTENTS (CONTINUED)

SECTION 1

INTRODUCTION

Much of the further development and application of fiber-reinforced composites in high performance structures now depends mainly on the fracture characterization of these materials. Unfortunately, the fracture behavior of these materials differs considerably from that of homogeneous isotropic materials.

Even though the mechanics of initiation and growth of cracks in composites is not well understood, it is generally believed that micro-flaws in the form, for example, of broken fibers, fiber-matrix interface debonds, and matrix cracks that exist in composites for various reasons, influence the fracture process as much as material inhomogeneity and anisotropy. Energy absorption during crack propagation in a multi-layered composite laminate is typically due to intralaminar transverse cracking, interlaminar delamination, fiber breaks, matrix cracks, fiber-matrix debonds, fiber pullouts and matrix yielding (see Figure 1). These failure modes depend on a number of factors such as fiber orientation, individual layer thickness, and the constitutive relations that describe the mechanical properties of the fiber, the matrix and the interface.

The large number of variables involved in the geometry of composites makes it very difficult to completely characterize their fracture behavior experimentally. An analytical model which can represent the various aspects of the intrinsic physical failure process is thus highly desirable. The main obstacle to deriving such a single analytical model is one of scale. The fiber breaks, matrix cracks and

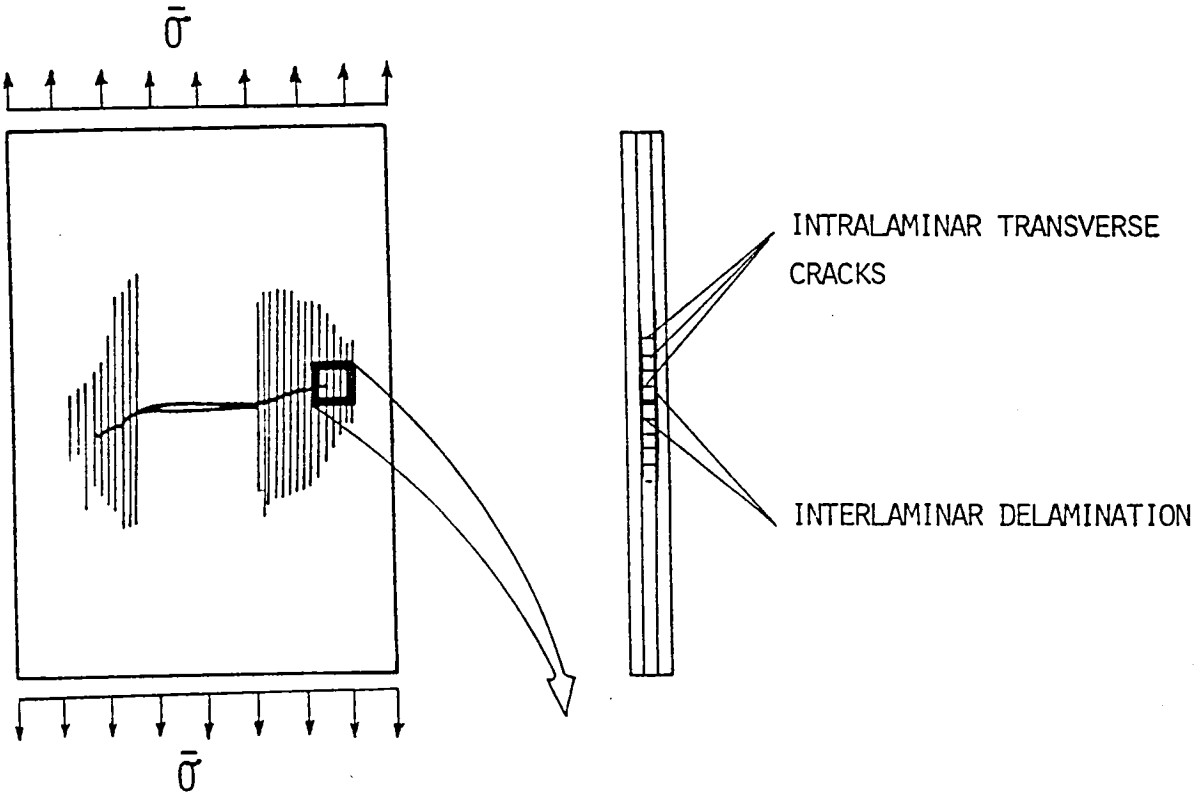

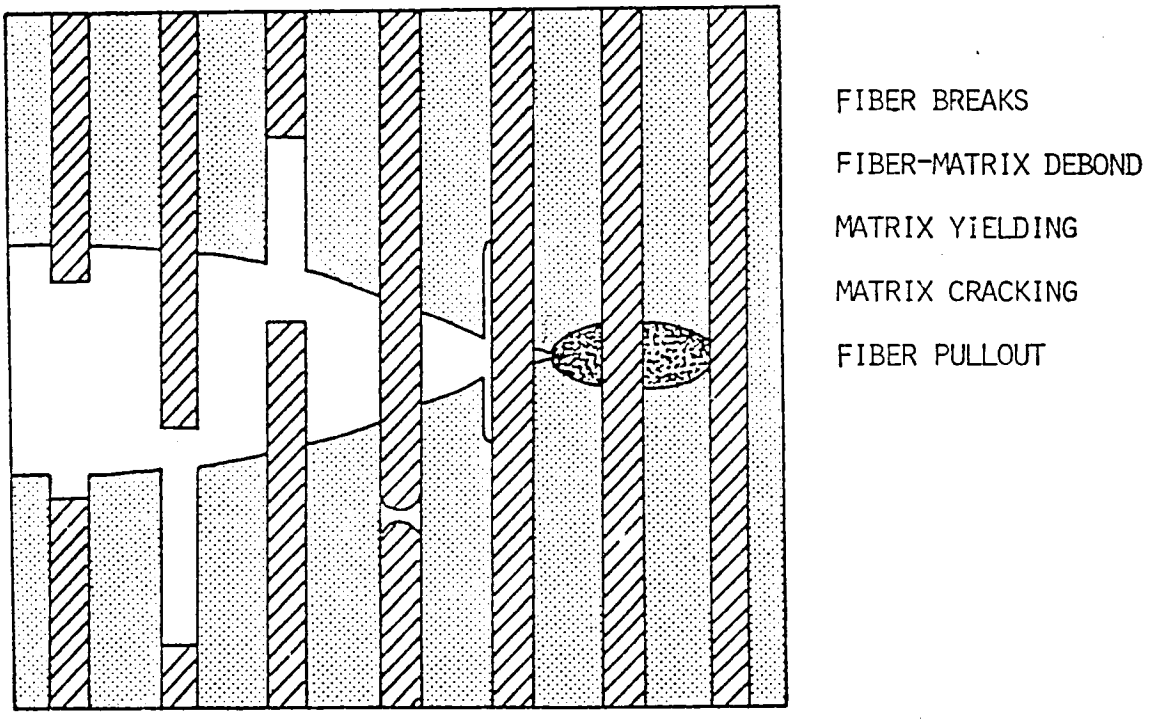

Figure 1. Energy Absorption Mechanisms During Crack Propagation in a Multilayered Fiber-Reinforced Composite Laminate.

fiber-matrix debonds are of the order of one fiber diameter in size, while the intralaminar transverse cracks and interlaminar delaminations are several orders of magnitude larger than the fiber diameter. Accordingly, two different analytical approaches are commonly used, viz., the macromechanics approach and the micromechanics approach. The macromechanics approach, which treats the composite as a homogeneous anisotropic continuum, has been relatively successful in predicting some macro scale failure modes. However, it does not account for failure modes associated with the material heterogeneity. On the other hand, the micromechanics approach has been very useful in studying the influence of microflaws on the fracture behavior of composites. Obviously a satisfactory approach is one that combines both the micromechanics and the macromechanics approaches.

The main objective of the present work was to develop a fracture criterion for composites based upon a combined micromechanics/macromechanics analysis. The historical development and present state of the art of fracture mechanics of composites are reviewed in Section 2. The theory associated with the proposed integrated micromechanics and macromechanics fracture criterion (IMMFC) for fiber-reinforced composites is explained in Section 3. A critical elastic strain energy release rate in the presence of plasticity has been defined and used as a criterion for crack initiation and propagation in both the micromechanics and the macromechanics analyses. The energy release rate criterion and the finite element technique of crack growth simulation in three-dimensional finite element models based on the virtual crack extension method are explained in Section 4. Preliminary results using the micromechanical analysis are given in Section 5. Graphite/epoxy

unidirectional composite models are used to study the initiation and propagation of microcracks from microscopic flaws. The fracture toughness values, which represent the energy release rate at the onset of fast fracture under different loading conditions, are evaluated using the crack growth resistance curve method. These values are subsequently used as critical energy release rates in the integrated analysis.

In Section 6, example results using the macromechanical analysis are presented. The initiation and propagation of a delamination crack in central notched and single-edge notched $[\pm 45/0]_s$ graphite/epoxy laminates subjected to inplane tensile stresses normal to the notch are studied. The delamination at ±45 and -45/0 interfaces, and material yielding at different stages of loading, are presented.

Section 7 contains the application of the integrated micromechanical and macromechanical fracture criterion to predict the onset and growth of cracks in a single-edge notched $[\pm 45/0]_s$ graphite/epoxy composite laminate. A qualitative comparison with experimental results is also presented.

Section 8 contains a summary, conclusions and suggestions for future work.

SECTION 2

BACKGROUND REVIEW

2.1 Classical Fracture Mechanics

Fracture mechanics is primarily concerned with the strength of materials in the presence of cracks. Until the early twentieth century, a satisfactory explanation had not been found for experimental observations that fracture occurs at a much lower stress level than that needed to separate adjacent atoms across the fracture surface. Griffith [1,2] proposed a theory based upon an energy balance associated with the fracture process, equating the release of elastic potential energy during crack extension under constant load point displacement to the surface energy of the newly created crack surface. Realizing that a certain amount of plastic deformation takes place near the crack tip in most engineering materials, Irwin [3] and Orowan [4] modified the Griffith energy balance equation by equating the energy release rate to the plastic energy dissipation rate and the surface energy absorption rate, which formed the basis for linear elastic fracture mechanics (LEFM).

Irwin [5] postulated that the critical energy release rate or "fracture toughness" can be related to the stress intensity factor, which is a measure of the strength of the elastic singularity of the crack tip strain field. Such a fracture characterization based on LEFM theory is applicable only to those materials in which plastic yielding is confined to a very small region around the crack tip, i.e., when the stress field associated with the crack tip is mainly elastic.

In the last two decades, a considerable amount of work has been done in developing methods to characterize fracture associated with medium to large scale plastic yielding in ductile materials. The plastic zone correction method by Irwin, et. al. [6], the J-integral method by Rice [7] and Cherepanov [8], the crack opening displacement (COD) method by Wells [9] and Cottrell [10], the near tip strain criterion by Ke and Liu [11], and the equivalent energy method by Witt [12] are some of the important theories that have been proposed to deal with crack tip plasticity in the absence of crack growth. The crack growth resistance curve (R-Curve) method [13], the nonlinear energy method by Liebowitz and Eftis [14], the strain energy density criterion by Sih [15], and the crack tip opening angle (CTOA) criterion by de Koning [16] and Shih, et. al. [17] are some of the theories proposed for ductile fracture associated with subcritical crack growth.

Irwin [6], in an early attempt, accounted for plastic yielding near the crack tip in the classical elastic analysis by assuming a slightly larger than actual crack size. This plastic zone correction method proposed by Irwin is essentially an empirical correction to the linear elastic solution.

Rice [7] and Cherepanov [8] independently introduced a path-independent integral (referred to as the J-integral), which is expressed as

$$J = \int_{\Gamma} (w dy - \sigma_{ij} n_j u_{i,x}) ds \tag{1}$$

where w is the strain energy density, Γ is any curvilinear path surrounding the crack tip, starting from any point on the lower crack surface and ending on the upper crack surface, traversing in a

counterclockwise direction, n_j is the outward unit normal vector to the curve, σ_{ij} is the traction vector parallel with n_j, $u_{i,x}$ is the derivative of the displacement vector, and s is the arc length. It has been shown [18,19] that the J-integral represents the energy release rate, and that its value at the onset of cracking (J_c) can be used as a fracture criterion.

The concept of crack opening displacement (COD) introduced by Wells [9] and Cottrel [10] was successful in taking into account the considerable amount of plastic flow associated with fracture in high toughness materials. For the fracture of elastic-perfectly plastic materials in plane stress, the can be energy release rate G related to the crack opening displacement δ as

$$G = \sigma_y \delta \tag{2}$$

where σ_y is the yield stress of the material in simple tension. Hence the COD can be used as an effective fracture criterion. In recent studies of elastic-plastic fracture mechanics, the COD has been found to be a valuable concept to describe stable crack growth.

The near tip strain criterion proposed by Ke and Liu [11] is based on the fact that the transverse strains near a crack tip at the onset of fracture are independent of the specimen geometry and type of loading. It has been argued [20] that the plastic strains at all points closer than a certain small characteristic distance from the crack tip attain a value equal to or greater than a critical value; this distance can be treated as a fracture criterion for growing cracks. Experimentally it is difficult to measure the strains at the midplane of a plate. However,

available experimental results based on surface strains [11] indicate significant promise in using strain as a fracture criterion for plates of all thicknesses.

The crack growth resistance curve (R-Curve) concept [13], in which the resistance to crack growth is plotted against crack extension, has been successfully used to explain the slow and stable crack growth in ductile materials which precedes unstable crack growth. The R-Curve, which has been shown to be independent of the initial crack size [13], represents the energy balance equation $G = R$, where G is the energy release rate and R is the energy absorption rate. The point of crack instability occurs when

$$\frac{dG}{da} = \frac{dR}{da} \tag{3}$$

The nonlinear energy method introduced by Liebowitz and Eftis [14] takes into account the nonlinearity of the compliance curve of a nonlinear elastic material. A new fracture parameter $\tilde{G}$, which is considered to be more accurate than the linear elastic fracture toughness G_C, is defined as

$$\tilde{G} = CG_C \tag{4}$$

where C is a constant determined by the geometry of the nonlinear compliance curve. The parameter $\tilde{G}$ is applicable to subcritical crack growth as well. It has been claimed that the $\tilde{G}$ value corresponding to the onset of stable fracture is independent of the geometry effect of the material (including the thickness), whereas G_C corresponding to the onset of rapid fracture depends on the thickness of the material.

The strain energy density theory originally proposed by Sih [15] for linear elastic fracture was later extended to explain ductile fracture and slow stable crack growth as well [21]. According to this theory, the crack extension is postulated to occur in the direction of minimum strain energy density when the strain energy density factor S reaches a critical value S_c.

The strain energy density factor S is given by

$$S = r_c\left(\frac{du}{dv}\right) \tag{5}$$

where $\left(\frac{du}{dv}\right)$ is the strain energy density and r_c is the radius of the core region surrounding the crack tip, which is a characteristic of the material.

Shih [17] and de Koning [16] have suggested that the crack tip opening angle (CTOA), measured as the angle subtended by the opened surface at a small but fixed distance behind the tip of the growing crack, is a satisfactory criterion for stable crack growth. Several investigators [17,20] have produced supporting theoretical and numerical results.

The theories discussed above identify certain parameters as a criterion for the onset and growth of cracks in ductile materials. However, each one has its own merits and demerits relative to the others. For materials exhibiting extensive plastic deformation, the obvious difference from elastic response is the irreversible strain followed by linear elastic unloading. The later feature of ductile fracture was not given much importance in the development of elastic-plastic fracture theories until recently, when Turner [22,23] noted that

the energy release rate in the presence of limit load plasticity is not G, but a term he called I, which is greater than G. The parameter I can be used as a criterion for the initiation and slow stable crack growth in ductile materials.

2.2 Fracture Mechanics of Composite Materials

The failure modes associated with fracture in fiber-reinforced composites differ considerably from those of homogeneous isotropic materials. The microscopic flaws pre-existing in composites for various reasons, typically in the form of broken fibers, matrix cracks and debonded fiber-matrix interfaces, influence the fracture process as much as material heterogeneity and anisotropy. The failure modes associated with fracture in composites are typically in the form of transverse cracking, delamination, fiber breaks, matrix yielding, matrix cracking, and fiber-matrix debonding (as previously indicated in Figure 1). As a result, the crack growth often does not occur in a self-similar fashion as in the case of isotropic materials. Obviously, the theories of classical fracture mechanics cannot be directly applied to composite materials.

Owing to the importance and complexity of the subject, a very large volume of literature dealing with different aspects of fracture in composites has accumulated within the past two decades. A number of theories have been proposed. The various approaches adopted for fracture characterization of composites can be broadly classified as

i) micromechanics approaches

ii) macromechanics approaches

iii) anisotropic continuum approaches

These approaches are discussed in more detail in the following sections.

2.2.1 Micromechanics Approaches

These approaches were primarily developed to estimate the mechanical properties of unidirectional composites based on the properties of their constituent materials. The early development of simple self-consistent mechanics models [24-29], variational models [30-34] and exact models [35-44] are discussed in References [45-47]. The "material model" approach developed by Hedgepath and Van Dyke [48] for the stress concentration around a single broken fiber, and the associated matrix damage in a unidirectional composite, has been extended by Goree and Gross for the case of an arbitrary number of broken fibers [49], as well as for longitudinal yielding and splitting of the matrix [50], in a three-dimensional model containing equally spaced unidirectional fibers. There are a number of papers dealing with cracks at interfaces between different materials. Some of these directly address the situation in composites [51,52]. In Reference [51], the stress intensity factors for a crack running into and crossing an interface are evaluated. The elastostatic interaction between a penny-shaped crack and elastic fibers has been discussed in Reference [52]. The effects of cracks and imperfections of the fiber-matrix interface contact surface on composite properties and the onset of brittle fracture are addressed in Reference [53].

In the fracture characterization of composites, even more important than a rigorous stress analysis [48-53] is the estimation of the energy absorption associated with the failure at microflaws. Simple estimations of the energy absorption during fiber pullout, fiber-matrix debonding, "stress relaxation" due to fiber breaks, "crack bridging" (a process in which the fibers are left intact as the crack propagates), and plastic

deformation of the matrix have been compiled by Phillips and Tetelman [54] and Cooper [55]. The different failure mechanisms and the associated energy absorption calculations have been reviewed in References [56,57].

By introducing a crack propagation capability into an elastoplastic, generalized plane strain finite element micromechanics model, the energy absorption mechanisms during crack propagation in a region of a broken fiber have been studied in References [58,59]. A "failed" element approach developed by Adams [60-64] for crack propagation in two-dimensional finite element models was used in these analyses.

The initiation and propagation of microcracks from broken fibers and matrix cracks in a single-fiber model composite has been studied by Mahishi and Adams [65-67] using an axisymmetric, elastoplastic finite element analysis. Similar single-fiber models have been used by several other authors, e.g., by Ko [68] to study stress concentrations due to the broken fiber, and by Gradin, et. al. [69] to study the debonding between the fiber and the matrix. Mahishi and Adams observed in their studies [65-67] that under fixed grip conditions, the microcracks originating from a broken fiber end or from a matrix crack grow in a slow and stable manner initially to a certain distance, before growing rapidly in an unstable manner across the model. The situation of slow and stable subcritical crack growth being similar to that observed in the case of crack growth in thin metallic plates led to their use of crack growth resistance curves (R-curves) to predict the point of crack instability in composites. The energy release rate corresponding to the point of instability has been defined as a measure of fracture toughness of the model composite. This is a very important development in the

micromechanics approach to fracture characterization of composites as, in addition to being able to predict a single fracture parameter (fracture toughness), it can be used to compare the severity of different types and sizes of microflaws. The axisymmetric model also has the advantage of being useful in correlations with experimental results. The requisite experiments are simple and easily performed. Such experiments are underway at a number of research laboratories [70], including within the Composite Materials Research Group at the University of Wyoming. Mahishi and Adams [67] have also used the axisymmetric model analysis to study the influence of weak fiber-matrix interfaces, curing-induced residual thermal stresses, and environmental moisture absorption on the fracture behavior of graphite/epoxy model composites. A three-dimensional finite element model has also been developed by these authors to study the stress state near a broken fiber in a unidirectional boron/aluminum composite [71]. The fibers were assumed to be packed in a regular square array; a repeating cell was identified consisting of a single broken fiber surrounded by an array of continuous fibers. This model has considerable flexibility in representing different types of microflaws and loading conditions.

By means of such rigorous three-dimensional finite element analyses it is possible to study the effects of sizes and density of different types of microflaws on the fracture toughness of a unidirectional composite. It is important to verify the predicted results of the analysis with experimental data. However, the reduction of experimental fracture mechanics data to identify different forms of microcracks is not straightforward. Beaumont and Anstice [72] have presented a statistical approach for the failure analysis of micromechanical fractures in

graphite fiber and glass fiber composites. Using a simple micromechanics model, they were able to estimate the energy dissipated during partial debonding of the fiber-matrix interface, during fiber fracture and during fiber pullout.

A two-dimensional, micromechanical finite element analysis has been used by Mandel, et. al. [73] to study the initiation of cracks in a steel-fiber-reinforced methacrylate polymer matrix, the results being compared with experimental data. Good agreement was obtained between the predicted and experimental values of loading required for the initiation of cracks in the matrix and subsequent crack arrest by the fibers. Badar, et. al. [74] have studied the micromechanisms of fracture in short-fiber-reinforced thermoplastics. Williams and Reifsnider [75] have used three-dimensional micromechanics models to evaluate the internal stress field in applying their strain energy release rate approach to the prediction of failure modes in composites. Wells and Beaumont [76] have used simple micromechanics models to calculate fracture energy associated with fiber debond and fiber pullout mechanisms. A general survey is presented by Hashin [77].

2.2.2 Macromechanics Approaches

A distinction should be made between different analytical approaches dealing with macroscale cracks in composite laminates, depending upon whether the macrocracks considered are at the lamina (ply) level or at the laminate level. The interlaminar delamination and intralaminar transverse cracking which occur at the lamina level are usually treated by idealizing the individual laminae as homogeneous anisotropic continua. The physical properties of the individual idealized laminae are thus represented by average values, based upon fiber

and matrix properties. In the present discussion, this approach to macroscale cracks in composites is classified as a macromechanics approach.

At the laminate level a phenomenological fracture analysis has been developed to study through-the-thickness cracks, by assuming the entire laminate as a homogeneous anisotropic continuum. This approach is discussed in the next section.

The delamination mode of crack growth, which is characteristic of multilayered composite laminates, has been attributed to the existence of interlaminar stresses near the free edges of the laminate [78,79]. A linear elastic stress analysis of the free edge in a composite laminate [80] suggests that the interlaminar stresses become singular near the free edges, and the signs of these stresses depend on the stacking sequence of the laminate [79-81]. Hence some laminates may be more prone to delamination than others depending on how the plies are stacked together. A review of interlaminar stress effects is given in Reference [82].

The singular behavior of the interlaminar stresses precludes use of any failure criterion based on maximum stress for predicting the onset and growth of the delamination. On the other hand, the homogeneous continuum idealization enables one to use classical fracture mechanics concepts. The critical energy release rate criterion has been used by Rybicki, et. al. [83] to predict the stable delamination crack growth in composite laminates. They used a finite element analysis and a numerical technique for evaluating energy release rates based on the Irwin crack-closure integral [84], a technique developed earlier by Rybicki and Kanninen [85]. This numerical technique has also been used by several

other investigators to characterize delamination crack growth in composite laminates under static tension, static compression, and fatigue loading conditions [86-103].

Wang and Crossman [86,95] have further developed the technique, to include transverse cracking as well. The principal assumptions in their energy release rate approach [86] are that the edge delamination involves only matrix-dominated fracture, which is assumed to be elastic and brittle, and that the crack surface is parallel to the ply interface. Even though the extent of delamination predicted by this energy release rate approach is in agreement with experimental observations [87-89, 97-100], there exists a difference between the experimentally measured energy release rate values and the predicted values. This is possibly because in reality the delamination crack does not propagate in a self-similar fashion parallel to the ply interface, but rather takes a zig-zag path. There is also some concern about possible material yielding in the vicinity of the crack tip.

Delamination crack growth in composite laminates is essentially a three-dimensional problem. A quasi three-dimensional finite element analysis was used in References [93,99,100]. A fully three-dimensional finite element analysis, in which the delamination growth surface can be fully simulated, has been used in Reference [91]. Wang and his associates [104-107] have used singular finite element, hybrid-stress models to study delamination crack growth in composites under both static and cyclic loadings. They used a mixed-mode failure criterion for crack growth. The energy release rate was calculated directly from the relation between stress intensity factors and energy release rates.

The transverse cracking mechanism in composite laminates has also been extensively studied [86,95]. Transverse cracks are caused by the in-plane tensile stress normal to the fiber direction in a unidirectional ply. The irregular spacing intervals of the multiple transverse cracks observed in experiments are attributed to the presence of microflaws. The energy release rate approach developed for delamination crack growth has been used to study transverse crack growth also [86,95].

While considerable progress has been made in understanding the delamination and transverse cracking mechanisms in composites incorporating brittle or quasi-brittle matrix materials, the problem of toughened polymer matrix or metal matrix composites, in which large scale yielding is associated with the cracking, requires special attention.

2.2.3 Anisotropic Continuum Approach

This is a phenomenological approach in which the composite is assumed to be a homogeneous anisotropic continuum. Perhaps the success of the homogeneous anisotropic continuum idealization in the stress and deformation analysis of composites led to the development of this approach for the fracture characterization of composites. But the fact is that the composite stresses and deformations are averaged properties, whereas failure is a localized process in which the material heterogeneity plays an important role. The single most important justification for such an idealization may be that the classical fracture mechanics concepts can be readily employed.

The anisotropic elasticity solutions [108,109] have been used in References [110-112] to evaluate the stress intensity factors for cracks of different sizes and orientations under various loading conditions.

A number of fracture mechanics theories have been proposed based on the LEFM concept [113,114]. These theories have been reviewed extensively in References [56,115]. Some of the more important of these theories are briefly discussed here.

Waddoups, et. al. [116] adapted the Bowie [117] solution for a crack emanating from a hole in an isotropic material, and derived an empirical expression for a crack of length 2a in an infinite body under tensile load normal to the crack, i.e.,

$$K_I = \sigma\pi(\ell + a)^{1/2} \tag{6}$$

where ℓ is the characteristic length of an "intense energy region" at the crack tip. The critical stress for crack extension is then

$$\sigma_C = \frac{K_{IC}}{\pi(\ell + a)^{1/2}} \tag{7}$$

The two parameters K_{IC} and ℓ were evaluated from experimental data. The predicted strengths were in good agreement with experimentally measured values. Cruse [118] represented a hole of radius R as a crack of half length a. The value of a was obtained through comparison of the hole and crack solutions for an orthotropic material. The strength of the laminate was then obtained using LEFM and an experimentally determined value of K_{IC}. Whitney and Nuismer [114], using a stress concentration approach, have proposed two stress criteria for the strength of notched composites. The first criterion assumes that fracture occurs when the normal stress perpendicular to and ahead of the crack reaches the strength of the unnotched laminate at a specific distance d_o from the

crack tip. The distance d_o is assumed to be a material property, independent of the laminate geometry and stress distribution. In the second criterion it is assumed that failure occurs when the average stress over a distance a_o ahead of the crack tip reaches the unnotched tensile strength of the laminate. Reasonably good agreement was obtained with the limited experimental results available.

Pipes, et. al. [119], generalizing the point stress and average stress criteria of Whitney and Nuismer [114], have introduced a three-parameter fracture criterion. A fictitious crack model has been presented by Backlund [120].

All of the theories discussed so far assume self-similar crack growth. In reality, cracks in composite laminates seldom grow in a self-similar fashion. This factor alone makes the application of these theories for the fracture characterization of composites somewhat less effective.

Harrison [121], to remove the restriction of self-similar crack growth, postulated different energy release rates for crack growth in the plane of the crack (denoted as G_x) and for crack growth normal to the crack (denoted as G_y). In his study of splitting in fiber-reinforced materials, Harrison gave the condition of splitting as

$$\frac{G_x}{G_y} < \frac{R_x}{R_y} \tag{8}$$

where R_x and R_y are the critical energy absorption rates for crack growth in the two directions. More general theories have been developed by Sih and Chen [122] and Wu [123,124]. The method of Sih and Chen is based on a strain energy density fracture criterion, which not only

predicts fracture but also the direction of fracture. This theory also introduces a parameter r_c, the radius of the core region in Eq. (5), which can be evaluated analytically or experimentally. The technique has been applied both to unidirectional composites and angle-ply laminates. Lukshminarayana, et. al. [125] have applied the same technique to cracks emanating from circular holes in cross-ply laminates. Experimental correlations were limited to transverse cracks running parallel to the fibers, but were in good agreement.

Wu's theory [123,124] also predicts fracture and the direction of fracture. The theory involves application of a failure criterion to the region ahead of a macroscopic crack in an anisotropic body. Wu assumes that the composite is a homogeneous anisotropic continuum containing randomly distributed microscopic cracks. For such configurations he further assumes that there exists a small but finite volume of dimension r_c that fully encapsulates a microscopic crack, such that the singular stresses are contained within the critical volume and the stresses external to the critical volume are bounded. He then postulates that failure occurs when the stress vector ($\bar{\sigma}_c$ acting on the outer surface of the critical volume reaches the value of the strength vector defining the failure surface for the material failure. Wu obtained excellent agreement with experiments on a Scotchply 1002 glass/epoxy laminate for mixed mode loading with cracks parallel to the fibers. In this theory, the failure surface must be obtained from experimental studies to determine remote properties.

There are other approaches which deal only with the specific mode of crack growth. One example is that of Kulkarni and Rosen [126], which is limited to crack growth normal to the crack plane, as observed for

both unidirectional and general laminates that contain 0° plies. This model was originally developed by Zweben [127], who used the detailed study of plasticity and crack blunting in an orthotropic body given by Tirosh [128]. In their model, Kulkarni and Rosen [126] have taken the region adjacent to the notch as a shear stress transfer region. The regions adjacent to the crack are subdivided into a region of shear stress transfer, a region of stress concentration, and a region of shear stress transfer in the average material. In the application of this approach to fracture normal to the original crack surface, it is necessary to determine two arbitrary parameters experimentally which define the size of the region of intense energy adjacent to the flaw, and the demarcation between Mode I and Mode II behavior.

In summary, the different approaches attempting to extend the classical fracture mechanics concepts to composite materials are, as noted by Kanninen, et. al. [115], nothing but curve-fitting techniques with parameters which can be adjusted to fit any experimental data. It can be concluded that the fracture behavior of composites is far more complex than can be modeled by LEFM. The main reason for the complexity is the material heterogeneity. A more general approach to study the fracture mechanics of composites should include the affects of material heterogeneity.

Kanninen, et. al. [115,129] have developed an approach which combines a micromechanical failure analysis with a macromechanical continuum analysis. At the crack tip, a local region is defined consisting of fibers, the surrounding matrix, and the associated interfaces. This local heterogeneous region (LHR) is considered to be surrounded by a homogeneous orthotropic continuum. The three constituent materials

(which include an interface material) are modeled using "spring-like" elements. The size of the LHR is assumed to be large enough such that its boundary displacements are given by continuum analyses, and small enough relative to the crack length that the singular behavior at the crack tip dominates. By varying the fracture properties, Kanninen, et. al. [129] were able to demonstrate the occurrence of axial splitting, matrix crazing, matrix bridging and fiber bridging. There was also qualitative agreement with the experimental results of Brinson and Yeow [130] on edge notched unidirectional graphite/epoxy laminates. Representation of the local heterogeneous region in a multilayered laminate, and in the case of continuous crack propagation, presents some practical limitations.

From this literature study of different approaches to fracture of composites it is clear that the micromechanics approach, which deals with microscopic failure processes, and the macromechanics approach, which deals with macroscale delaminations and transverse cracking failure processes, are very well developed. A conglomeration of both microscopic and macroscale failure processes represent the actual damage in a multilayered composite. Thus, a more general, integrated approach than that presented in Reference [115], but retaining all the basic features of the micromechanics and macromechanics approaches, is needed for the prediction of initiation and growth of damage in composites.

The main objective of the present work was to develop such an integrated approach.

SECTION 3

DEVELOPMENT OF AN INTEGRATED FRACTURE CRITERION

A method of developing a fracture criterion for heterogeneous anisotropic composites has been suggested by Wu [124], by re-examining the Griffith energy balance equation for homogeneous isotropic materials. By expressing the energy terms with greater generality, the fundamental assumptions and constraints of classical fracture mechanics can be relaxed to allow for material heterogeneity and anisotropy.

Griffith's energy balance equation for the instability of a crack in a brittle material is [1,2]

$$\frac{dW}{dA} - \frac{dU}{dA} \geq \mu \tag{9}$$

where W is the potential energy of the external forces, U is the elastic strain energy, μ is the surface energy per unit area of the crack surfaces and dA is the crack extension.

Irwin and Orowan [3,4] later modified the Griffith energy balance equation to account for the plastic deformation that occurs near the crack tip in most engineering materials as follows:

$$\frac{dW}{dA} - \frac{dU}{dA} \geq \frac{dU'}{dA} + \mu \tag{10}$$

where U' is the irreversible strain energy due to plastic deformation. Equation (10) is the basis of classical linear elastic fracture mechanics (LEFM).

The left-hand side of the Eq. (10) is the input energy rate that is released during an incremental crack growth, and the right-hand side is the energy absorption rate during the crack extension. The left-hand side of Eq. (10) is a function of loading conditions, geometry of the body and the orientation of the crack, whereas the right-hand side is a constant for a given material.

The underlying principle in the above mentioned criterion is that a crack in a continuum tends to extend when the left-hand side of Eq. (10) (i.e., the energy release rate G) reaches a critical right-hand side value (G_C), which is a material property, i.e., when

$$G = G_C \tag{11}$$

The above condition, i.e., Eq. (10), which has been derived from energy principles, is independent of the constitutive properties of the continuum. Therefore, the application of a general fracture criterion to composites requires only that the energy terms in Eq. (10) be redefined so as to account for the material heterogeneity and anisotropy.

To begin, we will assume that the composite is a homogeneous, anisotropic continuum, containing uniformly distributed microscopic flaws, the size and density of which are characteristics of the material and manufacturing process. In the vicinity of a microflaw tip (a high energy region), we assume that a number of microcracks initiate and propagate steadily with increasing external load. The microcracks subsequently coalesce and grow in an unstable manner, leading to an extension of the macrocrack.

The microscopic flaws in a reinforced composite are typically in the form of (see Figure 2):

a) broken fibers

b) matrix cracks

c) fiber-matrix interface debonds

d) weak sites in the fiber.

As mentioned earlier, the size and density of the different types of flaws depend on the constitutive materials and the manufacturing process. Since the size and density of the microflaws significantly influences the failure process in composites, it is necessary to include them as material parameters in a fracture criterion for these materials.

Assuming that the fibers in a unidirectional lamina are packed in a regular square array, we can represent all different types of flaws as shown in Figure 2. Because of the assumed periodicity, it is possible to isolate a repeating cell, such as the one containing a single broken fiber surrounded by an array of continuous fibers. A length of four times the fiber diameter has been shown [71] to be appropriate for the repeating cell in the fiber direction for complete load transfer from the broken fiber to the surrounding matrix.

The sizes of the microflaws within a repeating cell can be non-dimensionalized with respect to their individual maximum attainable values inside the cell. The microflaw parameters are defined as follows:

$$a_{frbk} = \frac{\text{Number of broken fibers in a repeating cell}}{\text{Total number of fibers in a repeating cell}} \tag{12}$$

$$a_{mcpl} = \frac{\text{Surface area of the matrix crack parallel to the fibers}}{\text{Maximum attainable size inside the repeating cell}}$$

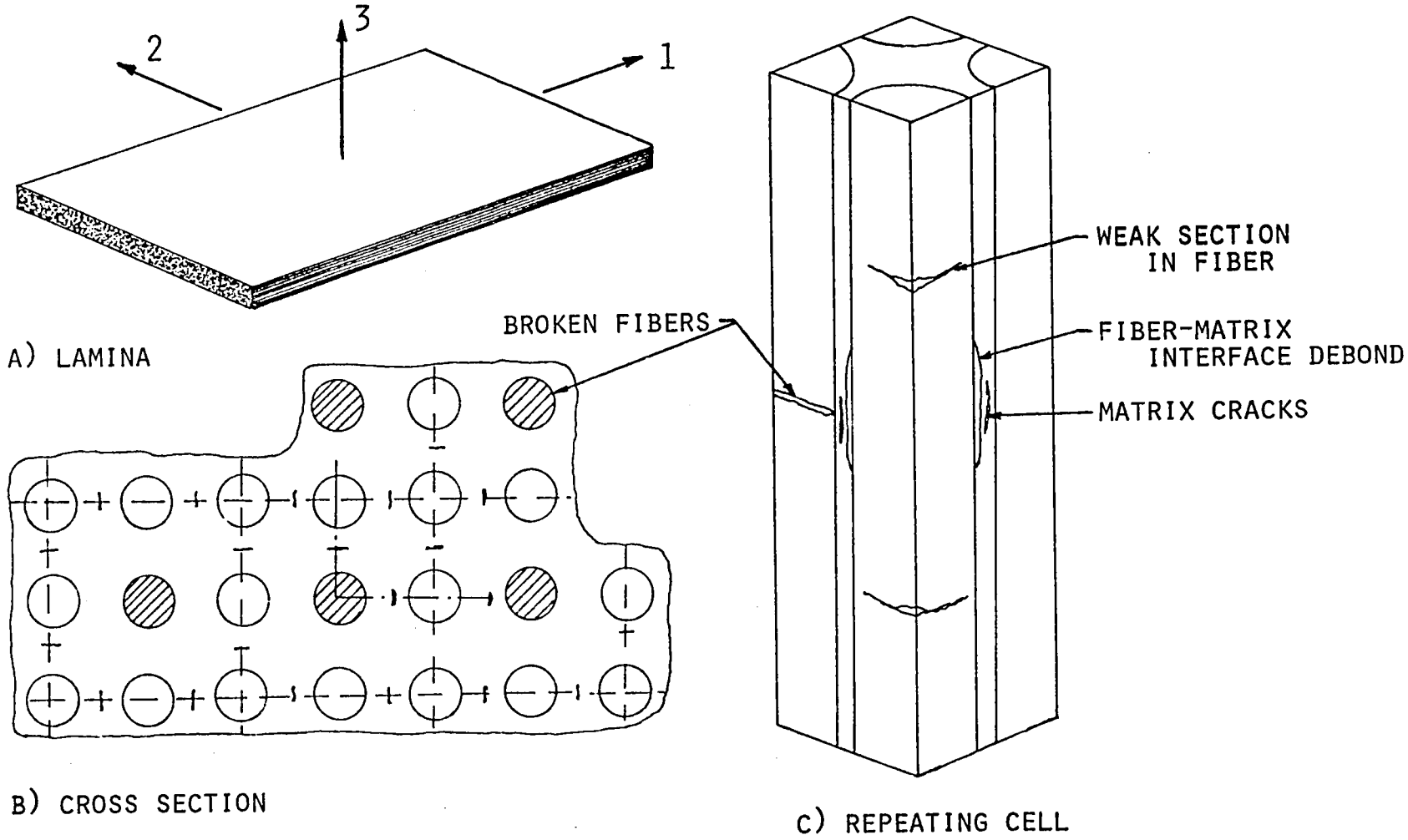

Figure 2. Typical Microscopic Flaws in a Unidirectional Lamina with Fibers Packed in a Square Array.

$$a_{mcpr} = \frac{\text{Surface area of the matrix crack perpendicular to the fibers}}{\text{Maximum attainable size inside the repeating cell}}$$

$$a_{fmid} = \frac{\text{Surface area of the fiber-matrix debond}}{\text{Maximum attainable size inside the repeating cell}}$$

The above parameters, along with the fiber volume content (V_f) and the mechanical properties of the constituent materials, uniquely define the unidirectional composite.

The repeating cell, which is a representative region of the unidirectional lamina, is an ideal model for a micromechanics analysis. But the two-material configuration, the presence of microflaws, and the complex boundary conditions can pose serious difficulties for a continuum analysis. All the above complexities can be easily incorporated in a numerical analysis, however, using a three-dimensional finite element approach. In such a numerical analysis it is also possible to simulate the onset and growth of microcracks from the microflaws. The energy absorption during the crack propagation can then be evaluated.

In accordance with our earlier assumption that the energy absorption during a macrocrack growth in a composite is in the form of fiber breaks, matrix cracks and fiber-matrix interface debonds instead of only surface energy of the crack surfaces as in the case of homogeneous isotropic materials, the term μ in Eq. (10) should be replaced by $\bar{\mu}$, which is defined as

$$\bar{\mu} = \frac{d}{dA}(U_{frbk} + U_{mopr} + U_{mcpl} + U_{fmid}) \tag{13}$$

where U_{frbk} = energy absorption due to fiber breaks

U_{mcpr} = energy absorption due to matrix cracks perpendicular to

the fiber direction

U_{mcpl} = energy absorption due to matrix cracks parallel to the fiber direction

U_{fmid} = energy absorption due to fiber-matrix interface debonding

The energy balance equation for crack instability in a fiber reinforced composite can thus be written as

$$\frac{dW}{dA} - \frac{dU}{dA} \geq \frac{dU'}{dA} + \frac{d}{dA}\left(U_{frbk} + U_{mcpr} + U_{mcpl} + U_{fmid}\right) \tag{14}$$

The left-hand side of Eq. (14) is the global elastic energy release rate, which can be evaluated from a macromechanics analysis, treating the composite as a homogeneous anisotropic continuum. The right-hand side of the equation is the global energy absorption rate, which is a material property. It depends on the size and density of the microflaws, and the constituent material properties. The right-hand side should be evaluated by means of a rigorous micromechanics analysis, preserving the material heterogeneity. Eq. (14) therefore forms the basis of an integrated micromechanical and macromechanical fracture criterion (IMMFC) for composites.

The IMMFC can be stated as the onset of a macrocrack in a composite laminate that occurs when the energy release rate during a virtual crack growth, evaluated from a macromechanics analysis while treating the composite laminate as a homogeneous continuum, reaches a critical value. We define the critical energy release rate as that corresponding to the onset of an unstable crack growth from a microflaw.

In the micromechanics analysis, in which a repeating cell containing microflaws is analyzed for the initiation and propagation of microcracks under fixed boundary displacement conditions, microcracks are likely to grow in a slow and stable manner initially up to a certain distance, beyond which they become unstable and grow rapidly across the model. The point of crack instability can be established from crack growth resistance curves (R-curves). The energy release rate corresponding to the point of crack instability is a measure of the critical energy release rate (toughness) of the material in that particular fracture mode.

Since the critical energy release rate depends on the direction of the loading on the micromechanics model, the three-dimensional micromechanics analysis will yield six different values of critical energy release rate, corresponding to the six independent applied stress components, viz., G_{C11}, G_{C22}, G_{C33}, G_{C23}, G_{C13} and G_{C12}, where subscripts 1, 2 and 3 denote the material coordinates (Figure 2). These critical energy release rates, which have the dimensions of force, can be transformed to any other coordinate system by means of a transformation.

The onset of the macrocrack will be in the direction in which the energy release rate reaches a critical value in that direction. Thus, the IMMFC can also predict the direction of fracture in the composite.

SECTION 4

CRACK GROWTH SIMULATION IN A THREE-DIMENSIONAL FINITE ELEMENT ANALYSIS

The application of the integrated micromechanical and macromechanical fracture criterion (IMMFC) to composites requires an accurate estimation of energy absorption during crack propagation from microflaws, in both the micromechanics and macromechanics analyses. As discussed in the previous section, both analyses are three-dimensional in nature, and thus require a three-dimensional analysis.

The finite element method has been previously used in both two-dimensional and three-dimensional fracture mechanics analyses. There are a number of special elements to represent the stress singularity that exists near a crack tip. A review of the application of the finite element method to fracture mechanics is given by Gallaghar [131]. Fundamental to the study of fracture mechanics is the study of the onset and growth of cracks in a continuum. It is possible in a finite element analysis to propagate a crack after initiation. Crack propagation in a finite element analysis was introduced by Anderson [132]. In his crack propagation simulation, Anderson proposed a method of nodal relaxation in which the cohesive crack tip forces at node points ahead of the crack are cancelled by applying equal and opposite forces to represent the crack extension. Anderson used a constant crack opening angle as a fracture criterion and was able to simulate stable crack growth in elastic-plastic materials. Light and Luxmoore [133] used the energy release rate criterion to predict crack growth. The numerical errors associated with a finite element simulation of crack growth in an

elastic-plastic material have been investigated by Bleackley and Luxmoore [134]. A "stiffness derivative" finite element technique has been developed by Parks [135] for determining elastic crack tip stress intensity factors, which has been further used to derive a virtual crack extension analysis for elastic materials by Parks [136] and Hellen [137], and for nonlinear materials by Parks [138]. Younan, et al. [139,140] used a technique similar to the stiffness derivative method with the critical energy release rate criterion to study the crack propagation in a heterogeneous anisotropic weldment.

Existing analytical modeling of crack propagation in composite materials is very limited. The crack-closure method [81,83] and the failed element [61-64] approaches used for delamination crack growth and micromechanics analyses, respectively, were already discussed in Section 2. In the following sections, a crack propagation simulation in a three-dimensional, elastoplastic, finite element analysis will be presented.

4.1 General Requirements

Crack growth simulation in a three-dimensional finite element analysis is extremely complex. There are nine possible modes in which a stationary crack can advance. Use of failure strength theories (based on stress or strain fields) has to be totally ruled out as they cannot effectively predict the mode of fracture. One cannot resort to the failed element approach [61-64] since this will be grossly inaccurate for the present analysis. More general criteria, e.g., the J-integral criterion or the strain energy density factor criterion, which have been shown to be successful in planar configurations, have practical limitations in a three-dimensional application. Since both the micromechanics

and macromechanics analyses are envisaged to include elastoplastic materials, it is not possible to continuously refine the finite element grid ahead of the propagating crack as in the nodal grafting technique [141] since in an elastoplastic analysis the stress history at fixed points in the material must be maintained. This would restrict the crack propagation to occur only between the element surfaces of the original grid. To allow sufficient freedom to the propagating crack, the finite element grid would have to be very fine and uniform.

The virtual crack extension method [135,136] combined with the energy release rate criterion seems to be the most appropriate approach to crack growth simulation in a three-dimensional finite element analysis. However, for elastoplastic materials the energy release rate during an increment of crack growth has to be redefined. Turner [22] has shown that the energy release rate in the presence of plasticity is higher than that estimated from the linear elastic approximation.

4.2 Energy Release Rate in the Presence of Plasticity

A simple estimation of the elastic energy release rate in the presence of plasticity can be made following the general approach of Turner [22], which is a direct extension of the well-known compliance method of calculating energy release rate G in the LEFM theory. Referring to Figure 3, the path OAB represents a typical nonlinear load-deformation curve for an edge cracked elastoplastic plate. If the effects of hysteresis are ignored, the elastic unloading path will be parallel to the initial loading path OA. If instead, an incremental crack growth Δa occurs at constant displacement, in elasticity theory the load drops to D due to a reduction in area $t\Delta a$, where t is the thickness of the plate, and $BD = -\sigma_n t\Delta a$, where σ_n is the net section

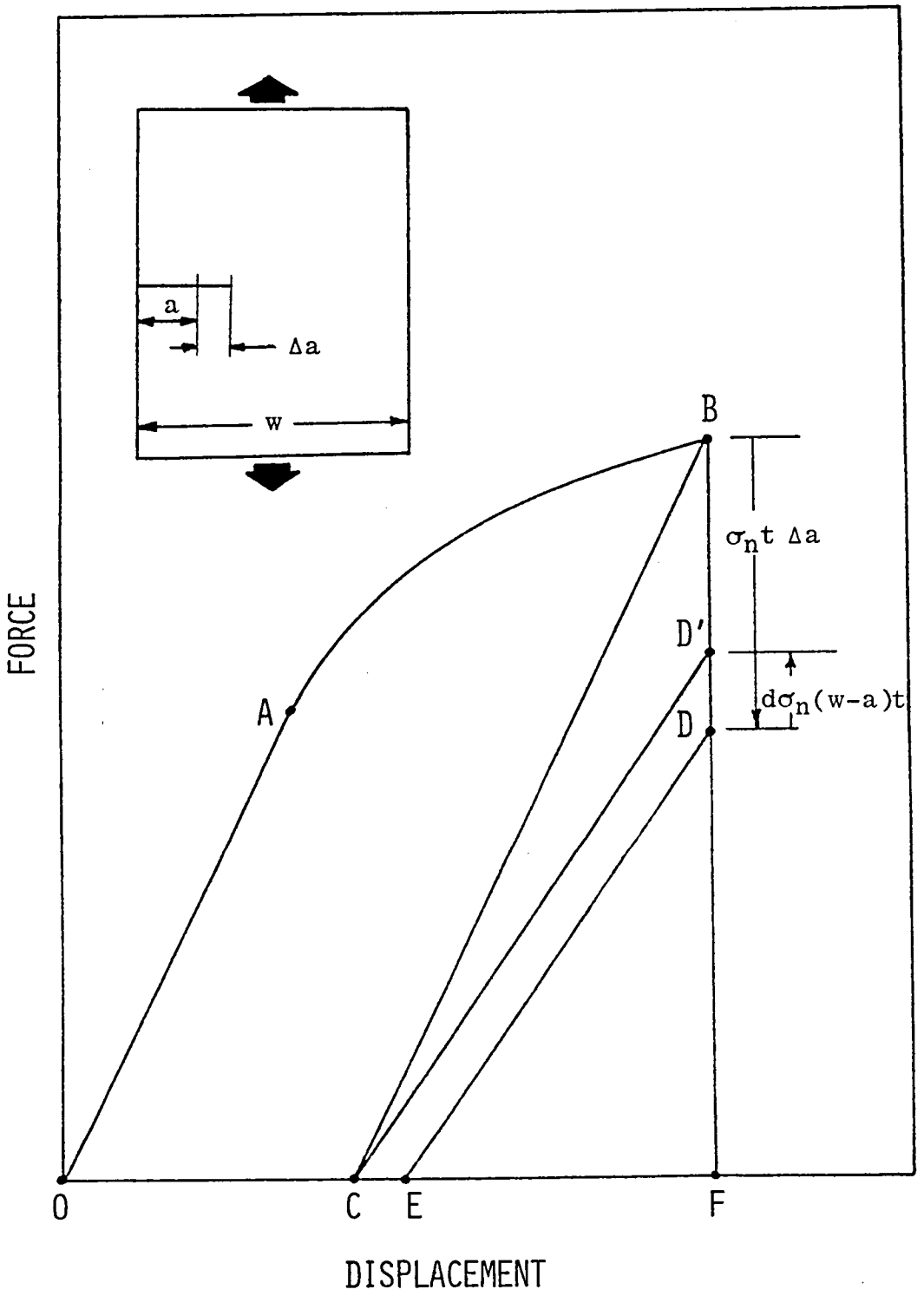

Figure 3. Estimation of the Elastic Strain Energy Release Rate I for an Elastoplastic Crack Growth.

stress on the cracked plane, and rises back to D' due to an increase in the net stress, i.e., $DD' = (w-a)td\sigma_n$, where w is the width of the plate. The ordinates BD and DD' can also be explained as follows. At point B, force equilibrium requires that

$$P = \sigma_n(w-a)t \tag{15}$$

where P is the remote applied force.

When the crack growth occurs under a condition of zero boundary displacement, the crack length, force, and net section stress change to $a+\Delta a$, P', and $\sigma_n+d\sigma_n$, respectively. Then force equilibrium requires that

$$P' = (\sigma_n+d\sigma_n)[w-(a+\Delta a)]t \tag{16}$$

The change in the force is

$$P'-P = (\sigma_n + d\sigma_n)[w - (a + \Delta a)]t - \sigma_n(w - a)t$$

which can be rewritten as

$$P-P' = \sigma_n t\Delta a - d\sigma_n(w - a)t + d\sigma_n t\Delta a \tag{17}$$

Neglecting the second order term $d\sigma_n t\Delta a$ Eq. (17) reduces to

$$P-P' = \sigma_n t\Delta a - d\sigma_n(w - a)t \tag{18}$$

in which $\sigma_n t\Delta a$ is the decrease in the force due to the incremental crack growth, and $d\sigma_n(w - a)t$ is the increase in the force due to the increase in the net section stress.

If the material is assumed to behave elastic-perfectly plastic, the net stress σ_n will be restricted to the yield stress σ_y and there will not be an increase in the force, i.e., DD' = 0. Unloading from point D will be parallel to the increased elastic compliance line D'C. In the case of perfect plasticity, the unloading line from D does not pass through the transposed origin C. The elastic strain energy release rate in the presence of plasticity is represented by area BCED. The area BCD' corresponds to the strain energy release rate if the crack growth is purely an elastic event. The energy release rate corresponding to the area D'CED is the additional energy available in an elastoplastic crack growth. It is also possible to actually include the strain hardening of the material in the plastic zone near the crack tip instead of assuming perfectly plastic response, in which case there will be an increase in the net stress, reducing the total energy release rate. For all practical purposes, this reduction in the area D'CED due to strain hardening will be very small and can be neglected. The elastic strain energy release rate in the presence of plasticity as defined here has been denoted by I by Turner [22], to distinguish it from the energy release rate in the LEFM theory.

4.3 Fracture Modes and the Estimation of Local Energy Release Rates

The loading conditions corresponding to the three fundamental fracture modes near a crack front are shown in Figure 4. The nine possible modes in which a crack in a three-dimensional finite element

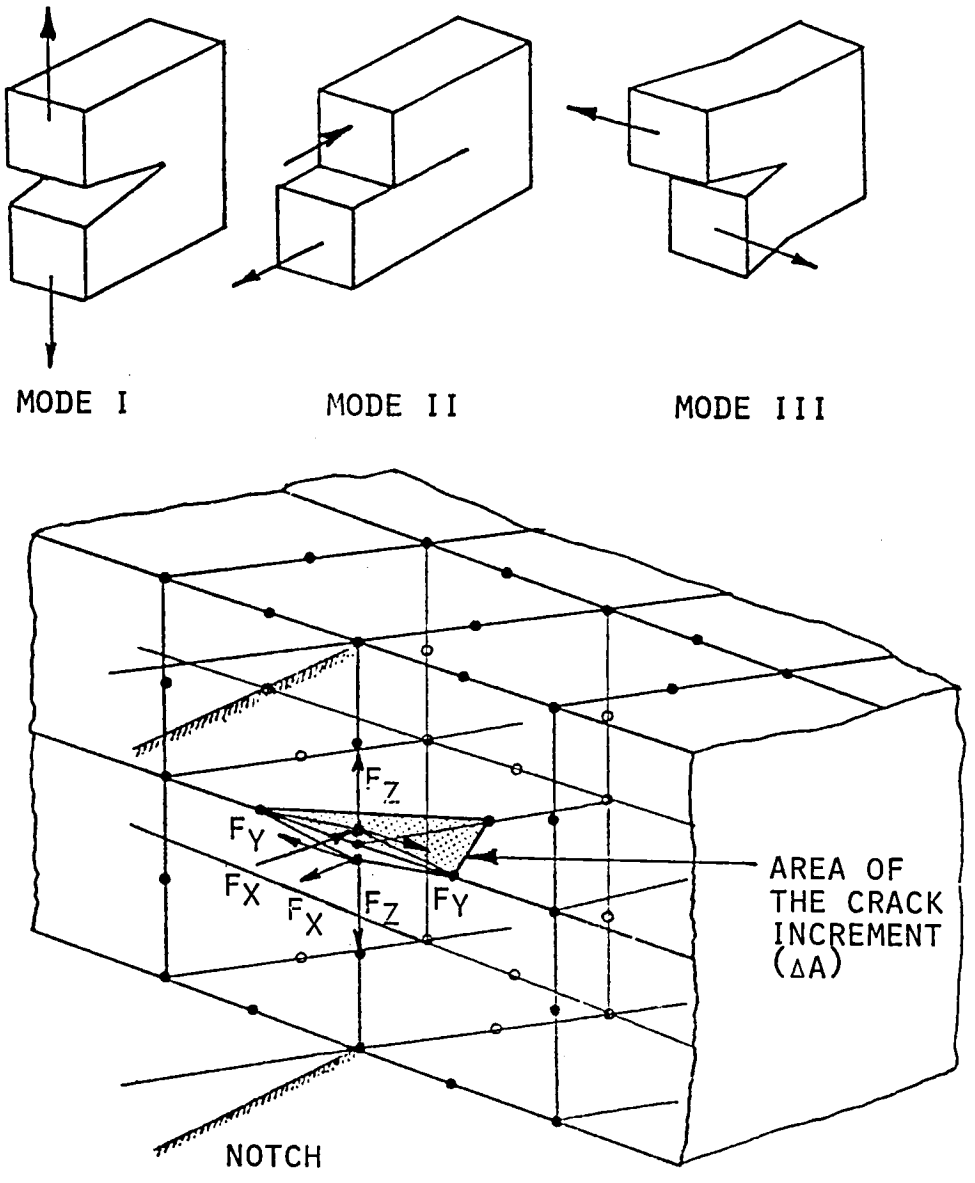

Figure 4. The Three Fundamental Modes of Fracture Near the Crack Tip in a Notched Composite Laminate as Represented in a Three-Dimensional Finite Element Model.

model can advance are shown in Figures 5 through 7. The nine modes of fracture are designated as

M_{XI}, M_{XII} M_{XIII}, M_{YI}, M_{YII}, M_{YIII}, M_{ZI}, M_{ZII} and M_{ZIII}.

As noted in the previous section, we can estimate the energy release rate in the presence of plasticity from the rate of change of compliance during an incremental crack growth. The relation between the rate of change of compliance and the energy release rate during an incremental crack growth in a linear elastic material is given by

$$G = \frac{1}{2t} P^2 \frac{dC}{da} \tag{19}$$

where P is the applied force and C is the compliance of the body (the inverse of the stiffness K).

If C_1 is the compliance of the body before an incremental crack growth and C_2 is the compliance after an incremental crack growth of an amount Δa, then the rate of change of compliance can be written as

$$\frac{dC}{da} = \frac{C_1 - C_2}{\Delta a} \tag{20}$$

Thus,

$$G = \frac{1}{2} P^2 \frac{C_1 - C_2}{t\Delta a} \tag{21}$$

or

$$G = \frac{1}{2} \frac{P^2}{t\Delta a} \left(\frac{1}{K_1} - \frac{1}{K_2}\right) \tag{22}$$

where K_1 and K_2 are stiffnesses corresponding to C_1 and C_2.

Computation of energy release rate in a finite element analysis directly using Eq. (22) will involve the solution of the global system

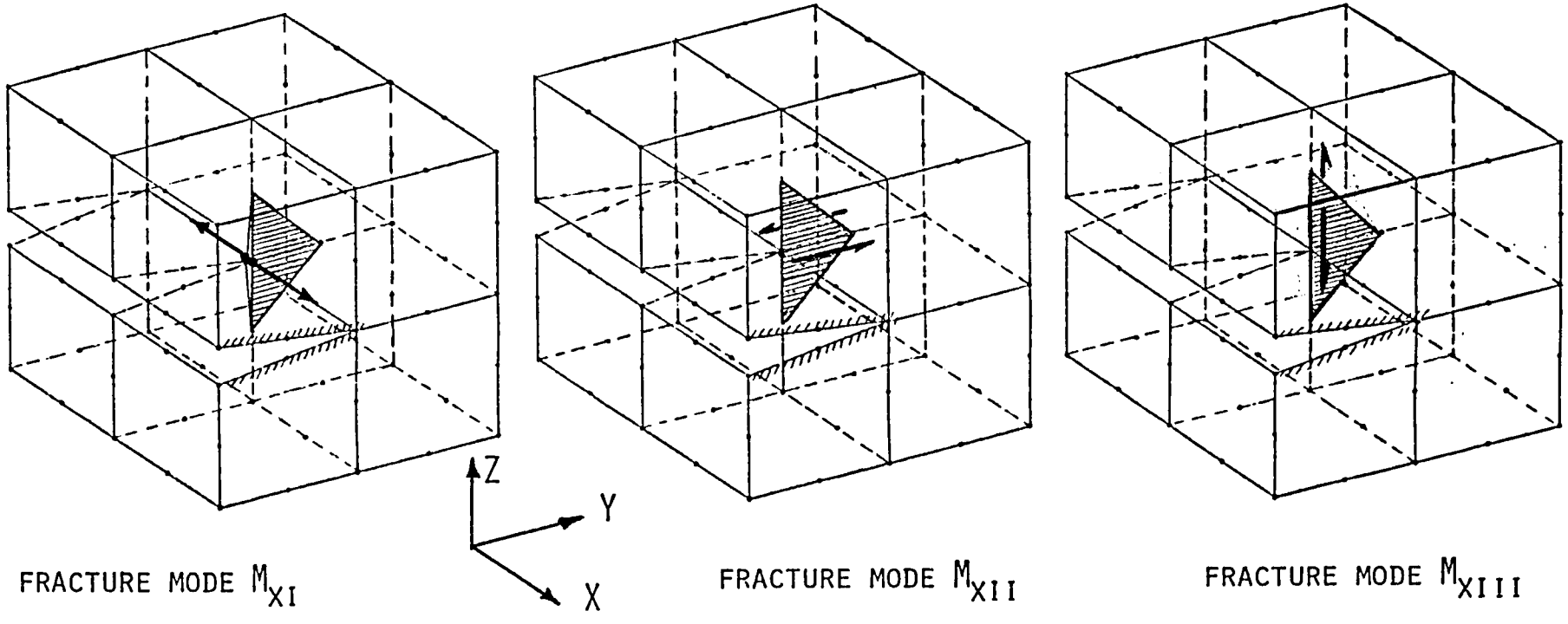

Figure 5. Modes M_{XI}, M_{XII} and M_{XIII} with Virtual Crack Plane Normal to the X Coordinate Direction.

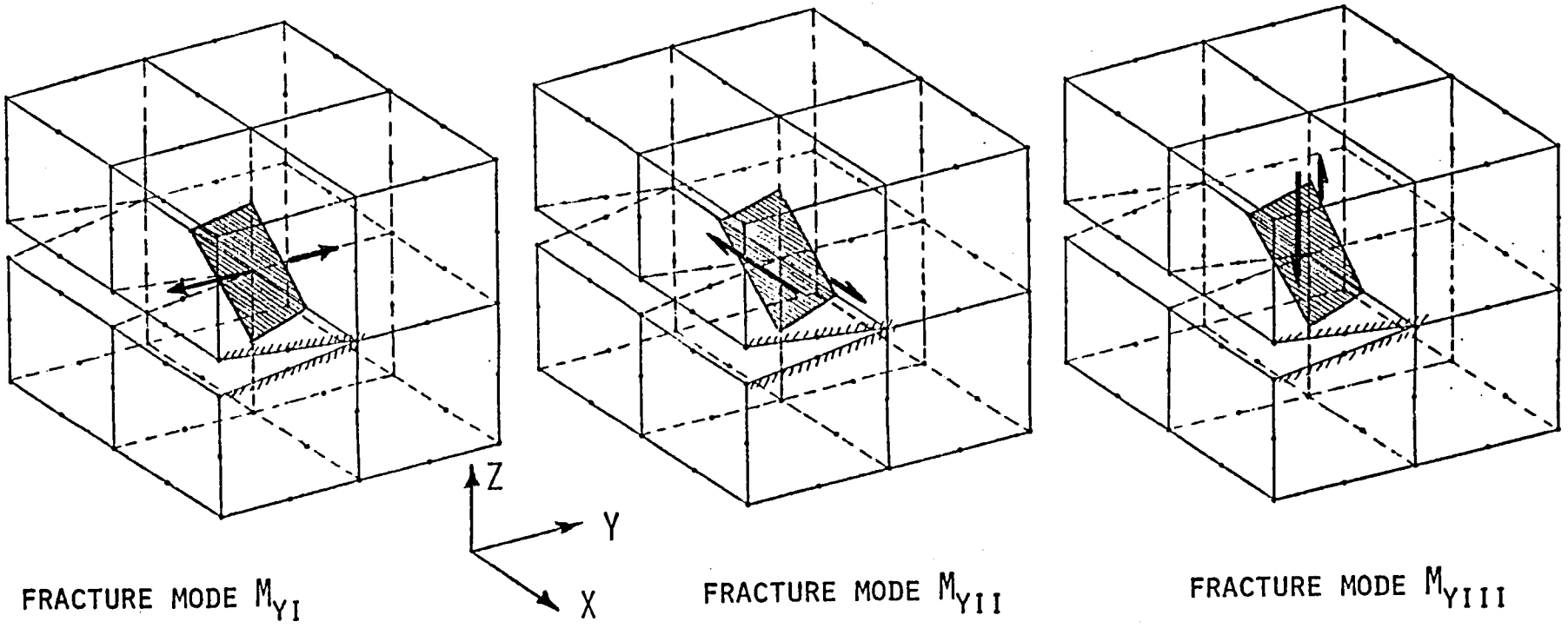

Figure 6. Modes M_{YI}, M_{YII} and M_{YIII} with Virtual Crack Plane Normal to the Y Coordinate Direction.

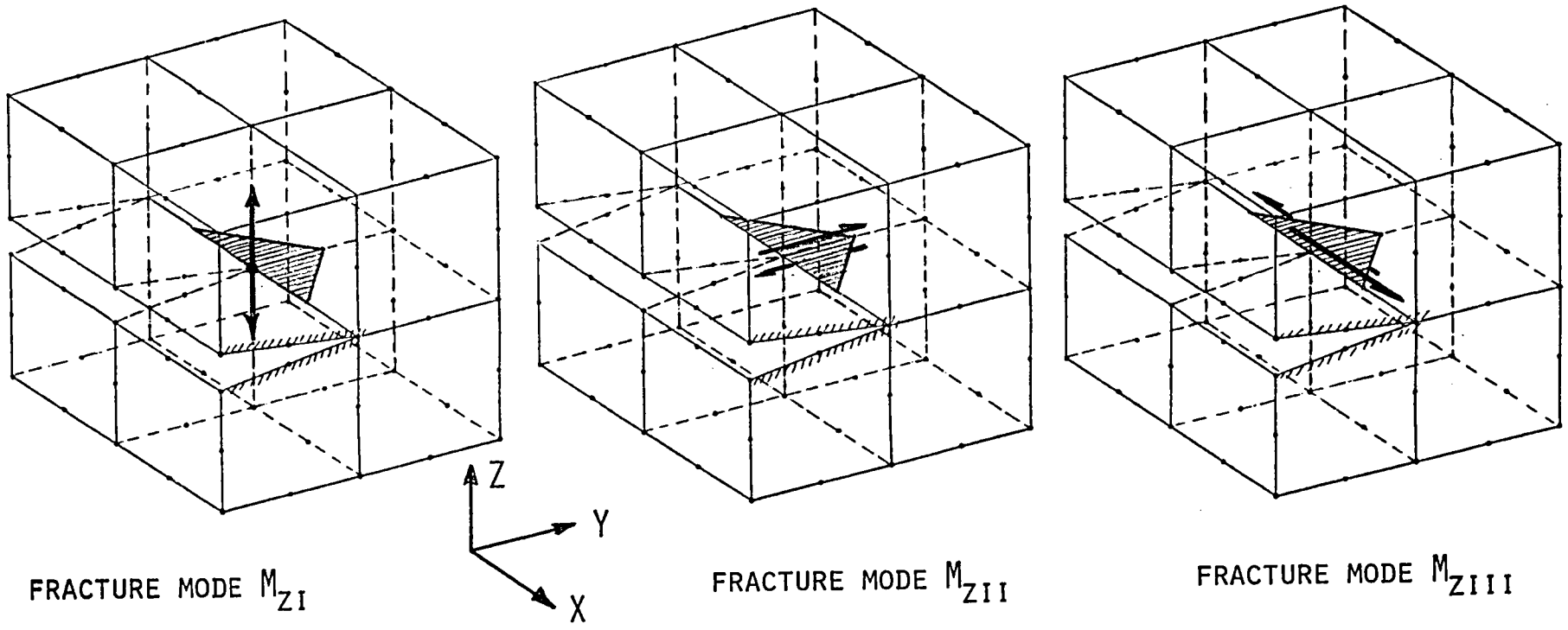

Figure 7. Modes M_{ZI}, M_{ZII} and M_{ZIII} with Virtual Crack Plane Normal to the Z Coordinate Direction.

of equations twice (once before an incremental crack growth and once after introducing the crack growth). This procedure is not computationally practical for a continuous crack growth simulation.

For the simulation of crack growth in a finite element analysis, Parks [135] and Hellen [137] have shown that the crack extension affects only a few elements near the crack tip. The virtual crack extension method given by Hellen is as follows. The total potential energy Π of a continuum containing an initial crack of length a, in terms of the global stiffness matrix [K], global displacement vector {q}, and global load vector {P} in a finite element formulation is given by

$$\Pi = \frac{1}{2} \{q\}^T[K]\{q\} - \{q\}^T\{P\} \tag{23}$$

If the crack is extended virtually by an amount δa, the variation of the potential energy is

$$\delta\Pi = \frac{1}{2}\{q\}^T[\delta K]\{q\} + \{\delta q\}^T[K]\{q\} - \{\delta q\}^T\{P\} - \{q\}^T\{\delta P\} \tag{24}$$

where

[δK] is the change in the global stiffness matrix

{δq} is the change in the global displacement vector

{δP} is the change in the global force vector

If the loading forces are far from the crack and are kept constant during the virtual crack extension, $\delta P = 0$. Since $[K]\{q\} = \{P\}$, Eq. (24) reduces to

$$\delta\Pi = \frac{1}{2}\{q\}^T[\delta K]\{q\} \tag{25}$$

Then the energy release rate for a plate of thickness t is

$$G = -\frac{d\Pi}{da}\, t = -\frac{t}{2}\{q\}^T[\frac{dK}{da}]\{q\} \tag{26}$$

This method is sometimes termed the "stiffness derivative method". Only a small portion of the stiffness matrix [δK] is populated since the crack extension affects only a few elements near the crack tip.

A similar observation can be made for crack growth under constant boundary displacement (fixed grip) conditions. Since the work done by the external forces is zero, Eq. (24) becomes

$$\delta\Pi = \delta U_s = \frac{1}{2}\{q\}^T[\delta K]\{q\} + \{\delta q\}^T[K]\{q\} \tag{27}$$

or

$$\delta\Pi = \frac{1}{2}\{q\}^T[\delta K]\{q\} + \{\delta q\}^T\{P\} \tag{28}$$

where U_s is the strain energy of the system. But $\{\delta q\}^T\{P\} = 0$ since the displacements of the loading boundary are held constant.

Making use of the above observations, the computation of the energy release rate during an incremental crack growth in a finite element analysis can be made in terms of the local stiffnesses and forces at the crack tip node points.

In the present analysis, the energy release rate in the presence of plasticity I at the crack tip node points is evaluated using the rate of change of compliance method. The energy release rate I is defined in terms of the local forces and compliance changes. The local forces referred to here are the sum of the corresponding incremental force components required to move the crack tip node point through the corresponding incremental displacement of the node point. The method is

similar to that used in evaluating the energy release rate by the crack closure integral method [85]. In Figure 8, typical force-displacement relations corresponding to the three fracture modes (as indicated in Figure 4) are shown for an elastoplastic material.

In the incremental displacement finite element analysis, the linear elastic total stiffness K and reduced stiffness $\bar{K}$ required in calculating the local energy release rate can be determined in the first load increment, by assembling the contribution of the stiffness coefficients of all elements sharing a node point, before and after incremental crack growth, respectively.

The values of I for the three modes of fracture (Figure 8) are given by

$$I_I = \frac{1}{2\Delta A}[F_z^2/K_{zz} - (F_z - \sigma_{zz}^y \Delta A)^2/\bar{K}_{zz}]$$

$$I_{II} = \frac{1}{2\Delta A}[F_x^2/K_{zx} - (F_x - \tau_{zx}^y \Delta A)^2/\bar{K}_{zx}] \qquad (29)$$

$$I_{III} = \frac{1}{2\Delta A}[F_y^2/K_{zy} - (F_y - \tau_{zy}^y \Delta A)^2/\bar{K}_{zy}]$$

where ΔA is the area of the incremental crack, F_x, F_y and F_z are force components, K_{zz}, K_{zx}, K_{zy} are the total stiffness coefficients, $\bar{K}_{zz}$, $\bar{K}_{zx}$ and $\bar{K}_{zy}$ are the reduced stiffness coefficients, and σ_{zz}^y, τ_{zx}^y, τ_{zy}^y are the yield stress values. The total elastic strain energy release rate is

$$I = I_I + I_{II} + I_{III} \qquad (30)$$

Although the finite element technique of evaluating energy release rate was actually developed here for a general three-dimensional

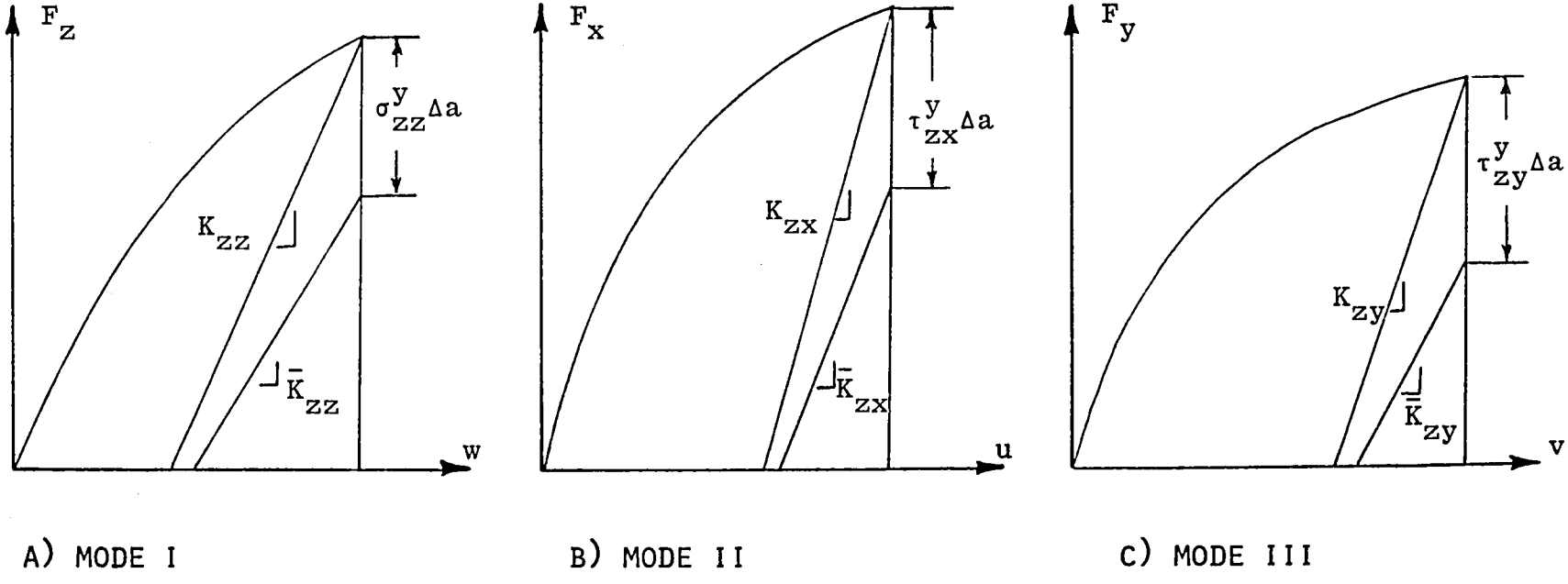

Figure 8. Force-Displacement Relations for Mode I, Mode II, and Mode III Crack Propagation.

analysis, the method can be explained more easily using a two-dimensional example. Shown in Figure 9a is a crack tip Node Point d surrounded by four finite elements (1,2,3 and 4). Under the first load increment the Point d gets displaced to d' by a displacement vector $\bar{u}_d(u_d,v_d)$. The deformation of the crack tip elements is shown by the dotted lines. With displacements of all node points held constant, the force vector $\bar{F}_d(F_{xd}, F_{yd})$ required to move the Point d to d' is evaluated by setting the displacement components u_d and v_d equal to zero in the matrix force-displacement relation for the crack tip elements

$$\{F\} = [K]\{q\} \tag{31}$$

where [K] is the stiffness matrix assembled from the four element stiffness matrices, {F} is the nodal force vector for the four elements, and {q} contains the nodal displacements. The ratio of the force components (F_{xd} and F_{yd}) to the corresponding displacement components gives the required total stiffness coefficients at Node Point d before the crack extension.

In Figure 9b, an incremental crack growth has been introduced by splitting the Node Point d' into d_1 and d_2. Under this new configuration, the Node Points d_1 and d_2 get displaced to d_1^1 and d_2^1 by displacement vectors $\bar{u}_{d1}$ and $\bar{u}_{d2}$. The force vectors required to move d_1 and d_2 to d_1^1 and d_2^1 can be computed, by setting $\bar{u}_{d1}$ and $\bar{u}_{d2}$ equal to zero in the corresponding force-displacement relations, similar to Eq. (31), in which the matrices are obtained by assembling only the top or bottom two element matrices. The ratios of the force vectors to the displacement

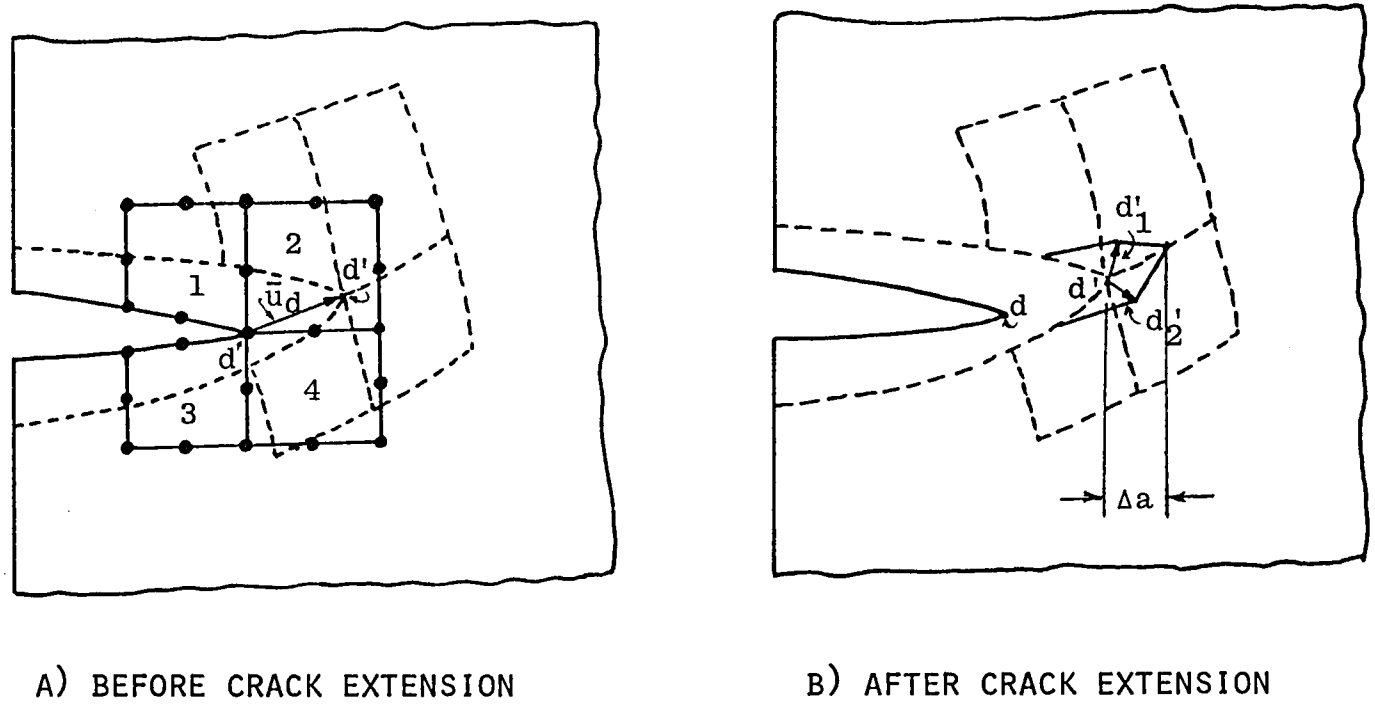

A) BEFORE CRACK EXTENSION

B) AFTER CRACK EXTENSION

Figure 9. Finite Element Technique Used to Calculate the Energy Release Rates.

vectors give the required reduced stiffness coefficients at Node Point d after an elastic increment of crack growth.

4.4 Evaluation of Accuracy

The finite element technique developed to compute the energy release rate during an incremental crack growth can be tested for accuracy by comparing the computed values with the values obtained by standard LEFM methods. The example problem to be considered here is a centrally cracked isotropic plate subjected to an inplane tensile force normal to the crack plane. The other methods to be used for comparison purposes are i) the compliance method, ii) the rate of change of total potential energy method, and iii) the stress intensity factor method.

In the compliance method, the rate of change of compliance $\frac{dC}{da}$ is calculated using Eq. (20). The compliances C_1 and C_2 are obtained from

$$C_1 = \frac{\delta}{P_1} \quad \text{and} \quad C_2 = \frac{\delta}{P_2} \tag{32}$$

where P_1 and P_2 are the forces on the boundary and δ is the applied constant displacement. The energy release rate is obtained using Eq. (21).

In the rate of change of total potential energy method, the energy release rate is given by

$$G = - \frac{\Pi_1 - \Pi_2}{t\Delta a} \tag{33}$$

where the total potential energies before and after an incremental crack growth are given by

$$\Pi_1 = U_1 - \Omega_1 \quad \text{and} \quad \Pi_2 = U_2 - \Omega_2 \tag{34}$$

where U_1 and U_2 represent the strain energy of the plate before and after the crack growth, respectively, and Ω_1 and Ω_2 are the corresponding potential energies of the external forces.

The finite element grid used to model the centrally cracked plate is shown in Figure 10. The plate was assumed to be made of a linearly elastic material having a Young's modulus E of 69 GPa (10.2 Msi) and a Poisson's ratio ν of 0.3. The plate dimensions were 15.2 cm (6 in) in length, 10.2 cm (4 in) in width, and 0.13 cm (0.05 in) in thickness. The two ratios of crack length a to width b considered were 0.2 and 0.3. A total of twenty eight 20-node quadratic isoparametric brick elements were used. In order to represent the $1/\sqrt{r}$ stress singularity near the crack tip, the 20-node elements were collapsed into 15-node quarter point, triangular wedge singular elements [142]. Tensile stresses were applied to the plate by prescribing uniform displacements at the boundary nodes. As can be seen from the results presented in Table 1, the agreement of the present analysis with existing analyses is excellent.

4.5 Crack Growth Simulation

A three-dimensional, elastoplastic, generally orthotropic finite element computer program patterned after that of Monib and Adams [144] was developed for use in the present work. The present program includes 20-node quadratic isoparametric brick elements and a crack propagation capability. The basic elastoplastic analysis theory and the structure of the present computer code are given in Appendix A.

At the node points near an existing crack, the energy release rates for all possible modes of fracture are evaluated at each load increment,

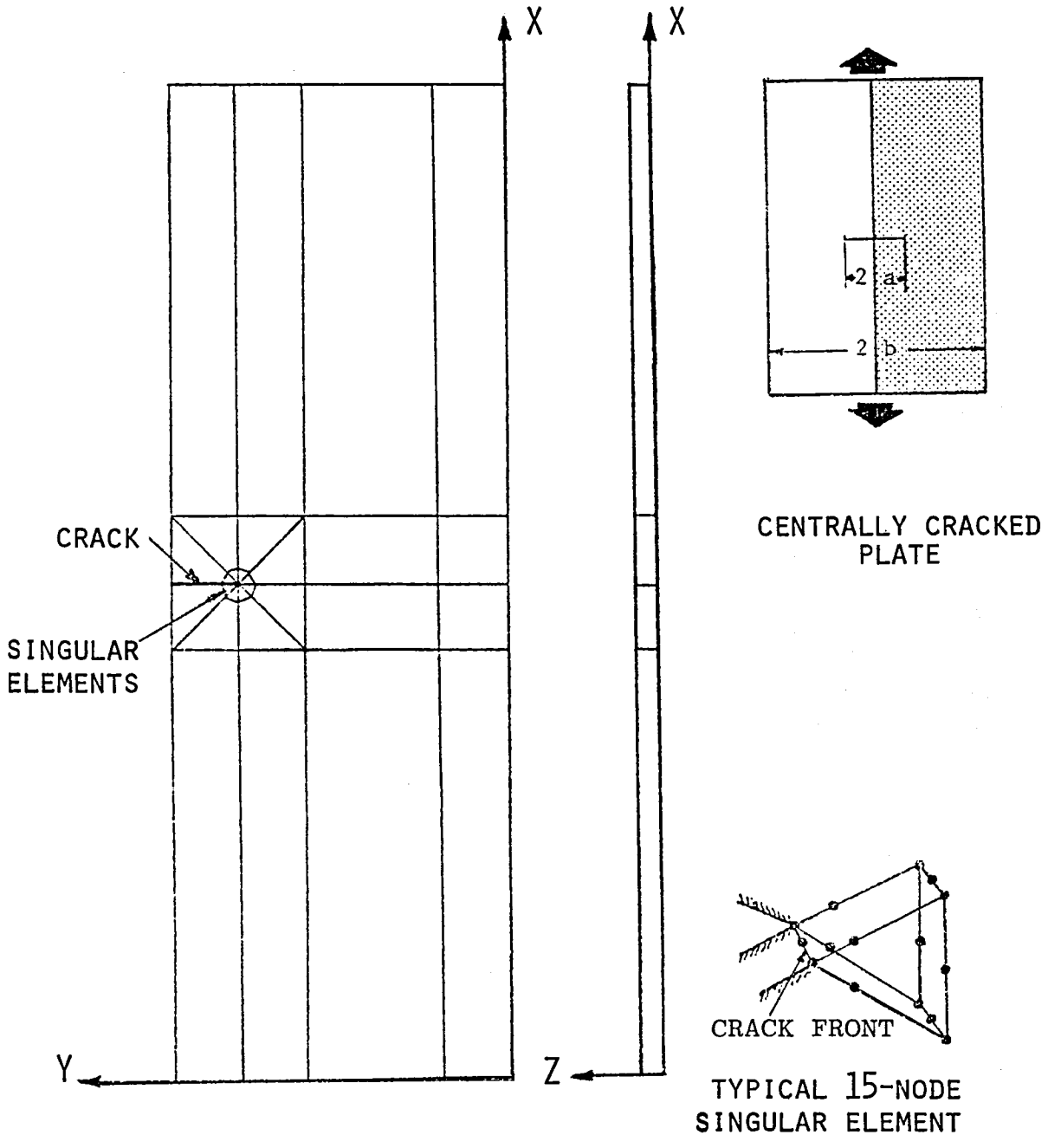

Figure 10. Finite Element Grid Used to Model the Centrally Cracked Isotropic Plate.

Table 1

Comparison of Energy Release Rates During an Incremental Crack Growth Obtained by Different Analytical Methods for a Central Cracked Isotropic Plate

Method	Energy Release Rate J/m^2	(lb/in)
Compliance Method (Eq. 21)		
$G = \frac{1}{2}\frac{P^2}{\Delta a t}(C_1 - C_2)$	6089	34.4
Rate of Change of Potential Energy (Eq. 33)		
$G = \frac{\Pi_1 - \Pi_2}{t\Delta a}$	5947	33.6
Stress Intensity Factor [143]		
$G = \frac{\pi K_I^2}{E}$, where $K_I = \frac{YP\sqrt{a}}{wt}$ and $Y = 1.82$	6106	34.5
Present Analysis	6053	34.2

and compared with the corresponding critical energy release rate values for the material. When the computed energy release rate at a node point is equal to the critical value in an increment, that node point is separated into two node points and the reaction forces are applied to the old and new node points. The element nodal connectivity of all elements sharing the new node point is changed to simulate the crack growth in the model. If the crack tip node point at which the energy release rate reaches a critical value happens to be a corner node, the crack is assumed to extend up to the nearest mid-side nodes; if the node point is a mid-side node, the extended crack surface is assumed to be that connecting the adjacent corner nodes and the mid-side node on the opposite side. The possible forms of crack extension are shown in Figure 11. Before applying the next load increment, the system of equations with new boundary conditions and reaction forces is solved again to check for any further crack growth. The crack growth simulation technique and its implementation in a three-dimensional elastoplastic finite element computer code is further explained in Appendix B.

4.6 Example Problem

The accuracy of the crack growth simulation technique developed in the present analysis was verified by applying it to predict self-similar crack growth in a centrally cracked 2024-T3 aluminum plate subjected to inplane Mode I loading.

The finite element grid and plate geometry were assumed as shown in Figure 10. The material properties used for the 2024-T3 aluminum alloy [143] were as follows: Young's modulus = 70.3 GPa (10.2 Msi), Poisson's ratio = 0.345, yield strength = 345 MPa (50 ksi), and tensile strength = 485 MPa (70 ksi). The nonlinear properties of 2024-T3 aluminum [143]

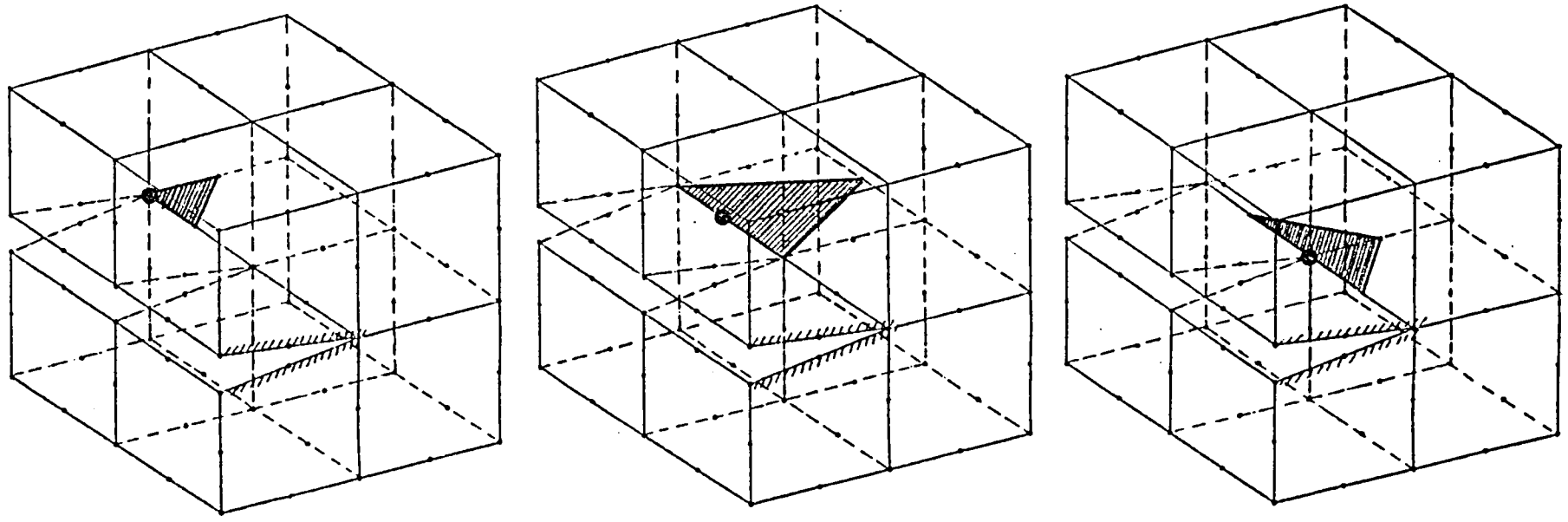

Figure 11. Area of the Incremental Crack Growth for Different Locations of the Crack Tip Node Point.

were incorporated in the analysis by expressing the stress-strain relation of the material in terms of Richard-Blacklock curve-fitting parameters (see Appendix). The displacement constraints on the collapsed nodes of the singular elements were removed, to represent the 1/r type of singularity of a perfectly plastic material. Such perfectly plastic singular elements are extensively used in elastoplastic fracture mechanics [145]. The thickness of the plate was taken as small as possible, viz., 0.0025 cm (0.001 in), to simulate plane stress conditions without introducing errors due to resulting large aspect ratios of the grid elements.

In Figure 12, the predicted crack extension at various applied stress levels and the associated extent of plastic yielding are shown. The shapes of the plastic yield zones were obtained by drawing smooth curves around the Gaussian integration points at which the material was predicted to have yielded. It should be mentioned here that in earlier trial runs in which greater plate thickness values were considered, the predicted yield zone sizes were smaller than those shown in Figure 12, and they varied in size through the thickness of the plate. The extent of plastic yielding at various applied stress levels predicted in the present analysis is in general agreement with those given in Reference [146] for a central cracked aluminum plate.

During the process of crack propagation (particularly for large scale yielding), the analysis also predicted that some of the elements which had previously plastically deformed start unloading as the crack passes by, as one might expect.

It was observed that the crack propagated in small increments initially, up to about half the plate width, and then propagated rapidly

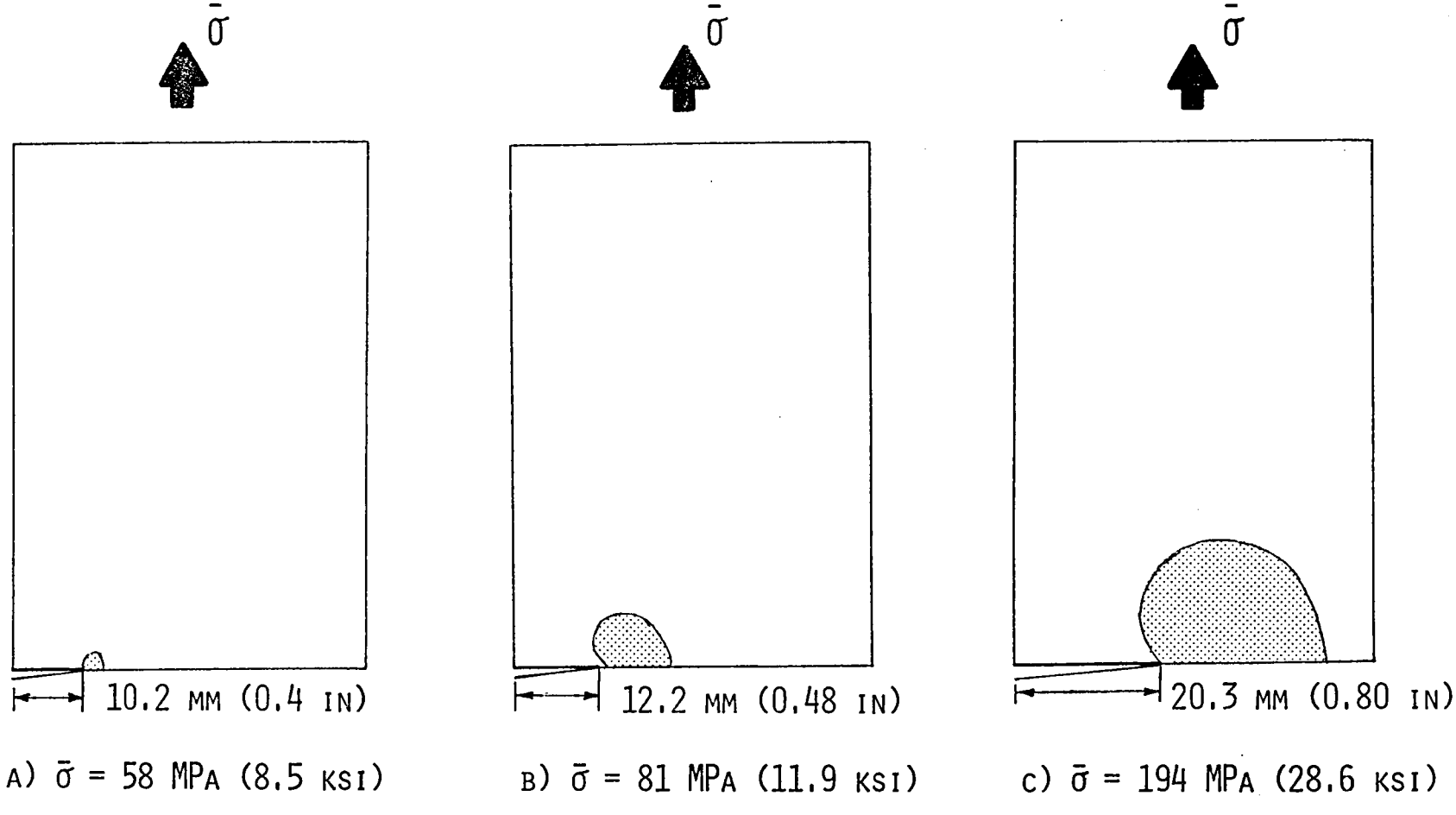

Figure 12. Crack Propagation and Associated Plastic Yielding in a Centrally Cracked 2024-T3 Aluminum Plate as Predicted by the Present Analysis.

across the plate. This may have been due to the coarseness of the finite element grid used, especially towards the later stages of crack growth, but the applied stress $\bar{\sigma}$ = 330 MPa (47.9 ksi) at the point of observed instability of the crack agreed with the critical stress value σ_c = 348 MPa (50.4 ksi) for the 2024-T3 aluminum [143]. The fracture toughness value of 41.8 MPa$\sqrt{m}$ (38 ksi$\sqrt{in}$) computed using $K_{IC} = \sqrt{GE}$, where G is the energy release rate at the onset of unstable crack growth and E is the Young's modulus of the material, was also in good agreement with the material toughness value of 44 MPa$\sqrt{m}$ (40 ksi$\sqrt{in}$) reported in Reference [143].

The predicted crack opening displacements (crack shapes) of the propagating crack are plotted in Figure 13. The effect of plastic yielding at higher applied stress levels in blunting the crack tip can be seen. Neither experimental nor analytical crack opening displacement values were available in the literature for the material and crack geometry used here, preventing comparisons with the crack opening displacements predicted here.

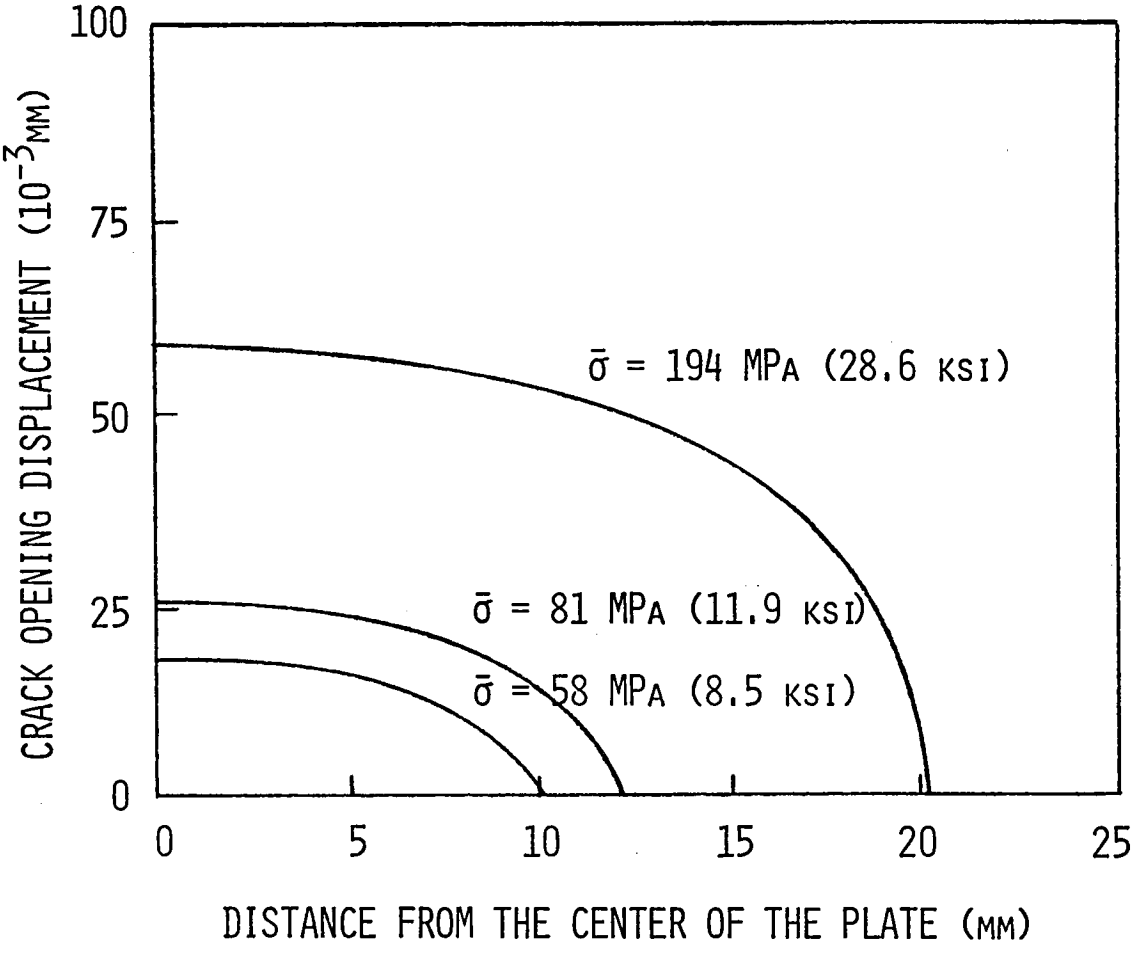

Figure 13. Crack Opening Displacements in the Centrally Cracked 2024-T3 Aluminum Plate at Various Applied Stress Levels.

SECTION 5

MICROMECHANICS ANALYSIS

5.1 Model Geometry

Assuming that the fibers in a unidirectional lamina are packed in a regular square array, a repeating cell can be identified. One such is that containing a single broken fiber surrounded by continuous unbroken fibers, as previously indicated in Figure 2. In this configuration, the density of the broken fibers is 25 percent of the total number of fibers. Other types of microflaws to be considered include matrix cracks parallel to the fibers, and fiber-matrix interface debonds. These microcracks are assumed to be distributed symmetrically with respect to three orthogonal planes.

Figures 14 and 15 show the two three-dimensional finite element models developed for the analysis. Taking advantage of the assumed symmetry, only one octant of the repeating cell need be modeled. The first model (Figure 14) contains a total of 282 20-node, quadratic isoparametric elements, whereas the second model (Figure 15) contains 144 similar elements. Due to the memory (including extended core) limits of the CDC Cyber 760 computer available for use at the University of Wyoming, it was not possible to run the first, more refined model. An attempt was made to run this model on the Department of Mechanical Engineering's Prime 550 minicomputer, but the running time per increment was prohibitively long. However, the limited results for the few incremental solutions which were obtained using the Prime 550 (with double precision) were later used to evaluate the much coarser second model (Figure 15). Stresses predicted using the two different models differed

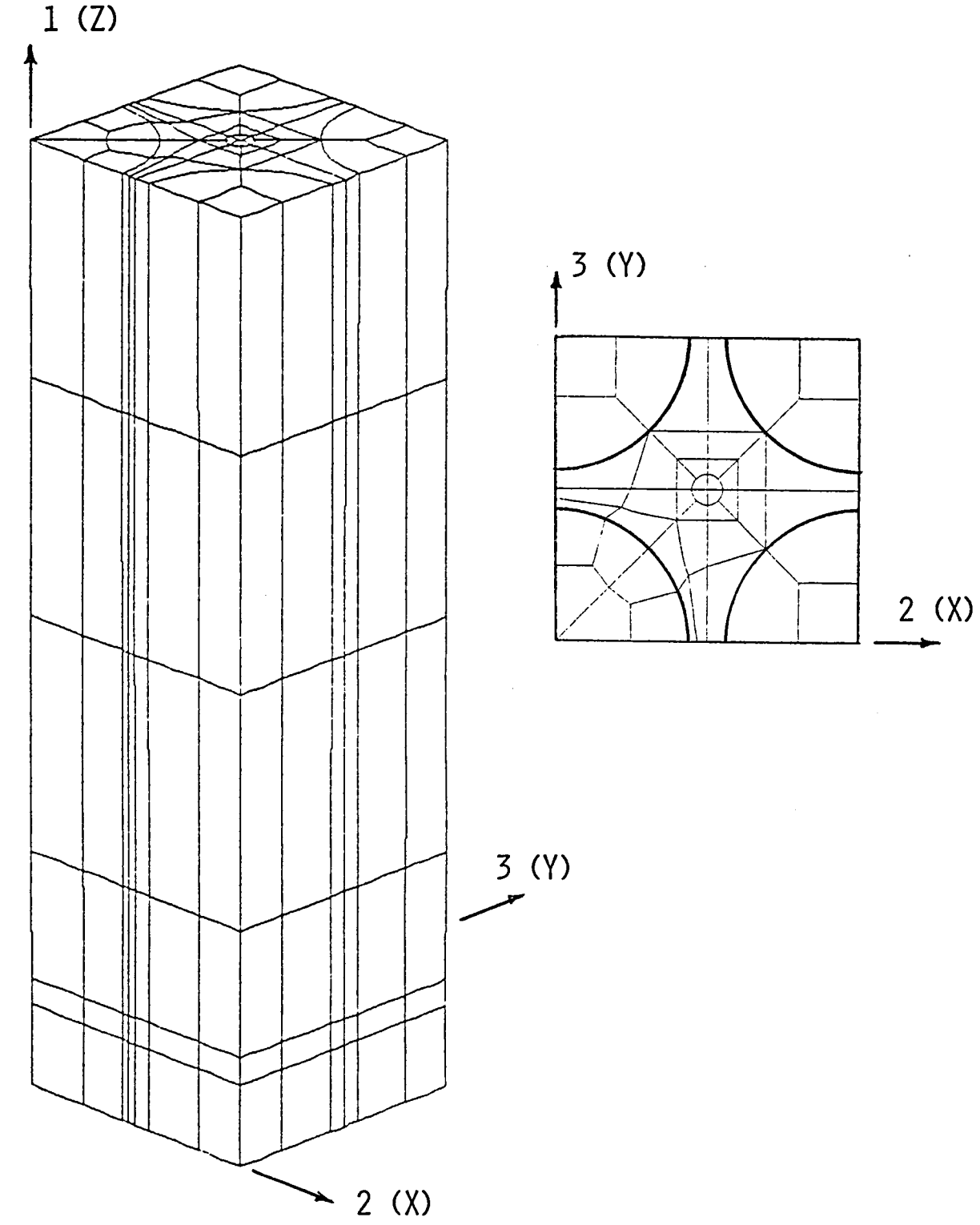

Figure 14. Finite Element Grid Developed for the Micromechanics Analysis.

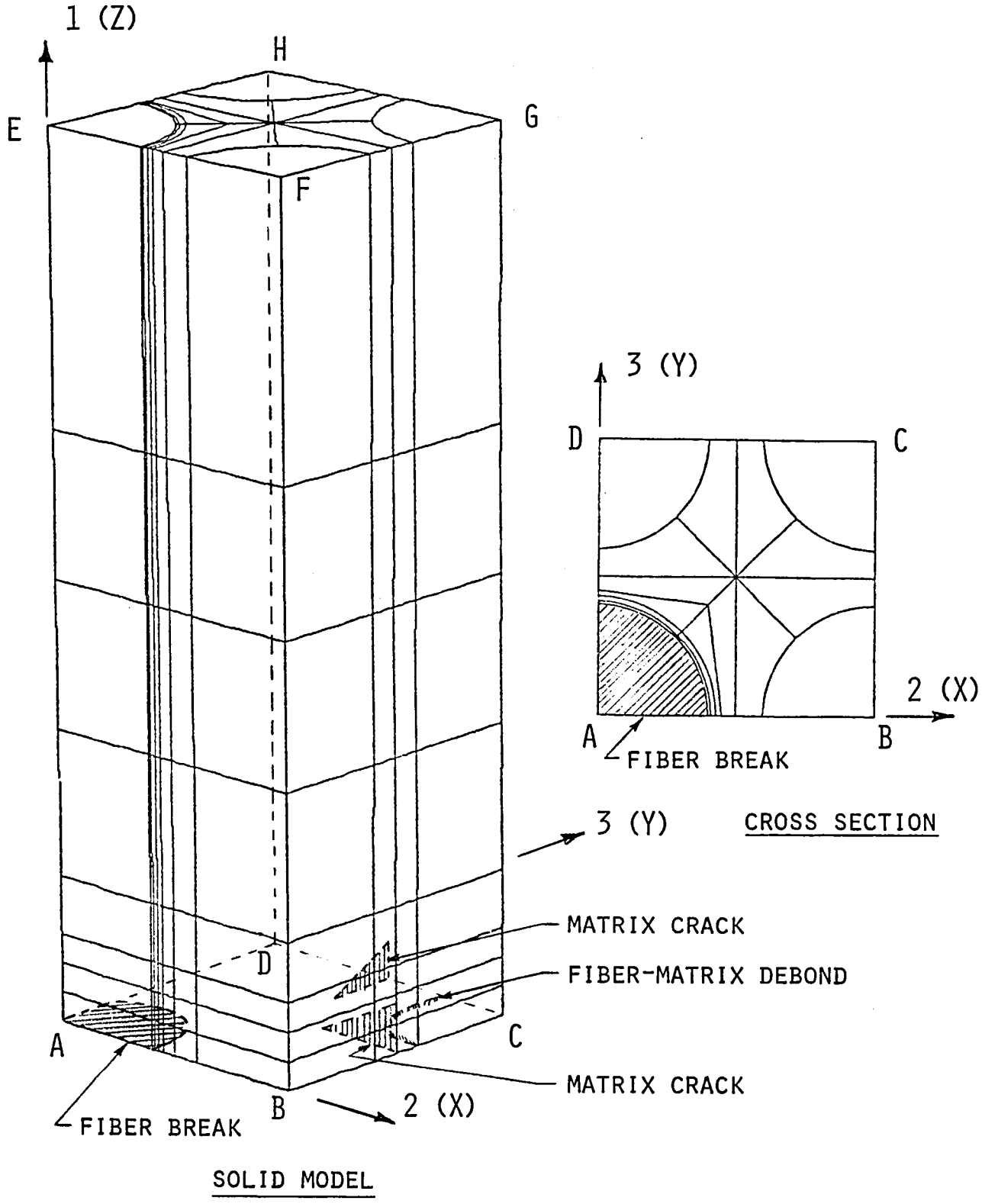

Figure 15. Finite Element Grid with Representative Microflaws Used in the Present Micromechanics Analysis.

by only 4 percent (maximum). The very large aspect ratios of the interface elements and the distortions of the fiber elements in the second model did not introduce significant errors.

There are 945 node points in the second model (1583 in the first). Three different microflaws, in the form of broken fibers, matrix cracks parallel to the fibers, and fiber-matrix interface debonds, have been represented in this model, by altering the boundary conditions. The material microflaw parameters (defined by Eqs. 12 in Section 3) used in the present analysis were:

$$a_{frbk} = 0.250$$

$$a_{mcpl} = 0.020$$

$$a_{fmid} = 0.017$$

The model incorporates a double-node concept at the junction of the broken fiber and the surrounding matrix, in order to represent the actual conditions of discontinuity of the fiber at the break, while retaining the continuity of the matrix material at the same point. The double nodes are constrained to have identical displacements in the x and in the y directions.

The displacement boundary conditions for the octant of the repeating cell shown in Figure 15 are that the normal displacements of all nodes on the vertical boundaries be uniform (from symmetry), and that the normal displacements of all nodes on the upper horizontal boundaries (surface EFGH) also be uniform (generalized plane strain loading). This complex boundary condition has been achieved in the present three-

dimensional model by assigning the same global degree of freedom to all nodes that are required to have same boundary displacements.

5.2 Material Properties

The constituent materials used for the unidirectional lamina were Hercules AS4 graphite fibers and Hercules 3501-6 epoxy matrix. The temperature- and moisture-dependent properties of the neat (unreinforced) matrix material as obtained by means of solid rod torsion tests [147] have been expressed in the present analysis in a polynomial form as

$$P(T,M) = C_1T + C_2M + C_3TM + C_4 \tag{35}$$

where P is the material property of interest, T is temperature (°C), M is the moisture content (weight percent) and the C's are coefficients of the polynomial (see Table 2). Temperature- and moisture-dependent octahedral shear stress-octahedral shear strain curves for the Hercules 3501-6 resin are shown in Figure 16. The matrix is treated as an isotropic, elastoplastic material in the analysis, by using a three-parameter Richard-Blacklock model [148].

The properties of the graphite fibers used in the analysis are given in Table 3. The anisotropic nature of the fibers has been taken into account in the present analysis, as explained in the Appendix.

5.3 Loading Conditions

The main objective of the present micromechanics analysis was to evaluate the six critical energy release rate values, viz, G_{C11}, G_{C22}, G_{C33}, G_{C23}, G_{C31} and G_{C12}. These critical energy release rate values correspond to the loading conditions denoted by their subscripts. In

Table 2

Coefficients of the Polynomial (Eq. 35) Used to Define the Temperature-and Moisture-Dependent Properties of the Hercules 3501-6 Epoxy Resin.

$$\text{Property} = C_1T + C_2M + C_3TM + C_4$$

Property	C_1	C_2	C_3	C_4
Shear Modulus, G (psi)*	-1.14×10^{3}	-2.49×10^{3}	-3.38×10^{1}	2.60×10^{5}
Richard Blacklock Curve-Fit Parameters n*	2.56×10^{-3}	2.78×10^{-3}	1.65×10^{-4}	1.54×10^{0}
τ_o (psi)*	-1.50×10^{2}	-1.36×10^{3}	6.46×10^{0}	2.67×10^{4}
Ultimate Shear Strength, τ_{ult} (psi)*	-8.73×10^{1}	-6.03×10^{2}	1.86×10^{0}	1.66×10^{4}
Coefficient of Thermal Expansion, α $(°C)^{-1}$	1.22×10^{-7}	1.04×10^{-6}	-5.90×10^{-10}	3.83×10^{-5}
Coefficient of Moisture Expansion, β $(\%M)^{-1}$	0	0	0	3.20×10^{-3}
Poisson's Ratio, ν	0	0	0	0.34×10^{0}

*Based on solid rod torsion shear data

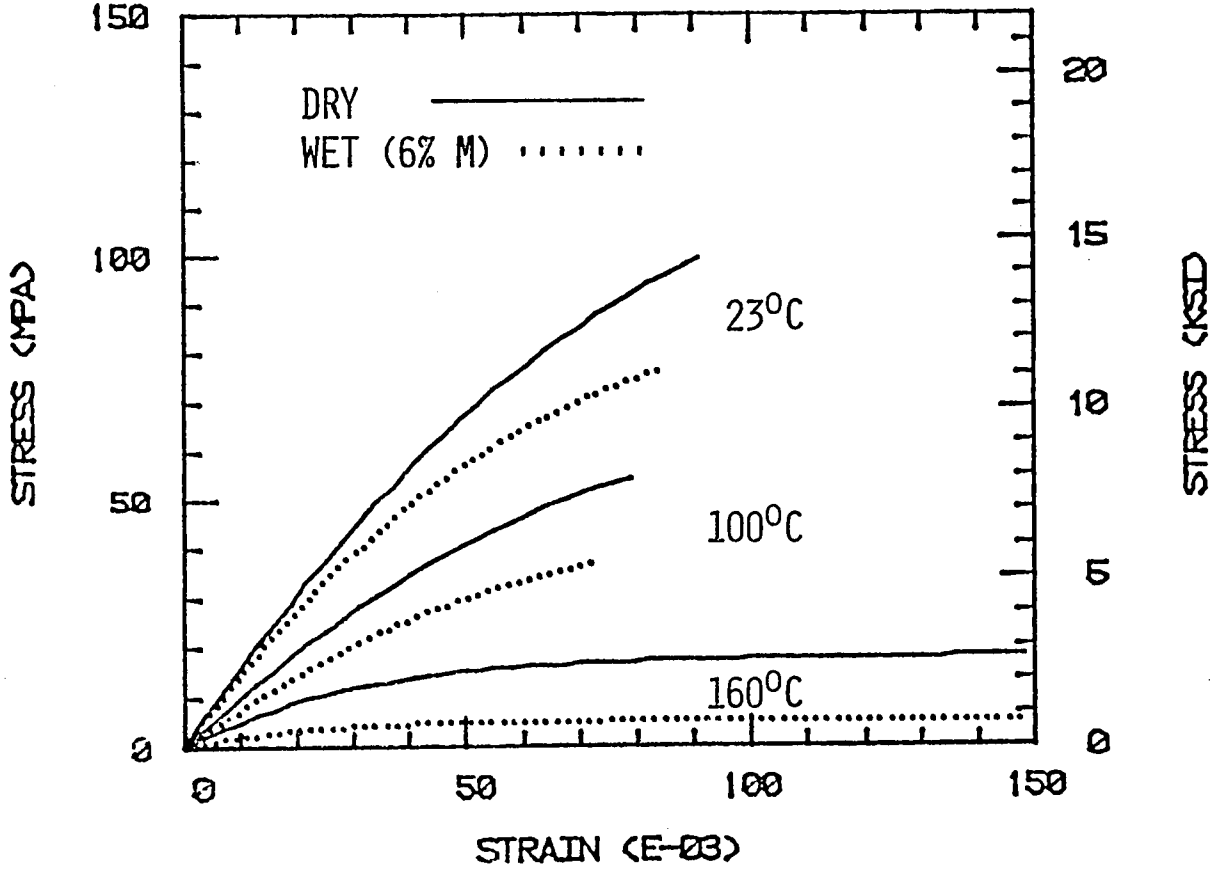

Figure 16. Temperature- and Moisture-Dependent Octahedral Shear Stress-Octahedral Shear Strain Curves for Hercules 3501-6 Epoxy Resin, as Obtained from Solid Rod Torsion Tests [147].

Table 3

Mechanical Properties of Hercules AS4 Graphite Fiber [147]

Longitudinal Modulus, E_ℓ	221 GPa	(32.0 Msi)
Transverse Modulus, E_t	13.8 GPa	(2.0 Msi)
Longitudinal Shear Modulus, $G_{\ell t}$	34.5 GPa	(5.0 Msi)
Transverse Shear Modulus, G_{tt}	5.52 GPa	(0.80 Msi)
Major Poisson's Ratio, $\nu_{\ell t}$	0.20	
In-Plane Poisson's Ratio, ν_{tt}	0.25	
Longitudinal Tensile Strength, σ^u_ℓ	3100 GPa	(450 ksi)
Transverse Tensile Strength, σ^u_t	345 GPa	(50 ksi)
Longitudinal Shear Strength, $\tau^u_{\ell t}$	1550 GPa	(225 ksi)
Transverse Shear Strength, τ^u_{tt}	172 GPa	(25 ksi)
Longitudinal Coefficient of Thermal Expansion, α_ℓ	$-0.36 \times 10^{-6}/°C$	
Transverse Coefficient of Thermal Expansion, α_t	$18.0 \times 10^{-6}/°C$	

general, to evaluate all six G_C values, the micromechanics model must be subjected to six separate loading conditions, viz, $\bar{\sigma}_{11}$, $\bar{\sigma}_{22}$, $\bar{\sigma}_{33}$, $\bar{\tau}_{23}$, $\bar{\tau}_{13}$ and $\bar{\tau}_{12}$. However, since the model and the microflaws are assumed to be symmetric about the x-z and y-z planes (in the transverse direction), $G_{C22} = G_{C33}$ and $G_{C13} = G_{C21}$.

This reduces the total number of loading conditions to four (viz, $\bar{\sigma}_{11}$, $\bar{\sigma}_{22}$, $\bar{\tau}_{21}$ and $\bar{\tau}_{23}$). Using the finite element model of the octant of the repeating cell (Figure 15), the longitudinal and transverse normal loads (see Figures 17a and 17b, respectively) are easily applied as prescribed boundary displacements, in increments, whereas the two longitudinal shear loading conditions (see Figures 17c and 17d) pose difficulties. Under shear loading, the assumption of three orthogonal planes of symmetry used in modeling an octant of the repeating cell is not valid. Longitudinal shear loading (Figure 17c) can be modeled directly, however, as presented in detail in Reference [40]. The longitudinal shear loading is applied by prescribing uniform displacements to all node points on face FBCG (Figure 15 or Figure 17c) in the longitudinal direction and removing the uniform displacement constraint on all node points on the top face (EFGH) except along lines EH and FG. A general approach to apply transverse shear loading in a two-dimensional micromechanics analysis is to identify a repeating cell with its sides at 45° to the transverse co-ordinates (2 and 3 in Figure 15), and then to apply equal and opposite normal stresses to the cell boundaries. It is not possible to identify such a repeating cell in the present case that has same percentage of broken fibers. However, the crack propagation due to shear loading in the transverse plane has been studied in the present analysis by applying equal and opposite normal stresses in

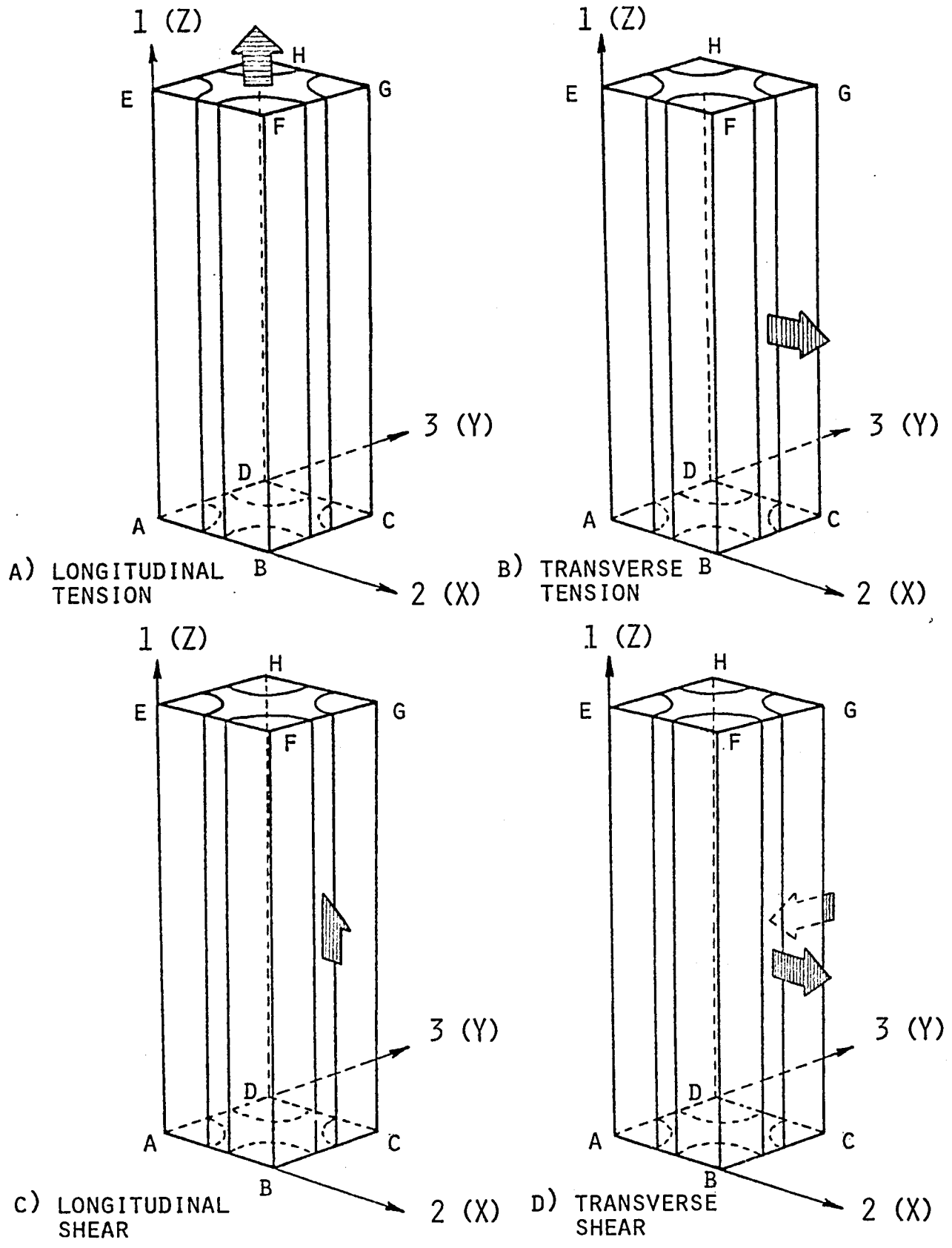

Figure 17. The Four Different Loading Conditions in the Present Three-Dimensional Micromechanics Analysis.

the two transverse directions (Directions 2 and 3 in Figure 17d). This is equivalent to transverse shear loading at 45° to the transverse co-ordinates.

Before applying any mechanical loads, the thermal conditions induced after curing the graphite/epoxy composite at (177°C) and then cooling down to room temperature (21°C) were simulated by reducing the stress-free reference temperature of 177°C to room temperature in 10 equal increments.

5.4 Crack Initiation and Propagation

For the three different types of microflaws considered in the present analysis (broken fibers, matrix cracks parallel to fibers, and fiber-matrix debonds) it could be judged beforehand that each individual flaw type would become critical only under certain loading conditions (e.g., the broken fiber will become critical only under longitudinal tension and longitudinal shear loading conditions). These observations considerably reduced the total number of computer runs required. The different combinations of types of microflaws and loading conditions actually considered are summarized in Table 4.

Table 4

Loading Conditions Considered with Different Types of Microflaws in the Present Analysis

Flaw Type	Loading Conditions			
Broken Fibers	$\bar{\sigma}_{11}$	-	$\bar{\tau}_{12}$	-
Matrix Cracks	-	$\bar{\sigma}_{22}$	-	$\bar{\tau}_{23}$
Fiber-Matrix Debond	-	$\bar{\sigma}_{22}$	-	$\bar{\tau}_{23}$

5.4.1 Broken Fibers

The fiber break is introduced in the finite element model (Figure 15) by simply removing the displacement constraint of all node points in the fiber lying in the plane of the break. If the fiber break is introduced before the cooling temperature increments are applied, the graphite fiber, which has a negative longitudinal coefficient of expansion, tends to extend beyond the symmetry plane. This has been prevented in the present analysis by not introducing the flaw until the system is cooled down to room temperature. The crack propagation flag is also turned off during the incremental loading.

The applied longitudinal displacement increments used were 0.0076 cm (0.003 in). In Figure 18, the predicted crack propagation at various applied stress levels is schematically shown. At the applied stress of 284 MPa (50 ksi), all nodes near the initial crack opened in modes M_{ZI}, M_{ZII} and M_{ZIII} (predominantly in M_{ZI}), forming a radial crack front. During subsequent load increments, the crack steadily grew until it reached the diagonally opposite fiber. The crack then spread all across the matrix. Although not shown here, plastic yielding was restricted to small volumes near the propagating crack. Comparisons of the sizes of the plastic yielding zones indicated that as the crack front advanced, the nodes previously yielded started unloading.

In Figure 19, the predicted crack growth from the broken fiber due to longitudinal shear loading is shown. The applied longitudinal displacement increments on the vertical face were 0.0076 cm (0.003 in). Two radial cracks initiated in the plane of the fiber break, and propagated around the adjacent fibers.

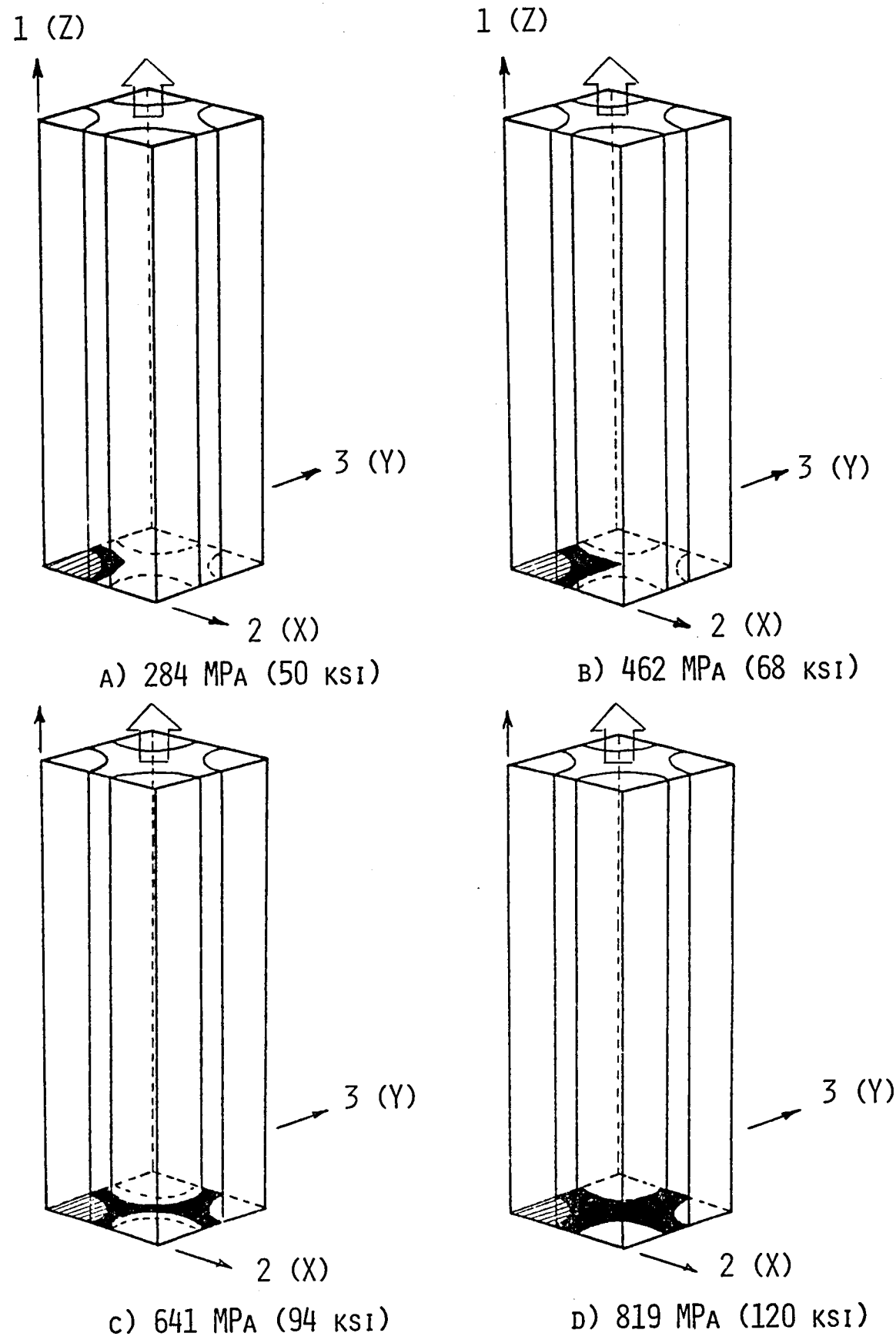

Figure 18. Initiation and Growth of a Crack from a Broken Fiber as a Function of Longitudinal Tensile Applied Stress.

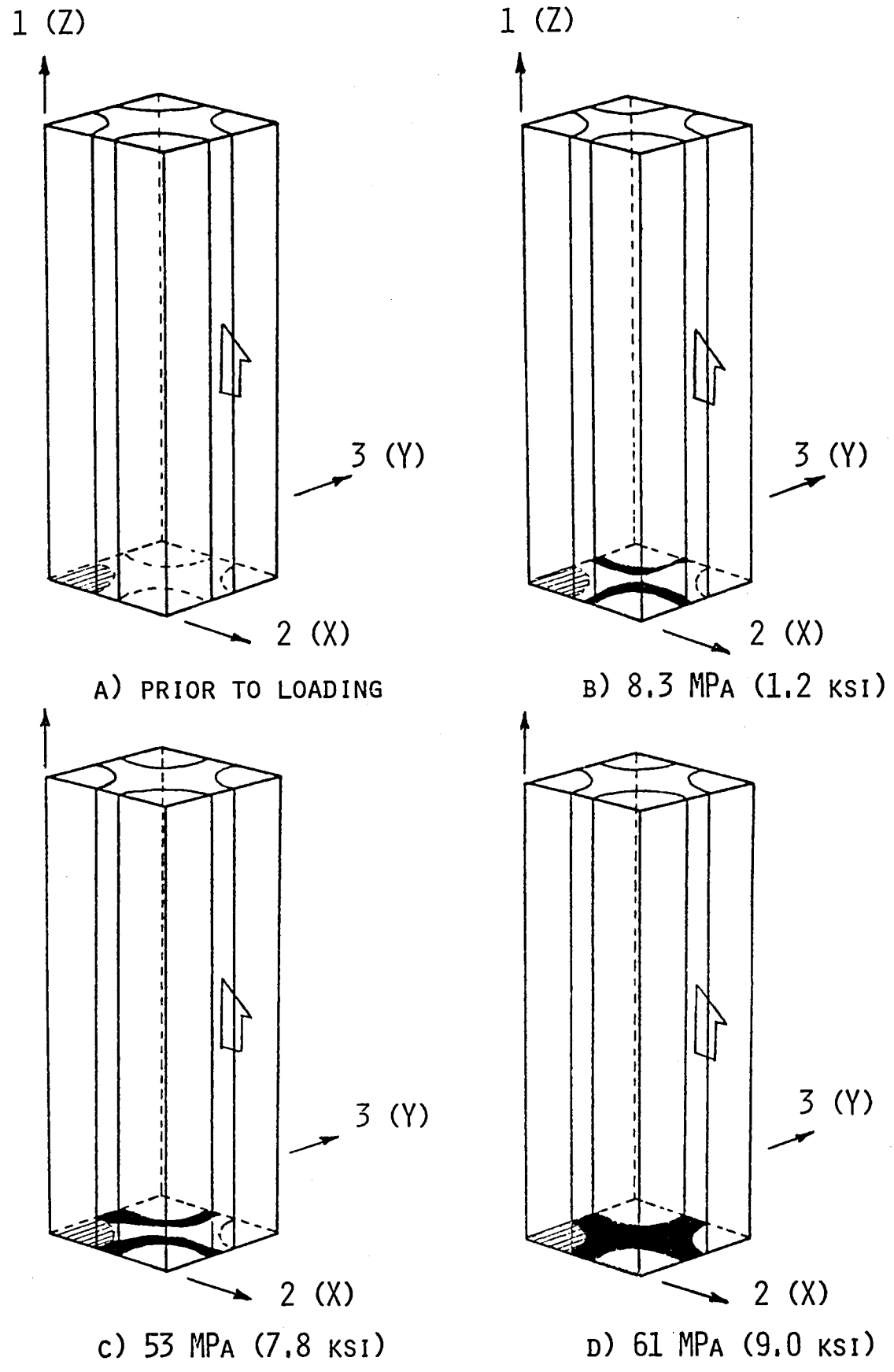

Figure 19. Initiation and Growth of Cracks from a Broken Fiber as a Function of Longitudinal Shear Applied Stress.

5.4.2 Matrix Cracks Parallel to Fibers

Two matrix cracks parallel to the fiber direction (Figure 20a) were introduced into the finite element model prior to loading by splitting the central node points on each of the sides into two nodes. The matrix cracks are symmetrically oriented with respect to a diagonal vertical plane, thus maintaining the transverse symmetry of the model.

Considering transverse normal loading first (see Table 4), the transverse normal incremental displacements applied were 0.0051 cm (0.002 in), on the face normal to the 2-axis (see Figure 20). Figure 20 shows the predicted crack propagation at various applied stress levels. The matrix crack normal to the load direction propagated in its initial plane up to the center of the model, and then suddenly changed its direction and propagated at 45° to the loading direction. In subsequent load increments, the crack growth was in the fiber direction. In an even later stage, the other initial matrix crack (parallel to the loading direction) started to propagate in its initial plane, all the way across the model (see Figures 20c and 20d), and then in the fiber direction.

The initiation and growth of microcracks from the initial matrix cracks under transverse shear loading is shown in Figure 21. The incremental displacements on the transverse faces were +0.0051 cm (+0.002 in) and -0.0051 cm (-0.002 in) in the 2- and 3-directions, respectively. As in the case of transverse tension, the initial crack, after running in its plane for some distance, changed its direction by 45° to the transverse plane.

The mixed mode crack growth predicted when the unidirectional composite containing matrix cracks is subjected to either transverse tension or transverse shear is important from another viewpoint also.

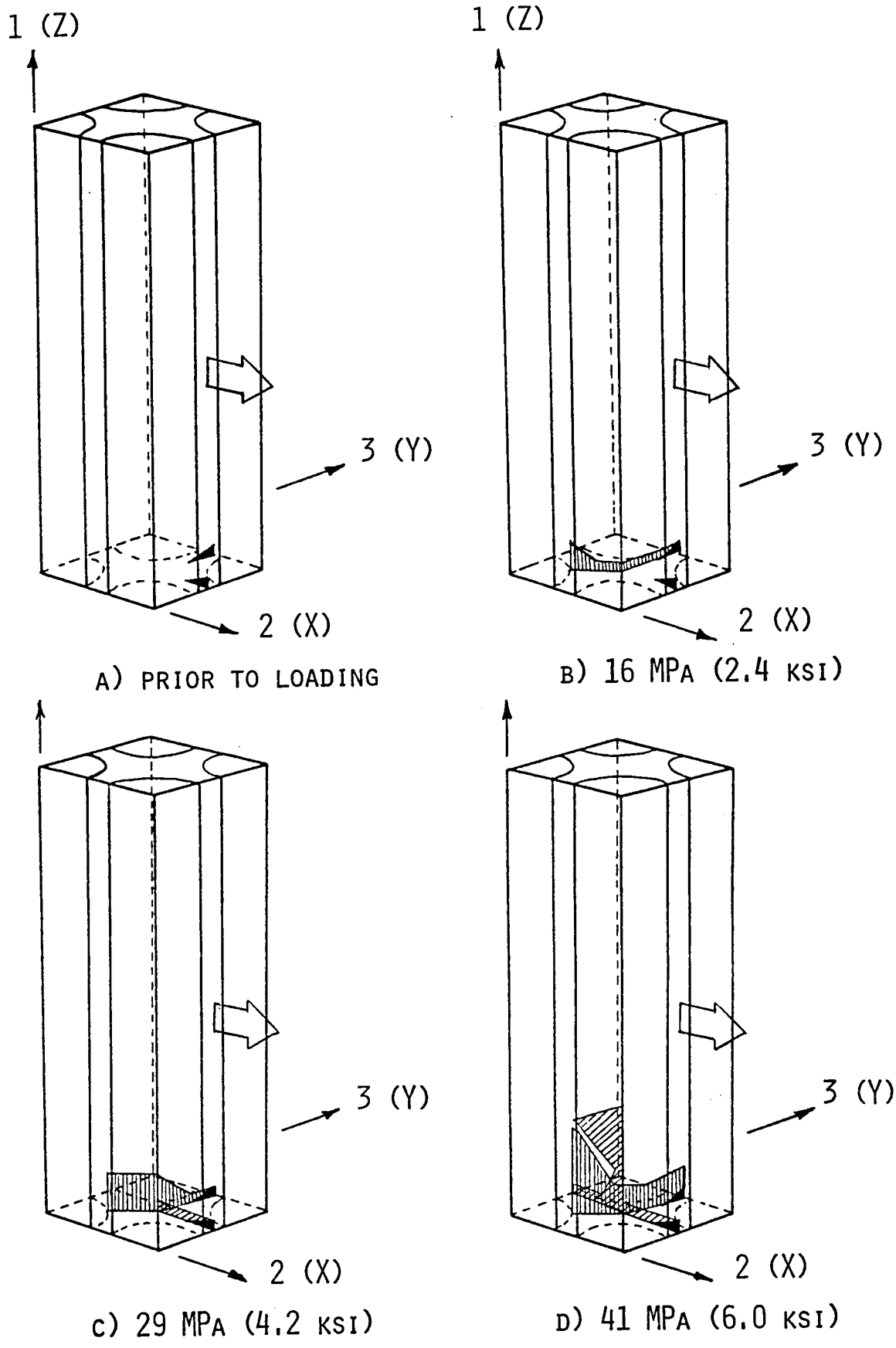

Figure 20. Initiation and Growth of Cracks from Pre-Existing Matrix Cracks as a Function of Transverse Tensile Applied Stress.

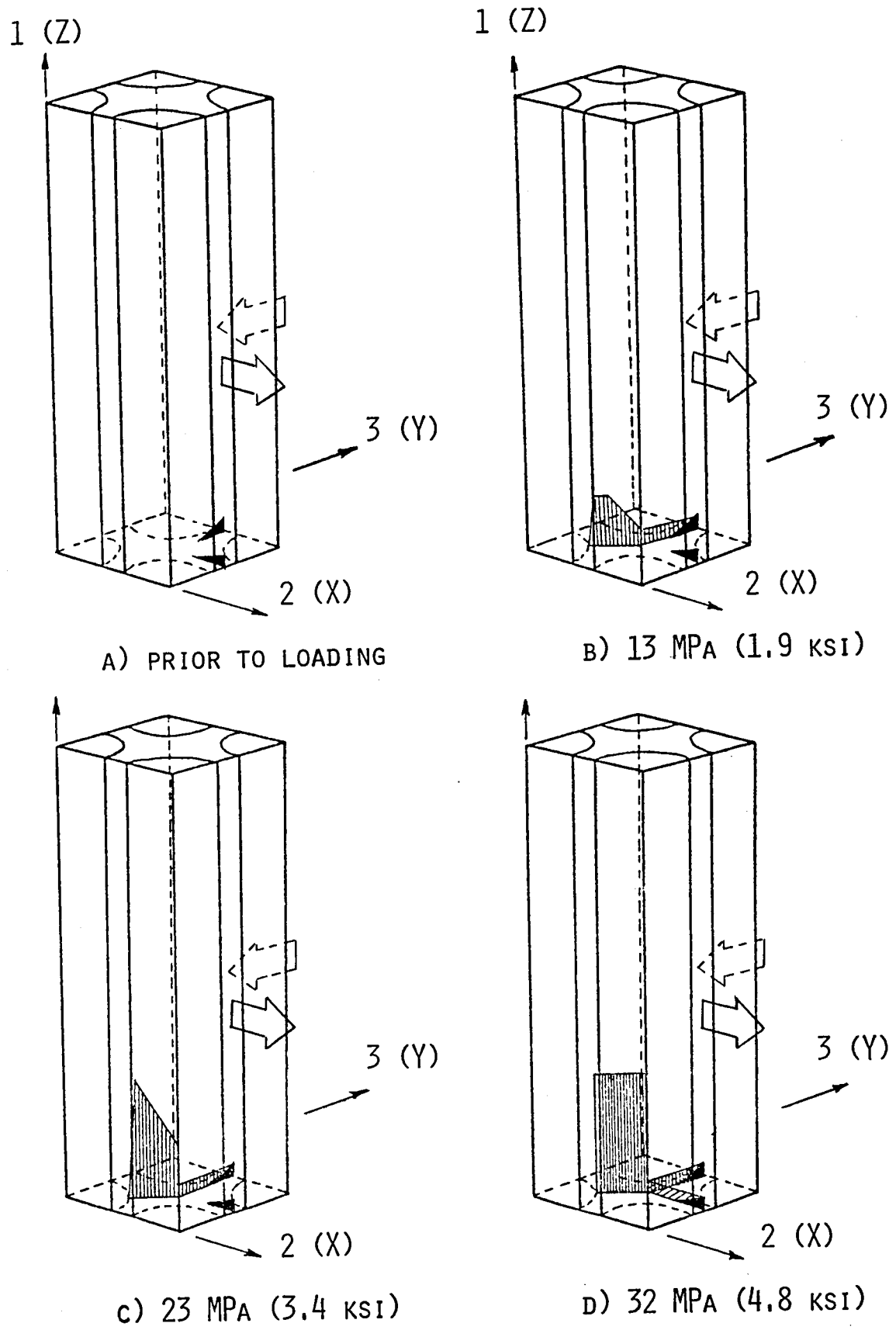

Figure 21. Initiation and Growth of Cracks from Pre-Existing Matrix Cracks as a Function of Transverse Shear Applied Stress.

The crack growth predicted may very well explain the experimentally observed zig-zag path of the delamination. It can be concluded that cohesive matrix cracks in the "resin-rich" zone at the ply interface are influenced by the presence of adjacent fibers, and change their path during propagation As a result, the "fracture toughness" of the composite also increases. This is in agreement with the experimental observation that the fracture toughness of the reinforced resin is higher than that of the neat resin. The transverse tension analysis can be directly correlated with the double-cantilever beam test in which a delamination is introduced between plies.

5.4.3 Fiber-Matrix Debond

In this flaw model, one of the fibers in the finite element model of the repeating cell was partially debonded from the matrix material by introducing double node points at the fiber-matrix interface in the x-y symmetry plane. The model was then subjected to transverse tension and transverse shear loads as in the case of the matrix crack flaw model. The crack growth at various stages of transverse tensile loading is shown in Figure 22. The crack growth pattern for transverse shear loading was similar. Only a part of the initial debond extended in the fiber direction, as shown in Figure 22.

5.5 Critical Energy Release Rates

The microcracks from the three different types of initial microflaws considered grew in a number of small increments. By further refining the finite element grid and reducing the load increment sizes, it should be possible to obtain slow and stable crack growth from microflaws. The fact that additional load increments are required to propagate a crack suggests that there is increasing resistance to crack

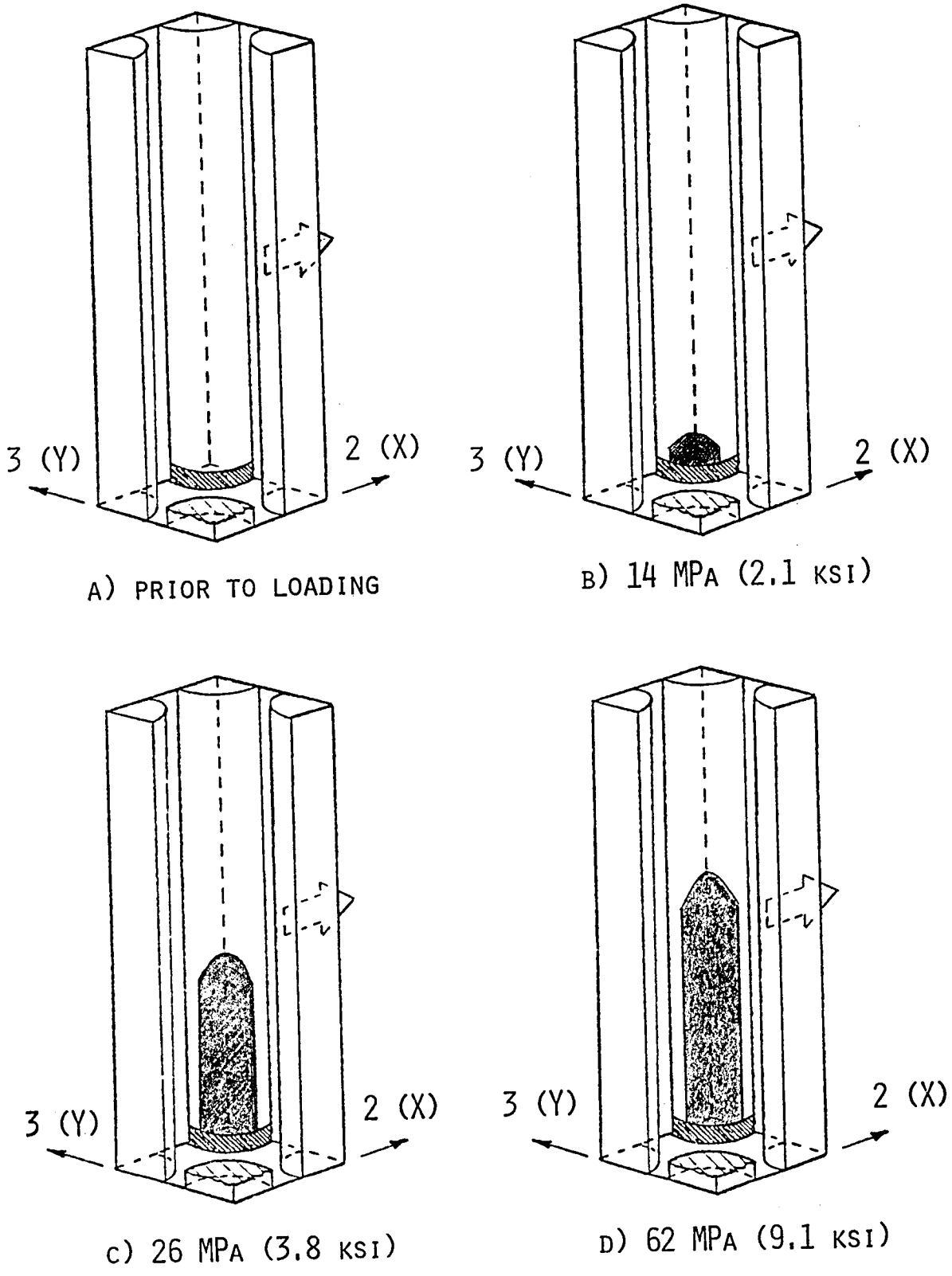

Figure 22. Initiation and Growth of a Crack from an Initial Fiber-Matrix Debond as a Function of Transverse Tensile Applied Stress. (Fiber on Vertical Axis Removed for Viewing Clarity)

growth. This situation is similar to that observed in the case of thin metal plates. The slow and stable crack growth in metals has been explained in terms of R-curves [13,149]. The energy release rate corresponding to the point of crack instability can be interpreted as the critical energy release rate or fracture toughness. However, in the present analysis, the loading increments were not small enough to generate adequate R-curves. Therefore, the energy release rate corresponding to only the first or second increment of crack growth was taken as the critical energy release rate here. The energy release rate was evaluated by dividing the difference between the global strain energy before and after an incremental crack growth by the total area of the incremental crack. The potential energy of the external forces was zero since the crack growth was modeled as occurring under fixed grip conditions. The computed critical energy release rates for the different types of microflaws and loading condition combinations are tabulated in Table 5.

Table 5

Computed Critical Energy Release Rates from the Micromechanics Analysis

Microflaw Type	Critical Energy Release Rate, J/m^2 ($in\text{-}lb/in^2$)			
	G_{C11}	G_{C22}	G_{C13}	G_{C23}
Broken Fibers	434 (2.45)	--	1873 (10.58)	--
Matrix Cracks	--	262 (1.48)	--	273 (1.54)
Fiber-Matrix Debond	--	119 (0.67)	--	350 (1.98)

For use in the macromechanics analysis to be presented in the next section, the lower of the values for a particular load increment was taken as the critical value. The six critical energy release rates actually used in the subsequent macromechanics analysis are given in Table 6.

Table 6

Computed Values of Critical Energy Release Rates Selected for Use in the Macromechanics Analysis

Parameter	(J/m^2)	$(in\text{-}lb/in^2)$
G_{C11}	434	2.45
G_{C22}	119	0.67
G_{C33}	119	0.67
G_{C23}	273	1.54
G_{C13}	1873	10.58
G_{C12}	1873	10.58

SECTION 6

MACROMECHANICS ANALYSIS

6.1 Notched Composite Laminates

The numerical results of a macromechanics analysis of the initiation and growth of a delamination crack near a through-the-thickness notch crack in a composite laminate is presented in this section. In the present macromechanics analysis, the individual laminae are treated as homogeneous anisotropic continua. A central notched and a single-edge notched $[\pm 45/0]_s$ graphite/epoxy laminate were considered. It was assumed that delamination involved only matrix-dominated fracture, and that the crack surface is parallel to the ply interface.

The matrix-dominated transverse normal, transverse shear and longitudinal shear properties of the lamina used in the present analysis are shown in Figure 23. These properties were generated using a two-dimensional finite element micromechanics analysis [147]. The nonlinear stress-strain response of the ply material indicates the need to use the elastoplastic stress analysis and fracture criterion for crack growth developed in the present analysis.

6.2 Finite Element Model

The finite element grid used to model the central and single-edge notched $[\pm 45/0]_s$ graphite/epoxy laminate is shown in Figure 24. The laminates were assumed to be 15.2 cm (6 in) in length, 10.2 cm (4 in) in width, and to have a notch length a to plate width b ratio of 0.2 in both cases. Twenty-node, quadratic, isoparametric elements were used. Each individual ply was modeled by a separate layer of elements. The model shown previously in Figure 10 is a single-layer model. Even though

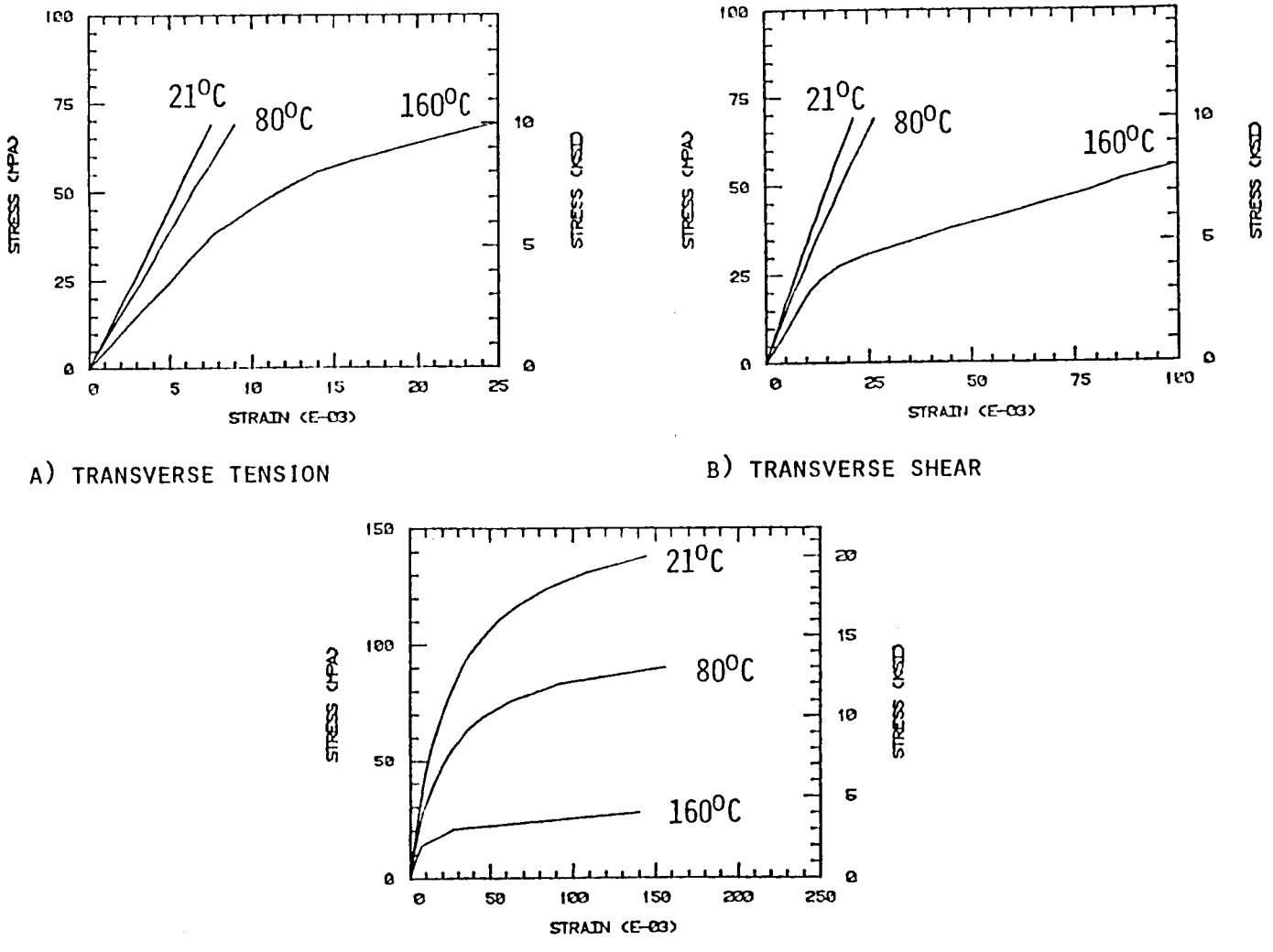

Figure 23. Matrix-Dominated Properties of a Unidirectional Hercules AS4/3501-6 Graphite/Epoxy Composite as Predicted by a Finite Element Micromechanics Analysis [147] (fiber volume = 60 percent).

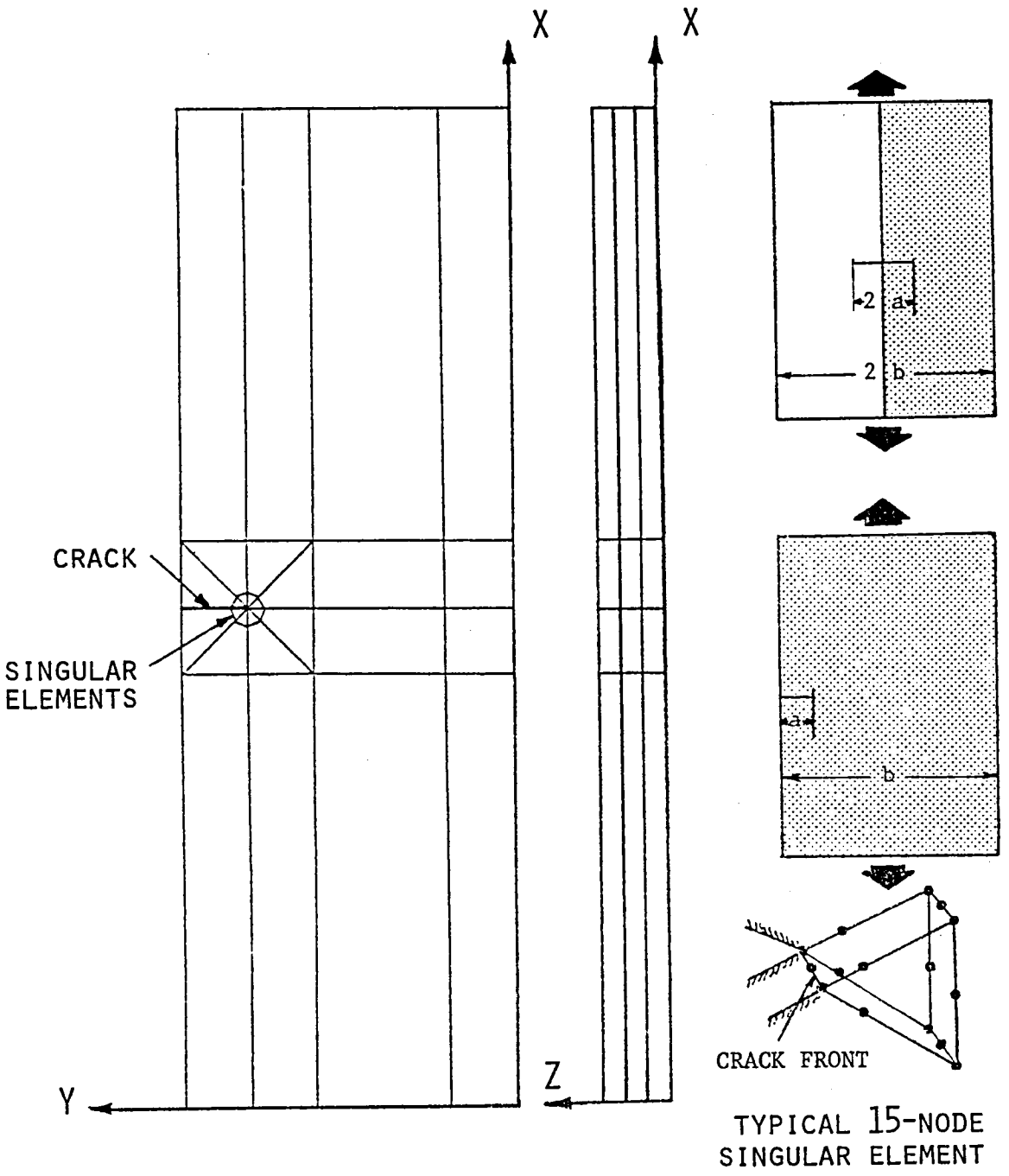

Figure 24. Finite Element Grid Used to Model the Central and Single-Edge Notched $[\pm 45/0]_s$ Graphite/Epoxy Laminate, a/b = 0.2.

the assumed material symmetry relative to the x-z plane does not actually exist in the case of a center notched laminate, it was assumed here that this does not affect the delamination crack growth in the one-half laminate modeled. In order to reduce the total number of 20-node elements required to accurately represent the stress state near the crack tip, the 20-node isoparametric elements were collapsed into 15-node, quarter-point, triangular, wedge-like, singular elements in this region [142]. These elements, if the collapsed nodes at the crack tip are not constrained to have the same displacements, represent a perfectly plastic (1/r type) singularity [150].

6.3 Crack Initiation and Propagation

The finite element model of the central notched and single-edge notched $[\pm 45/0]_s$ graphite/epoxy laminate was subjected to inplane uniaxial tensile stresses, applied in small increments by prescribing boundary displacements. At each increment of loading, the local elastic energy release rates were calculated at all node points lying near the crack tip in the +45/-45 and -45/0 interfaces. If the computed energy release rate at any of these nodes was equal to the critical energy release rate, the node was split into two nodes and the reaction forces were applied to the split nodes. Holding the boundary node displacements constant, the system of equations was solved again to check for further crack extension due to the reaction forces at the split nodes. Experimentally measured [100] fracture toughness values for a Hercules AS4/3501-6 graphite/epoxy composite, viz, G_{IC} = 130 J/m^2 and G_{IIC} = G_{IIIC} = 230 J/m^2, were used as critical energy release rates in the present analysis.

Figures 25 and 26 show the growth of the plastic zone near the crack tip between +45/-45 and -45/0 interfaces, for the central notched laminate during different stages of loading. Figures 27 and 28 show the growth of plastic yielding for the single-edge notched laminate. In both the central notched and single-edge notched laminates, the plastic yielding was confined to a very small region near the through-the-thickness crack tip.

Figures 25 through 28 presented the extent of interface yielding. The onset and growth of actual delamination cracks between the +45/-45 and -45/0 interfaces for the case of the central notched laminate are shown in Figures 29 and 30. The applied stress increments were kept small enough to cause only one increment of crack growth in an increment of applied stress. A particular mode (Mode I, II or III) was predominant in each incremental crack advance; this is indicated in Figures 29 and 30 by different shadings to represent the crack growth. The delamination crack growths in the case of a single-edge notched laminate are shown in Figures 31 and 32. In both the central and single-edge notched laminates, the delamination was more extensive between -45/0 interfaces than between +45/-45 interfaces.

6.4 Crack Growth Resistance and Fracture Toughness

In all cases, for loadings beyond the maximum applied stress levels shown in Figures 29 through 32, the analysis predicted a very large area of delamination. This was undoubtedly due to the very coarse finite element grid used in the present analysis. With a finer grid, the crack growth would likely continue further in the same slow and stable manner as observed during the initial phase in the present analysis. One of the explanations given for such stable crack growth behavior is that the

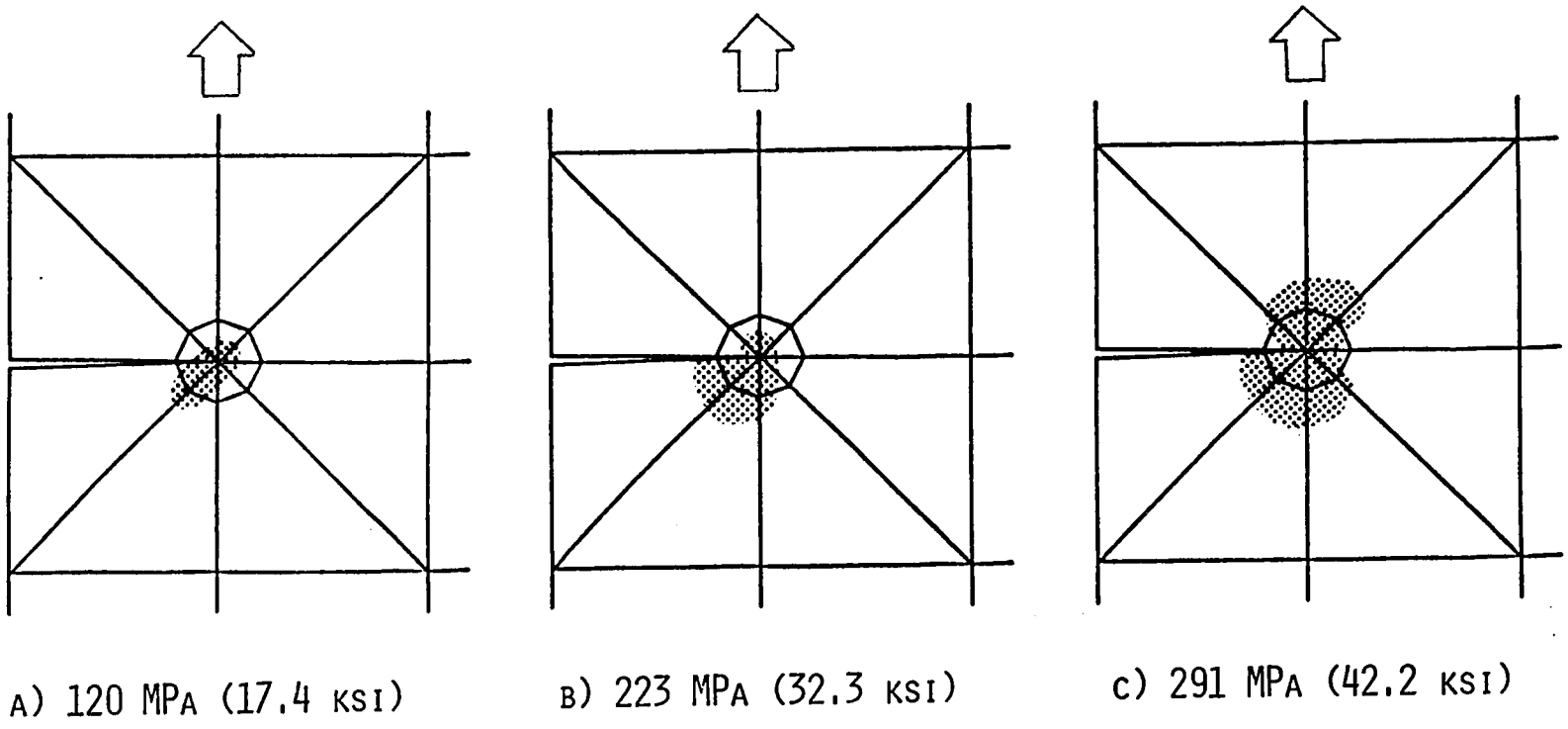

Figure 25. Material Yielding at Increasing Levels of Applied Axial Tensile Stress Near the Crack Tip at the +45/-45 Interface in a Central Notched $[\pm 45/0]_s$ Graphite/Epoxy Laminate.

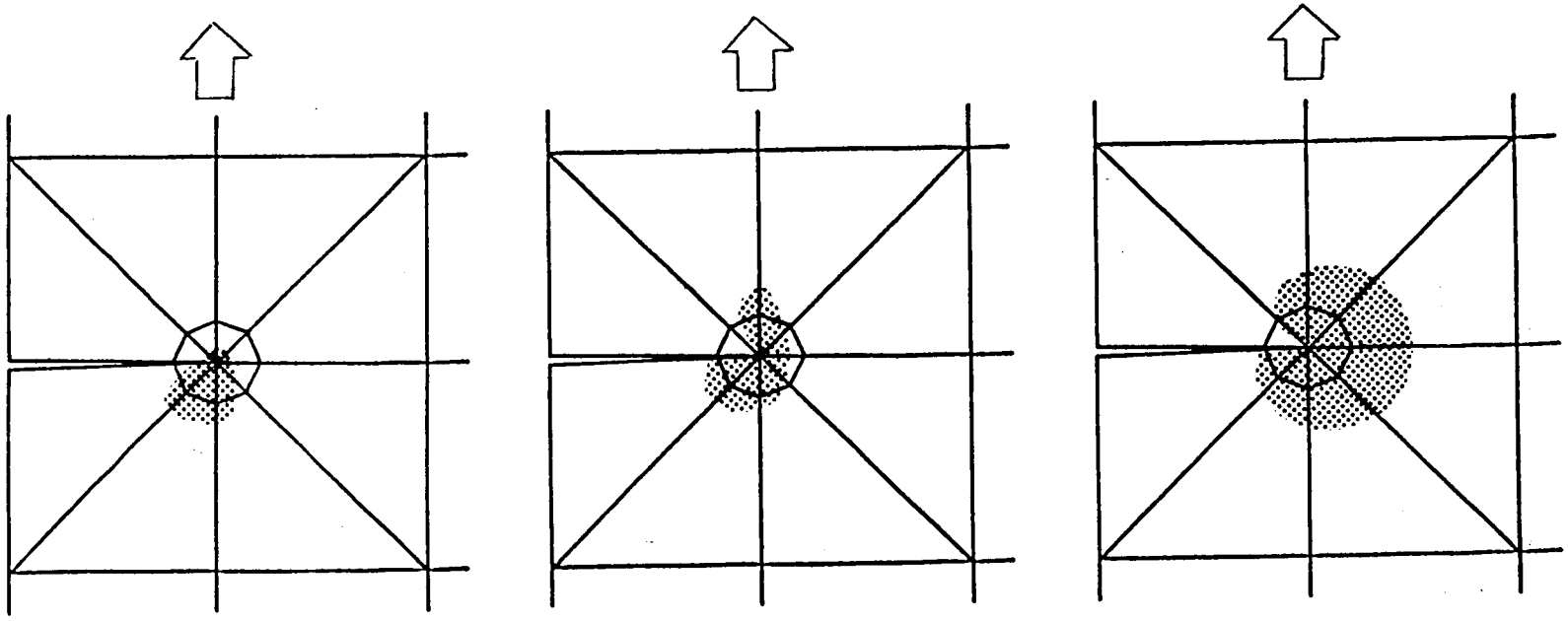

Figure 26. Material Yielding at Increasing Levels of Applied Axial Tensile Stress Near the Crack Tip at the -45/0 Interface in a Central Notched $[\pm 45/0]_s$ Graphite/Epoxy Laminate.

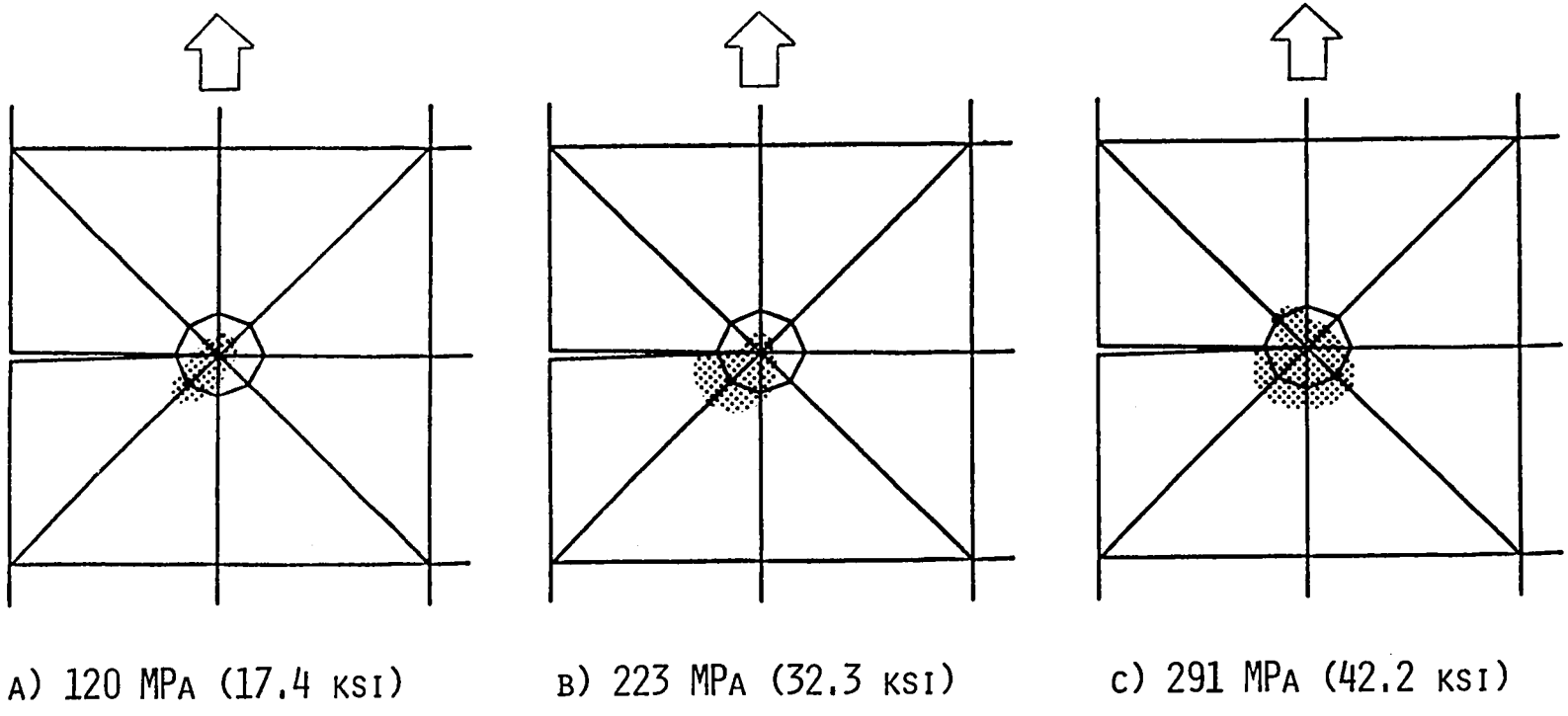

Figure 27. Material Yielding at Increasing Levels of Applied Axial Tensile Stress Near the Crack Tip at the +45/-45 Interface in a Single-Edge Notched $[\pm 45/0]_s$ Graphite/Epoxy Laminate.

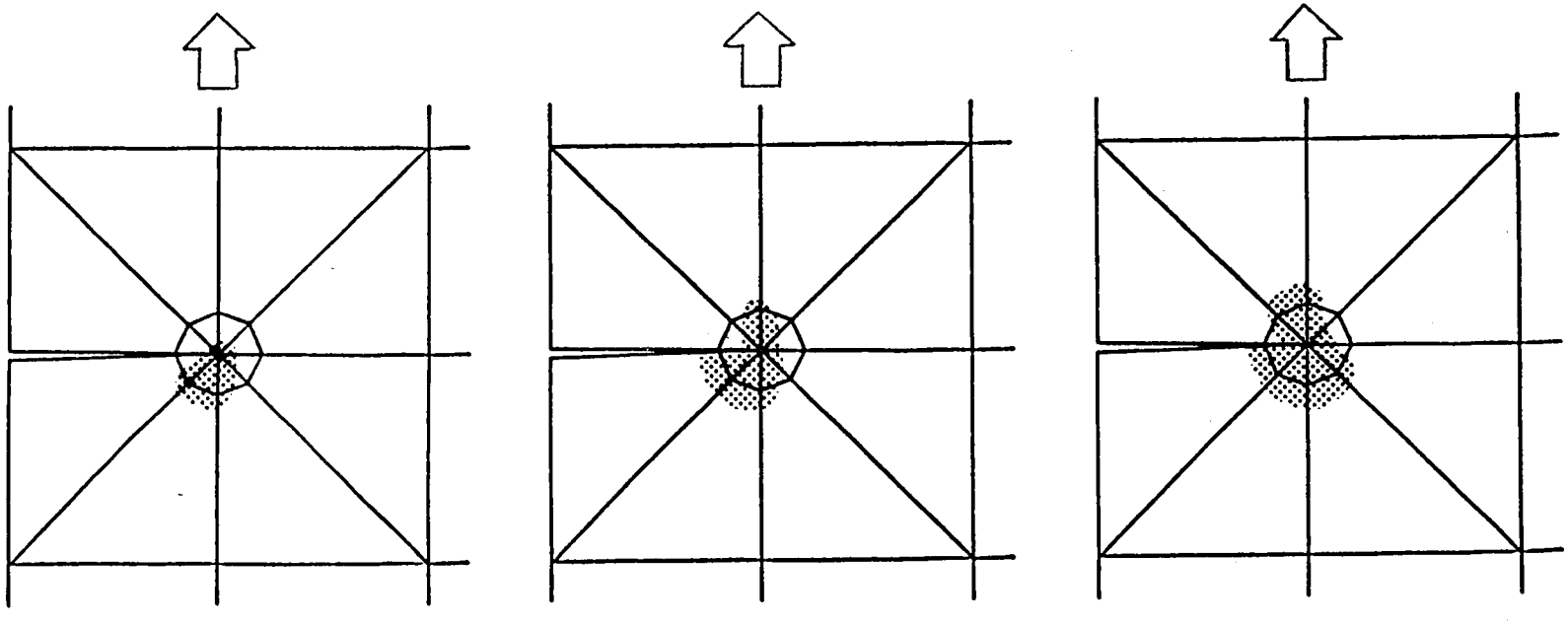

Figure 28. Material Yielding at Increasing Levels of Applied Axial Tensile Stress Near the Crack Tip at the -45/0 Interface in a Single-Edge Notched $[\pm 45/0]_s$ Graphite/Epoxy Laminate.

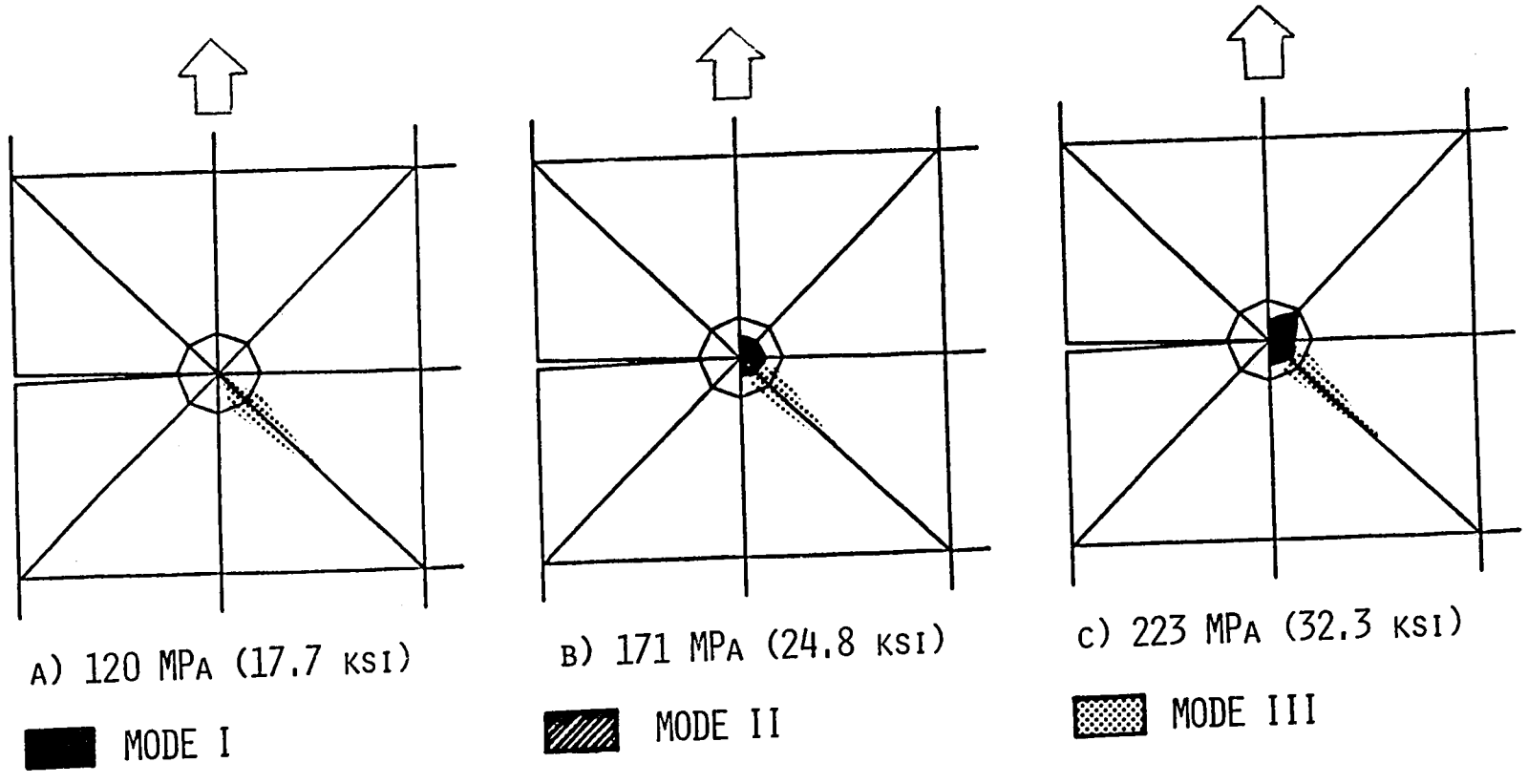

Figure 29. Delamination Growth Near the Crack Tip at the +45/-45 Interface in a Central Notched $[\pm 45/0]_s$ Graphite/Epoxy Laminate at Increasing Levels of Applied Axial Tensile Stress.

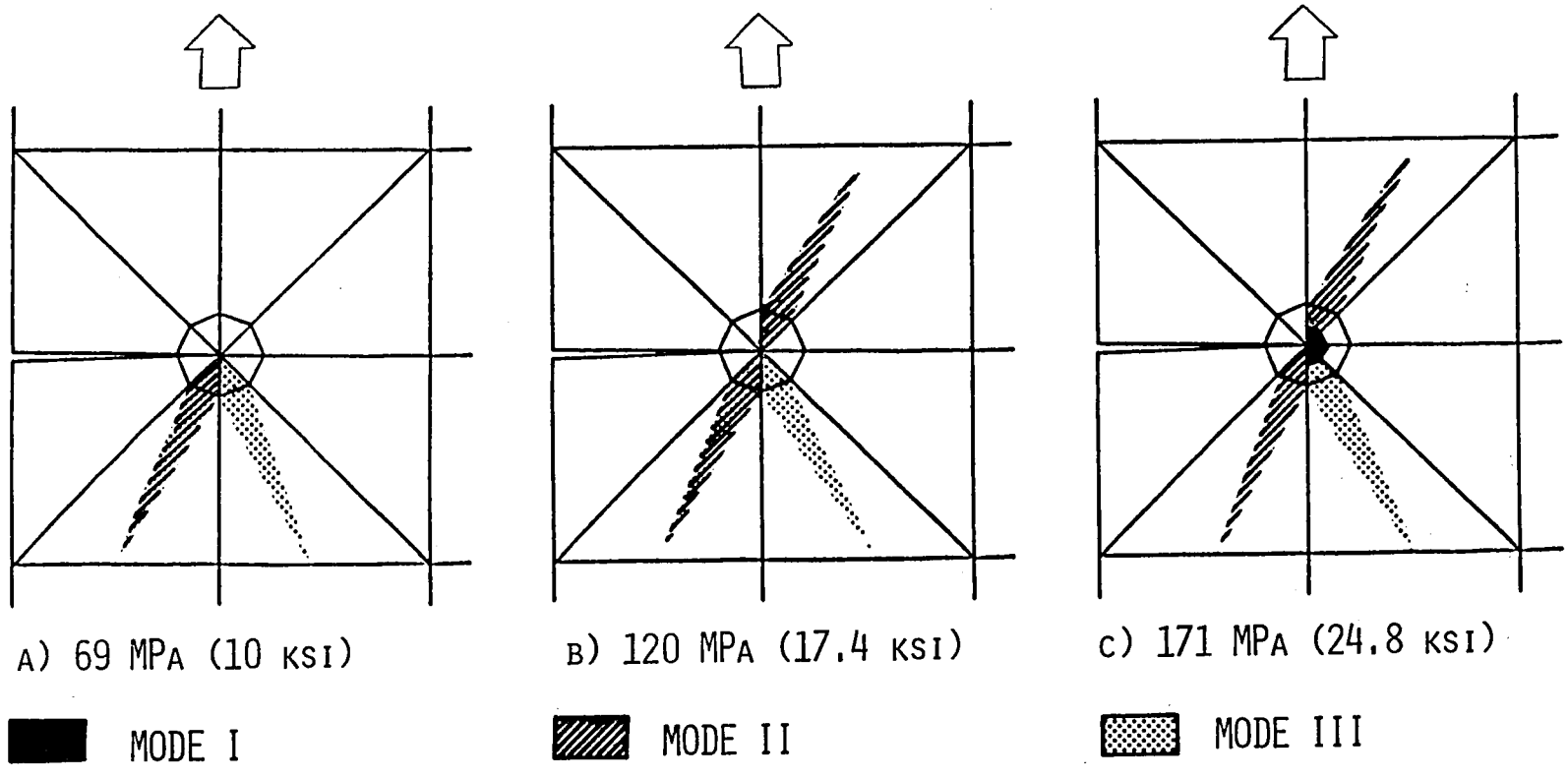

Figure 30. Delamination Growth Near the Crack Tip at the -45/0 Interface in a Central Notched $[\pm 45/0]_s$ Graphite/Epoxy Laminate at Increasing Levels of Applied Axial Tensile Stress.

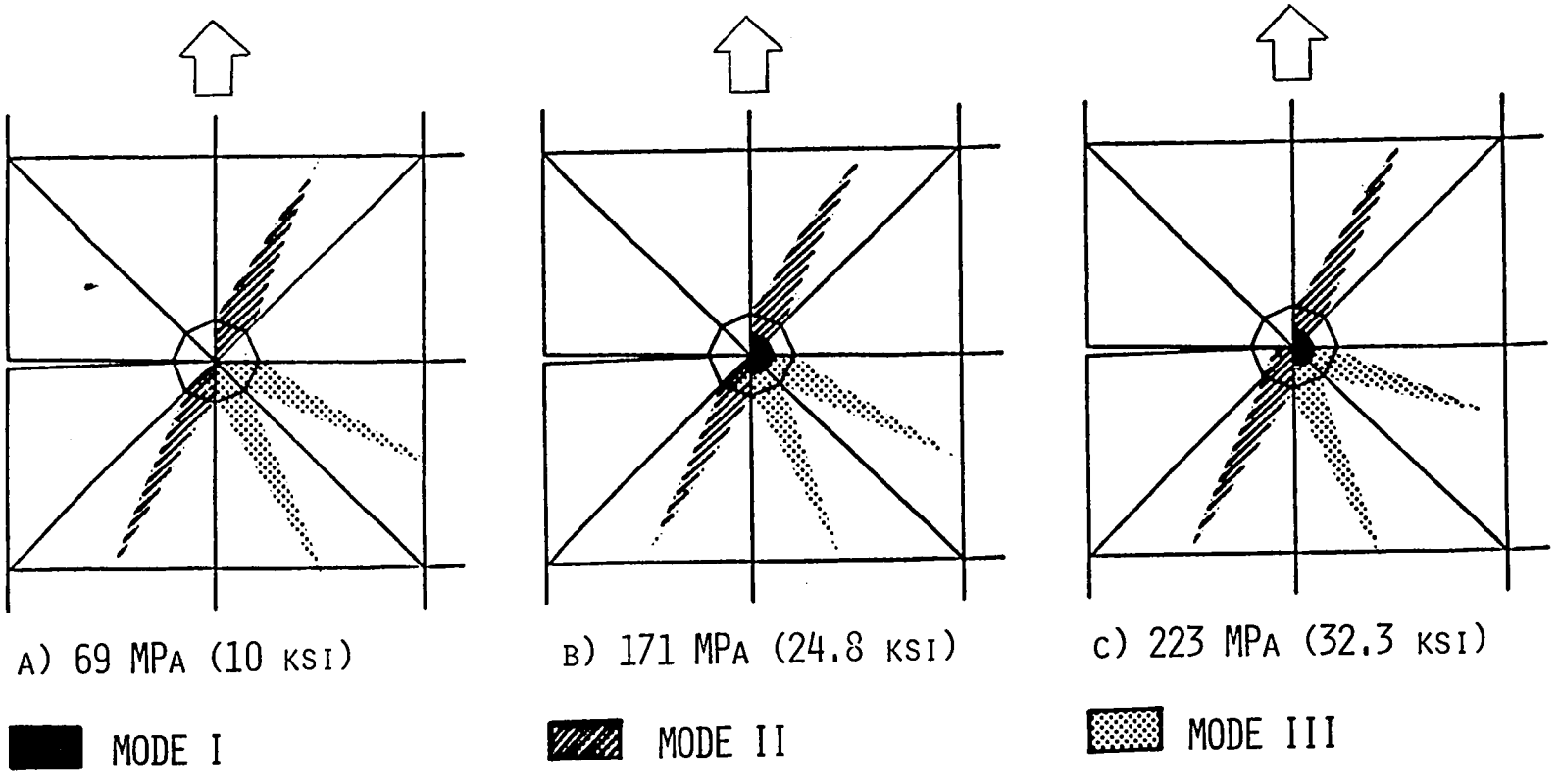

Figure 31. Delamination Growth Near the Crack Tip at the -45/0 Interface in a Central Notched $[\pm 45/0]_s$ Graphite/Epoxy Laminate at Increasing Levels of Applied Axial Tensile Stress.

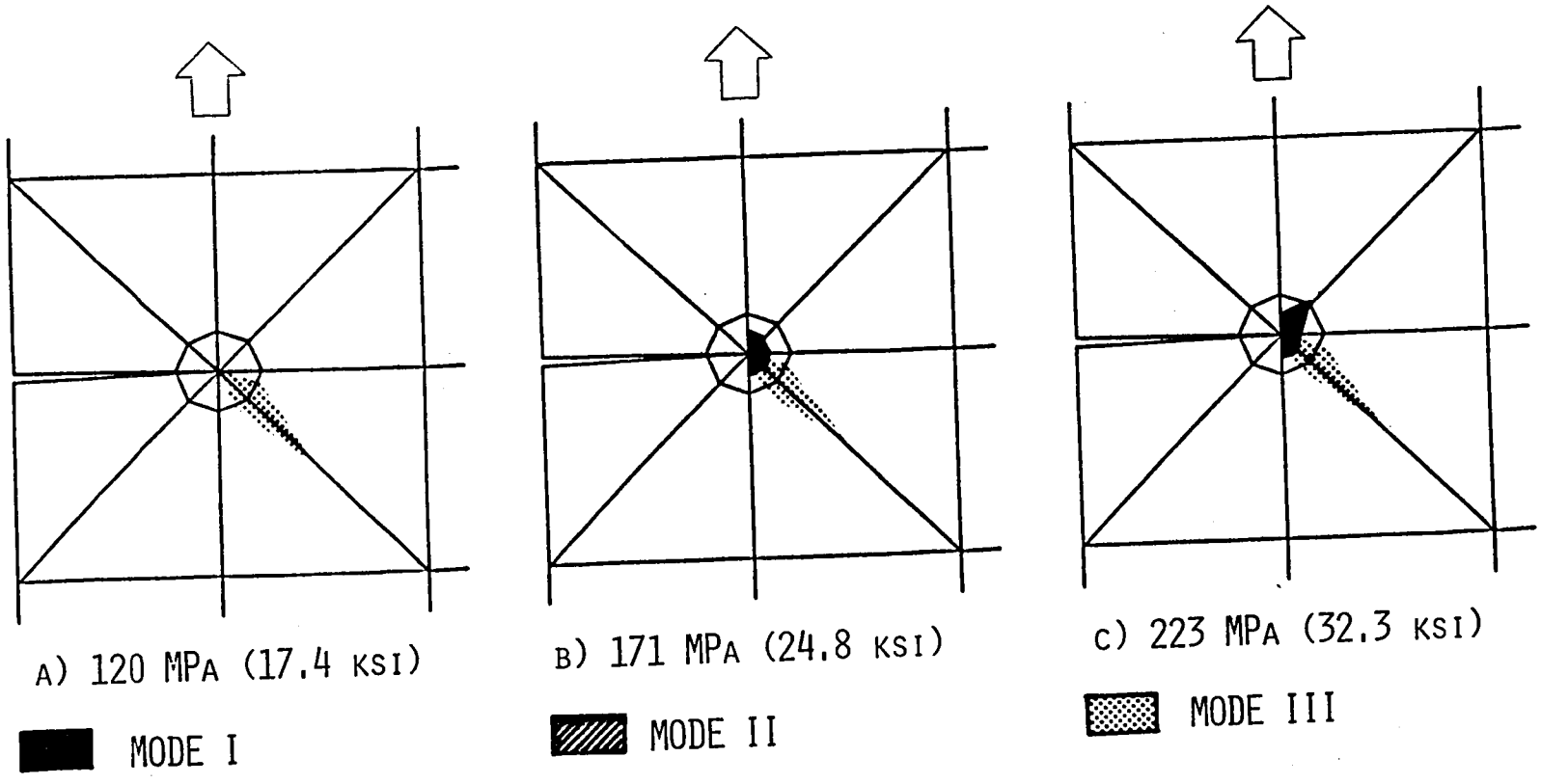

Figure 32. Delamination Growth Near the Crack Tip at the +45/-45 Interface in a Single-Edge Notched $[\pm 45/0]_s$ Graphite/Epoxy Laminate at Increasing Levels of Applied Axial Tensile Stress.

energy absorption rate continuously increases with increasing plastic zone size in front of the crack tip [95]. In the present analysis, the elastic strain energy release rate at the next node point attains the critical value only after sufficient material yielding. The delamination crack growth observed in the present analysis can be characterized by R-curves [150,151], and a point of instability can thus be established. The energy release rate corresponding to the onset of unstable crack growth is then defined as the delamination fracture toughness of the particular notched composite. Owing to the coarseness of the present finite element grid, crack growth beyond the singular crack tip elements is not considered accurate. Nevertheless, for general information, the energy release rates corresponding to the onset of the large delaminations observed in the present model are given in Table 7. It should be noted that in the present analysis, only delamination crack growth was allowed; all other possible modes of crack growth, e.g., transverse intralaminar cracking, were completely suppressed.

Table 7

Critical Energy Release Rates Predicted During Delamination Crack Growth in Notched $[\pm 45/0]_S$ Graphite/Epoxy Composite Laminates

Notch Geometry	Critical Energy Release Rate (J/m^2)	(lb/in)
Central Notch	515	2.92
Single-Edge Notch	511	2.89

SECTION 7

INTEGRATED ANALYSIS

The ability of the integrated micromechanical and macromechanical fracture criterion (IMMFC) and the crack propagation scheme developed in the present analysis to predict the onset and growth of cracks in general multilayered composite laminates will be demonstrated in this section by means of an example problem. A single-edge notched $[\pm 45/0]_s$ graphite/epoxy laminate is assumed to be subjected to inplane tensile stress normal to the notch (as shown previously in Figure 24). Individual laminae of the laminate are assumed to contain uniformly distributed microflaws of the same size and density as used in the micromechanics analysis of Section 4. In accordance with the IMMFC, the critical energy release rate values evaluated by a rigorous micromechanics analysis of the unidirectional lamina, as listed previously in Table 6, were used as the criterion for the onset of cracking. These G_c values, which were derived in material coordinates, were transformed here into laminate coordinates for the +45 and -45 plies.

The finite element grid, the layup of the laminate, and the notch dimensions were assumed to be the same as these used for the macromechanics analysis (see Figure 24 of Section 6).

7.1 Crack Propagation

The incremental inplane tensile stress was applied by prescribing uniform displacements to all appropriate boundary node points. Displacements of 0.00127 cm (0.0005 in) and 0.00254 cm (0.001 in) were applied in the first two increments, respectively, followed by increments of 0.00762 cm (0.003 in) in subsequent increments.

In Figures 33 through 35, perspective views of the total crack/damage growth are shown, at three successively increasing levels of loading. It must be noted that the sizes of the incremental cracks are a direct function of the finite element sizes. In Figure 36, the average laminate stress is plotted against the applied normal tensile strain. The several horizontal steps in this stress-strain curve correspond to the large-scale crack propagation which occurred at higher load levels. Beyond applied strains of 6.75 percent there was no increase in the stress level.

Details of the predicted crack/damage growth between and within individual plies at various applied stress levels are schematically shown in Figures 37 through 39. Due to the complex nature of the predicted crack growth, results are shown individually between each ply interface, and also on the top surface. It can be seen that, in addition to the self-similar growth of the original crack, a number of through-the-thickness transverse cracks running parallel to the fibers are initiated during the initial stages of loading. The delamination mode becomes predominant at the later stages of loading. In the present analysis, only node points in a narrow band on either side of the original crack were considered for possible cracking.

No experimental results were available in the literature for the specific layup sequence and laminate geometry used in the present example problem. However, the predicted strength and crack propagation extent are in very good agreement with general experimental observations [151]. This example problem demonstrates that the IMMFC and crack propagation scheme developed in the present analysis are very effective

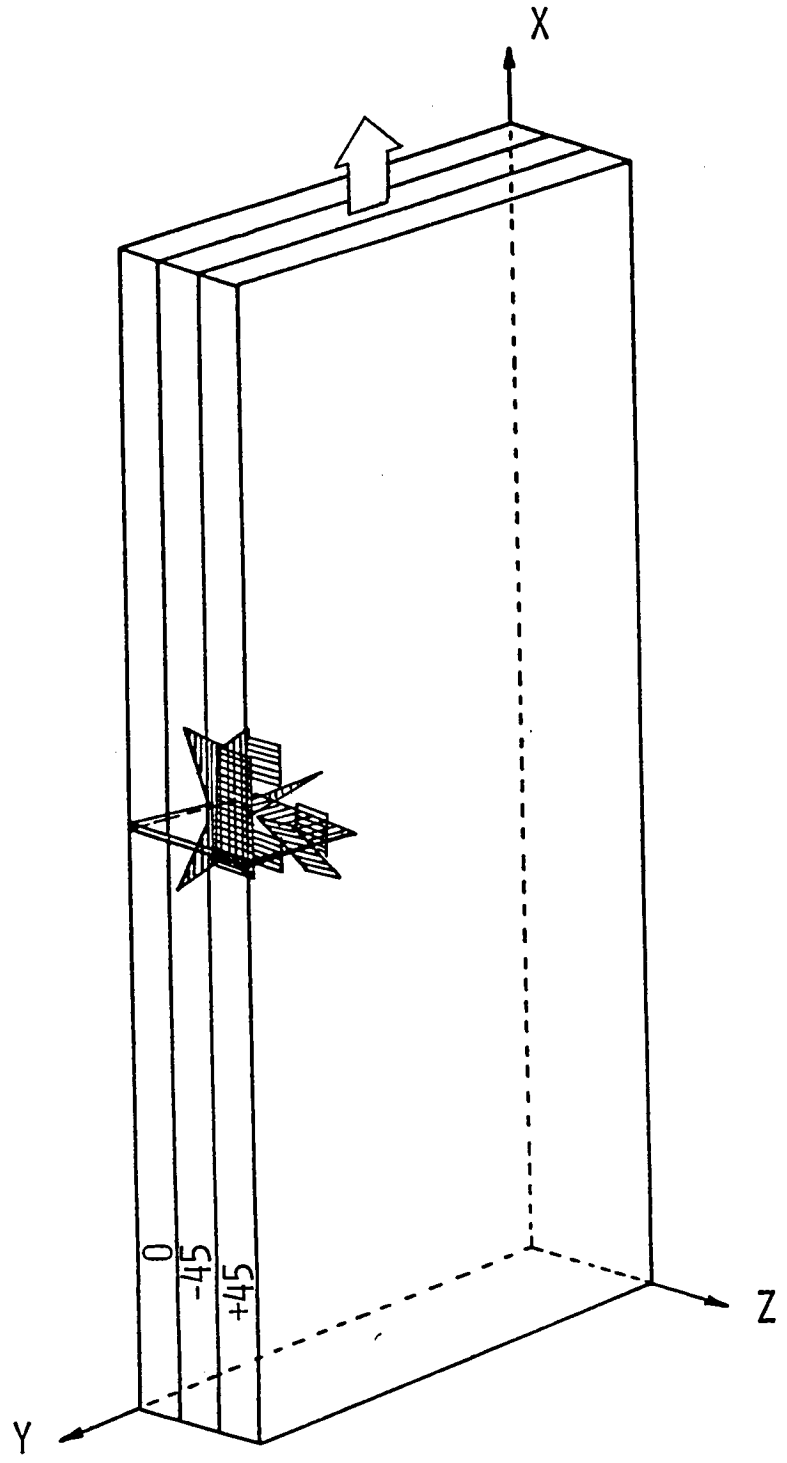

Figure 33. Three-Dimensional View of the Predicted Crack/Delamination Growth in a Single-Edge Notched $[\pm 45/0]_s$ Laminate at an Applied Axial Tensile Stress of 105 MPa (15 ksi).

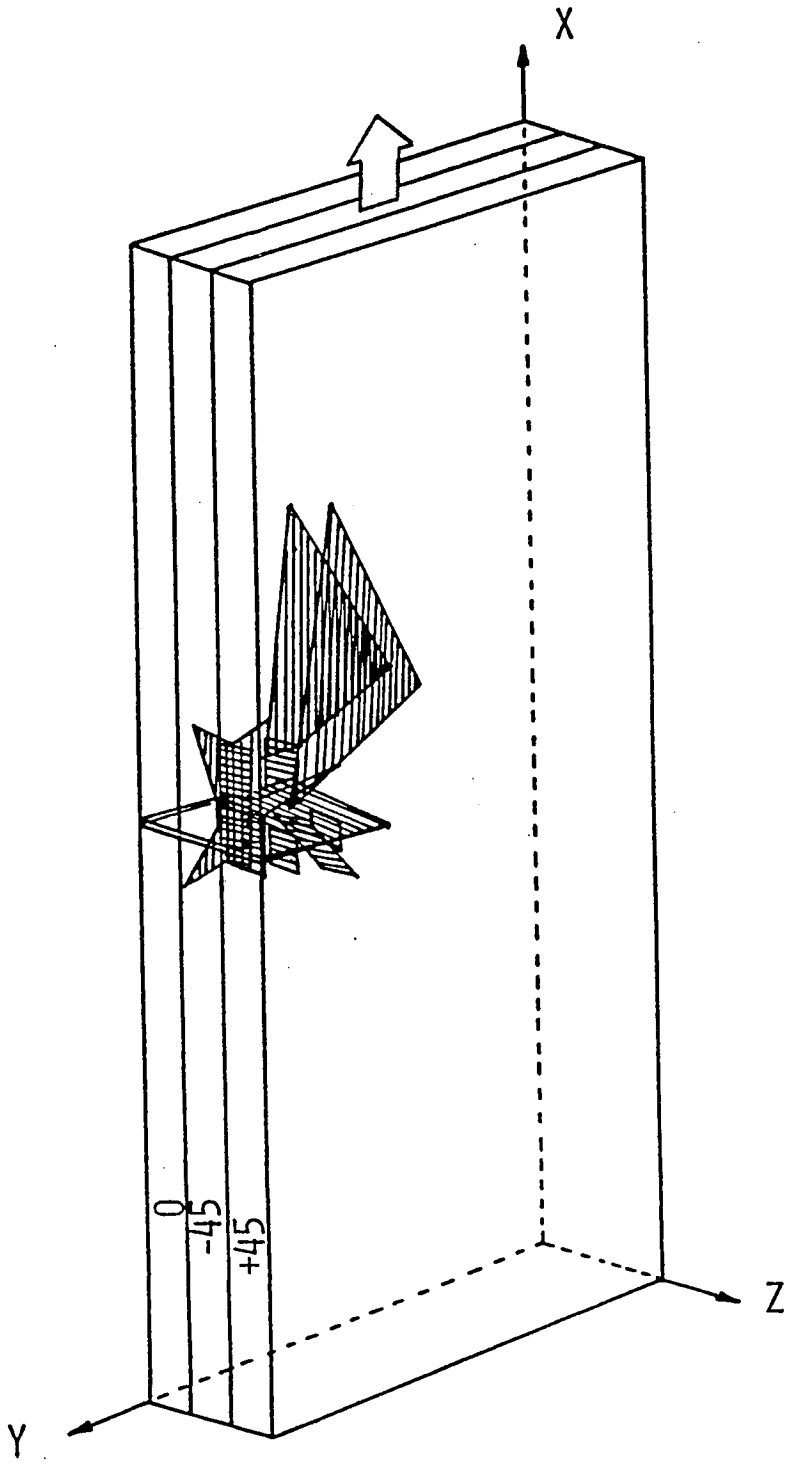

Figure 34. Three-Dimensional View of the Predicted Crack/Delamination Growth in a Single-Edge Notched $[\pm 45/0]_s$ Laminate at an Applied Axial Tensile Stress of 300 MPa (44 ksi).

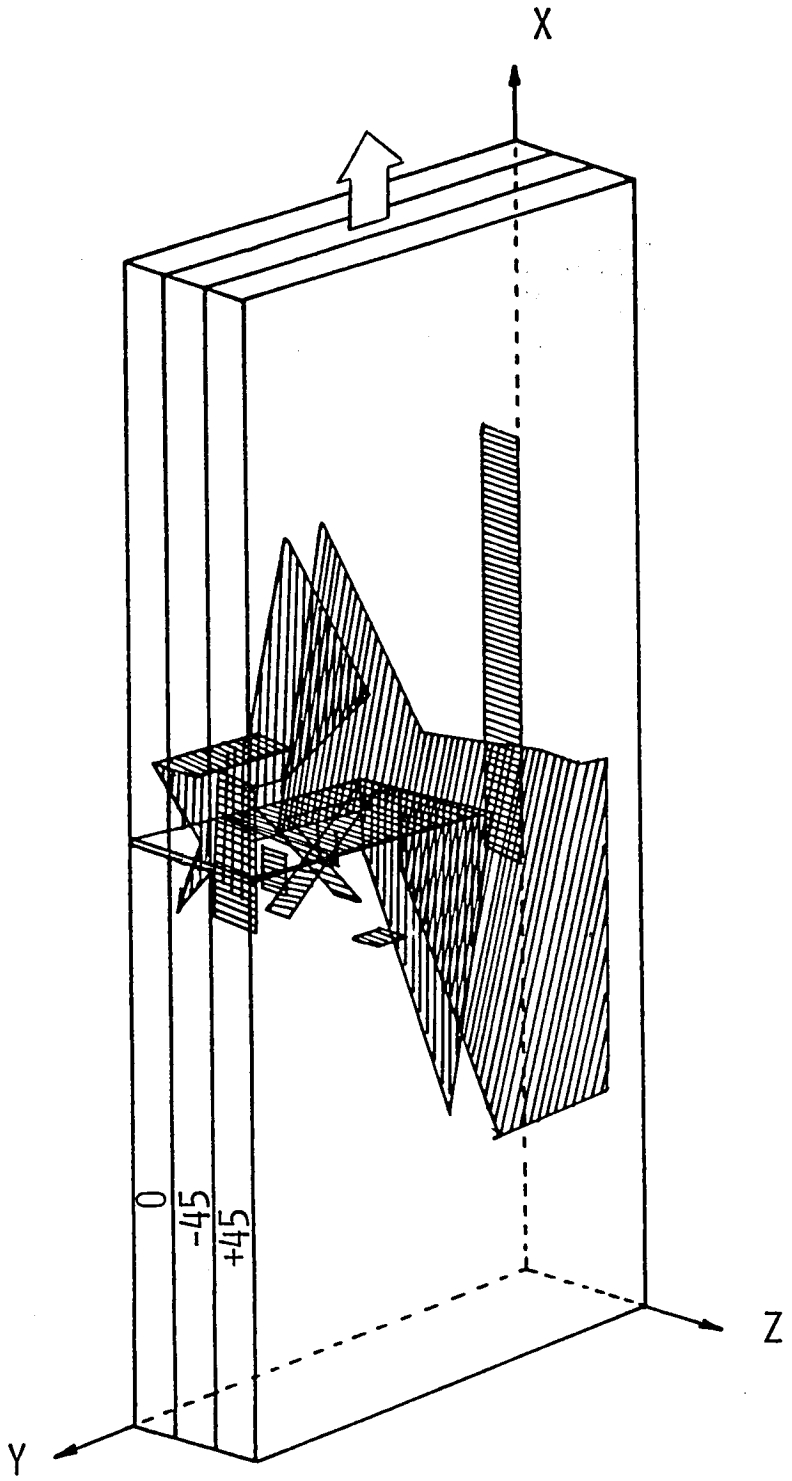

Figure 35. Three-Dimensional View of the Predicted Crack/Delamination Growth in a Single-Edge Notched $[\pm 45/0]_s$ Laminate at an Applied Axial Tensile Stress of 434 MPa (64 ksi).

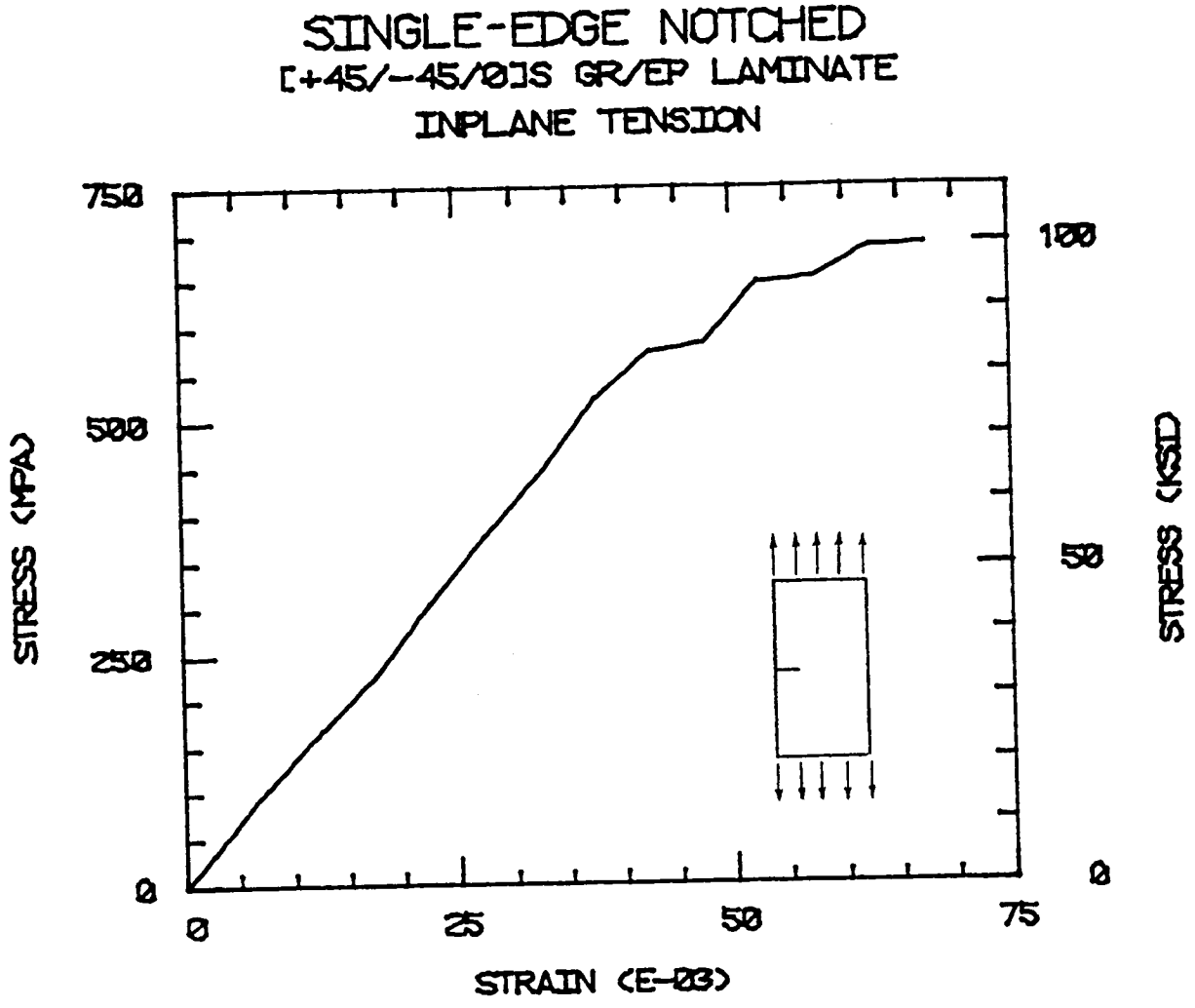

Figure 36. Predicted Stress-Strain Response of a Single-Edge Notched $[\pm 45/0]_s$ Graphite/Epoxy Laminate Subjected to an Axial Tensile Stress.

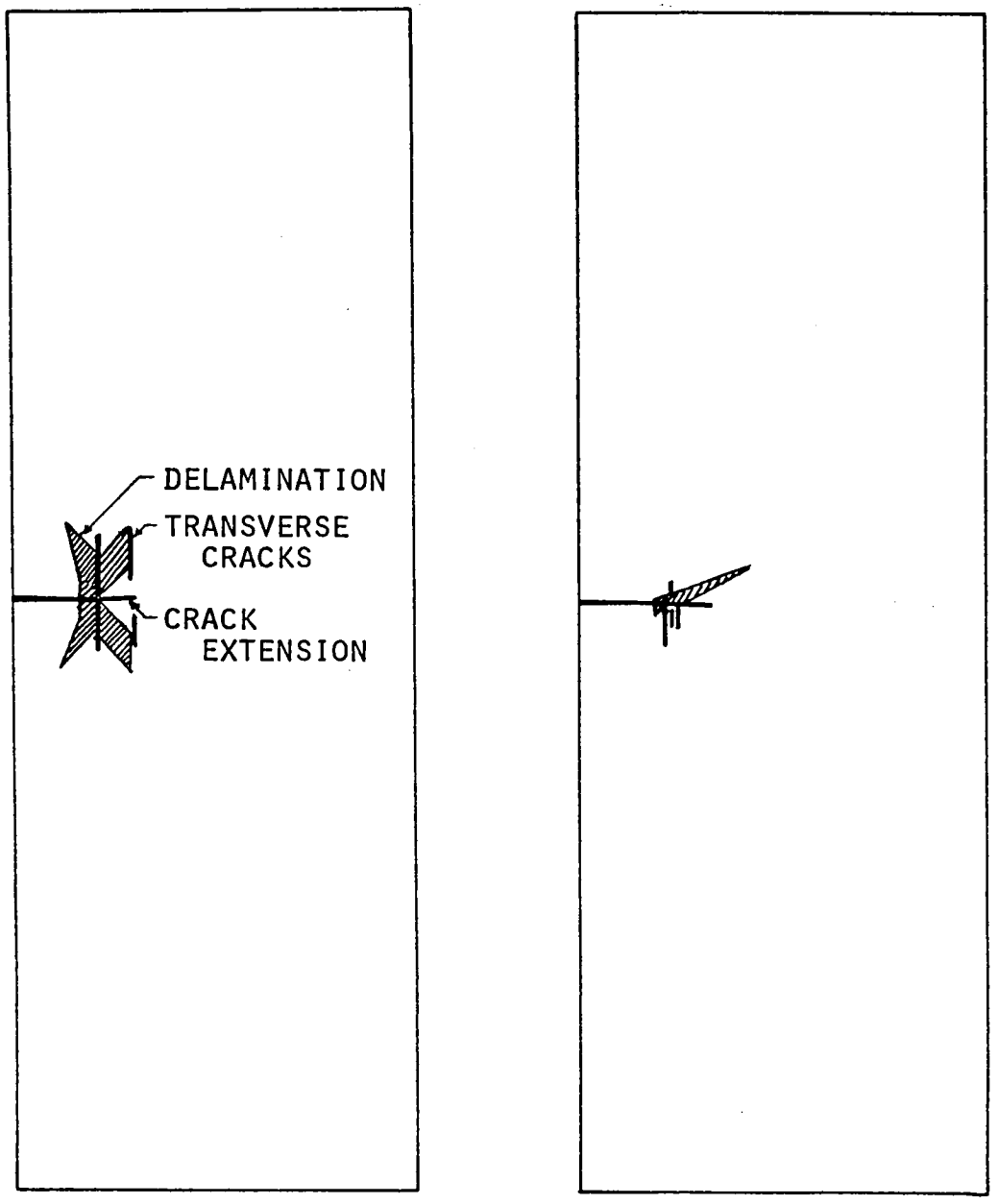

Figure 37. Crack/Delamination Growth in a Single-Edge Notched $[\pm 45/0]_s$ Graphite/Epoxy Laminate at an Applied Axial Tensile Stress of 105 MPa (15.2 ksi).

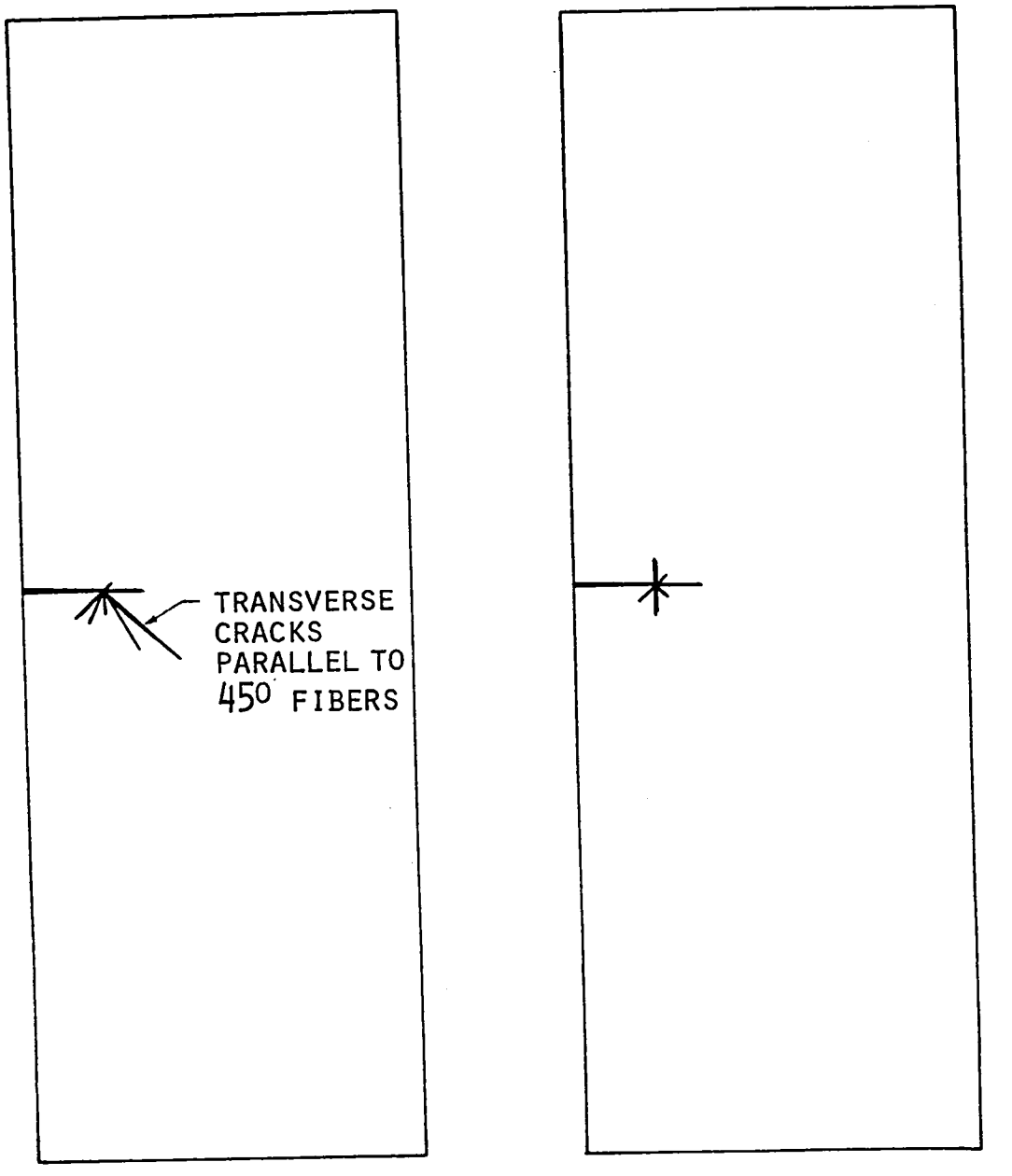

Figure 37 (Continued). Crack/Delamination Growth in a Single-Edge Notched $[\pm 45/0]_s$ Graphite/Epoxy Laminate at an Applied Axial Tensile Stress of 105 MPa (15.2 ksi).

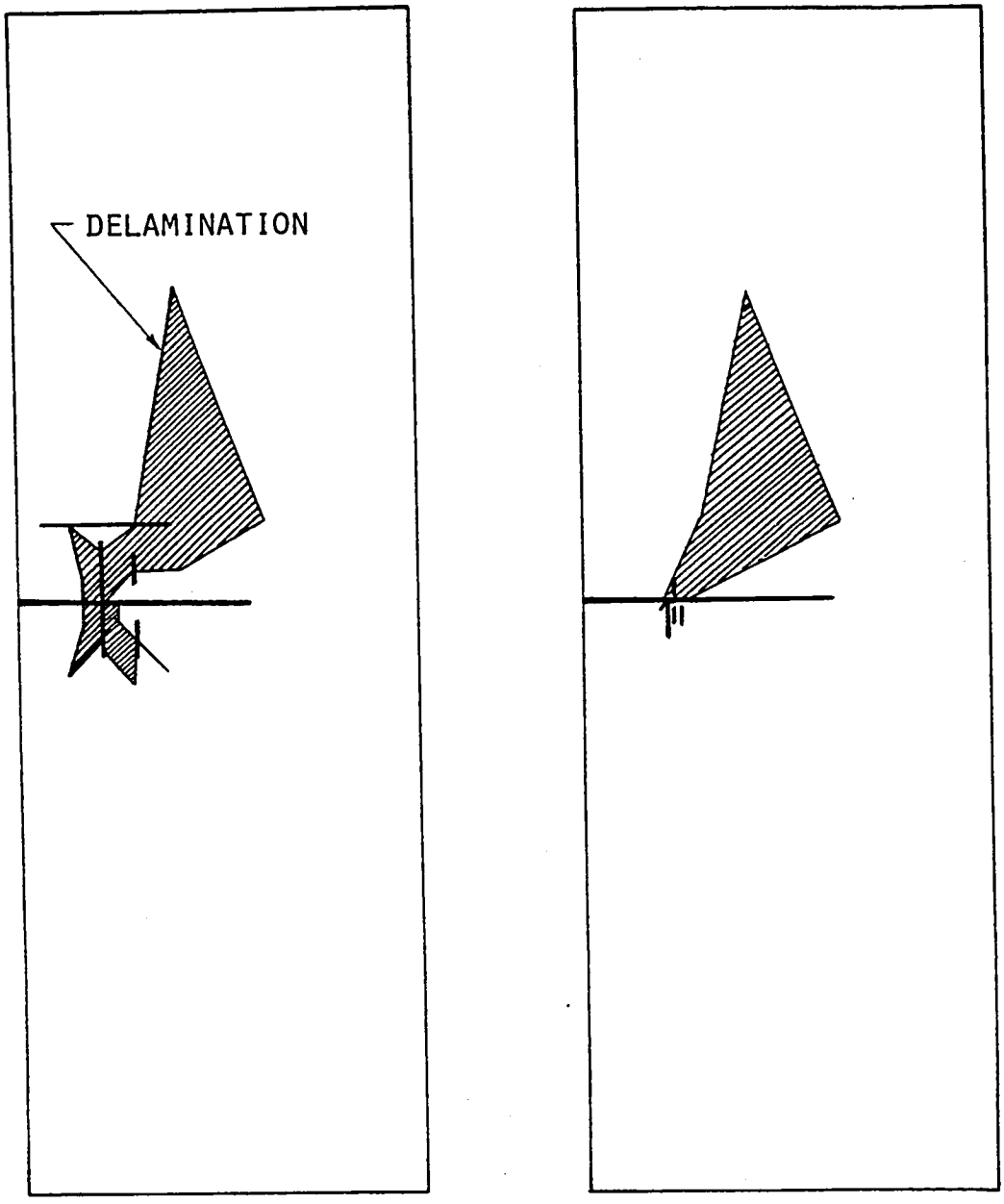

Figure 38. Crack/Delamination Growth in a Single-Edge Notched $[\pm 45/0]_s$ Graphite/Epoxy Laminate at an Applied Axial Tensile Stress of 300 MPa (44 ksi).

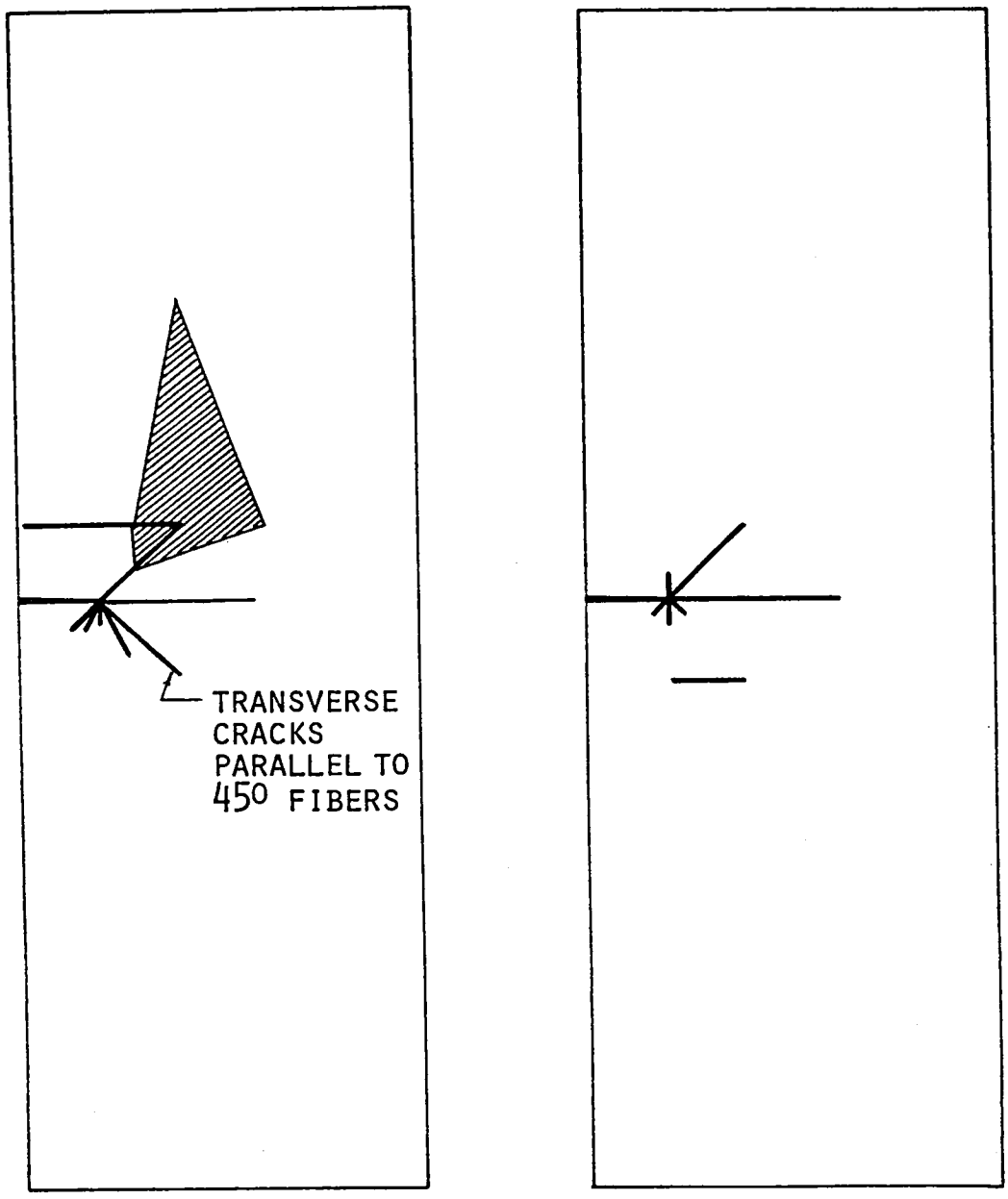

Figure 38 (Continued). Crack/Delamination Growth in a Single-Edge Notched $[\pm 45/0]_s$ Graphite/Epoxy Laminate at an Applied Axial Tensile Stress of 300 MPa (44 ksi).

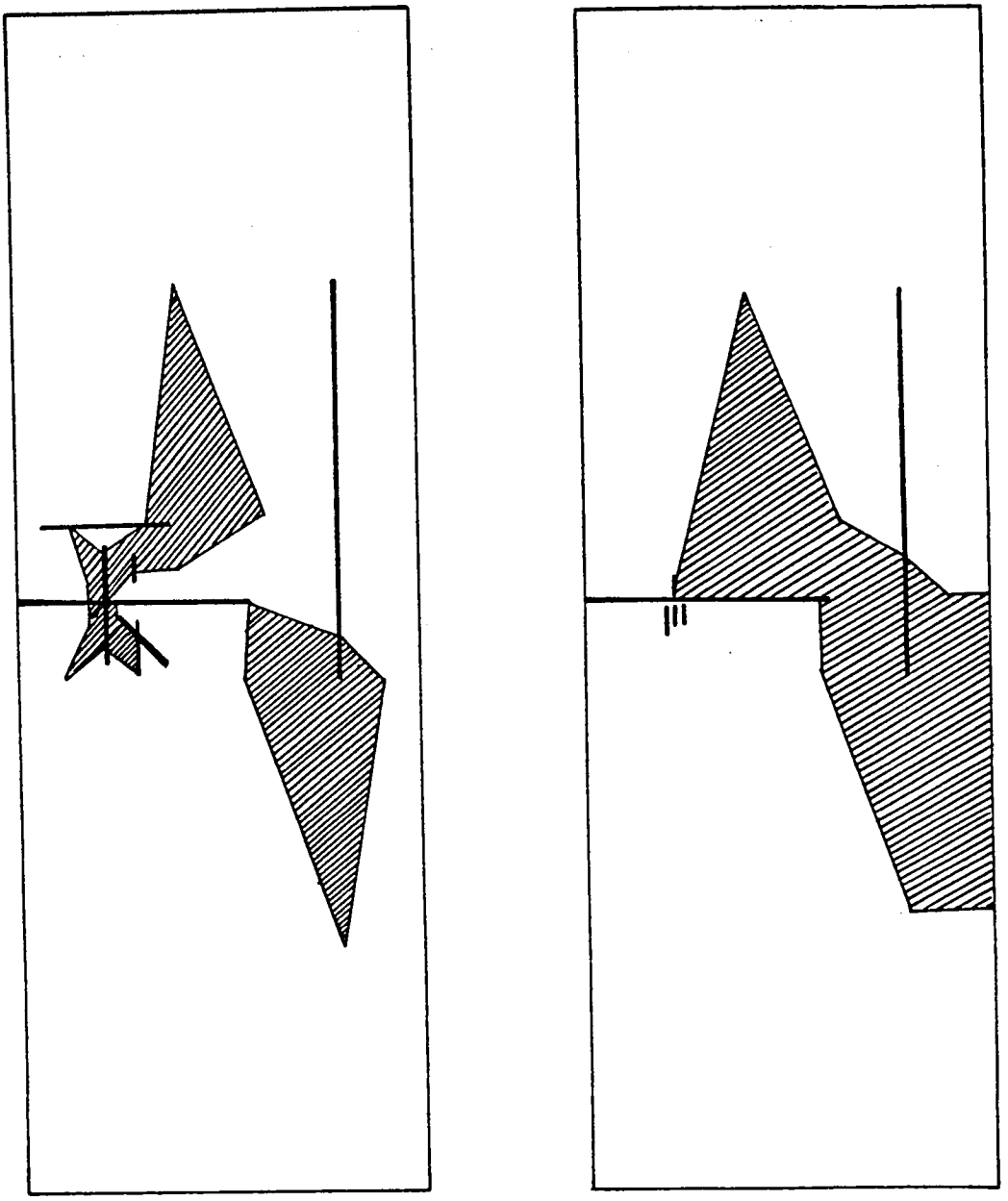

Figure 39. Crack/Delaminatino Growth in a Single-Edge Notched $[\pm 45/0]_s$ Graphite/Epoxy Laminate at an Applied Axial Tensile Stress of 434 MPa (63 ksi).

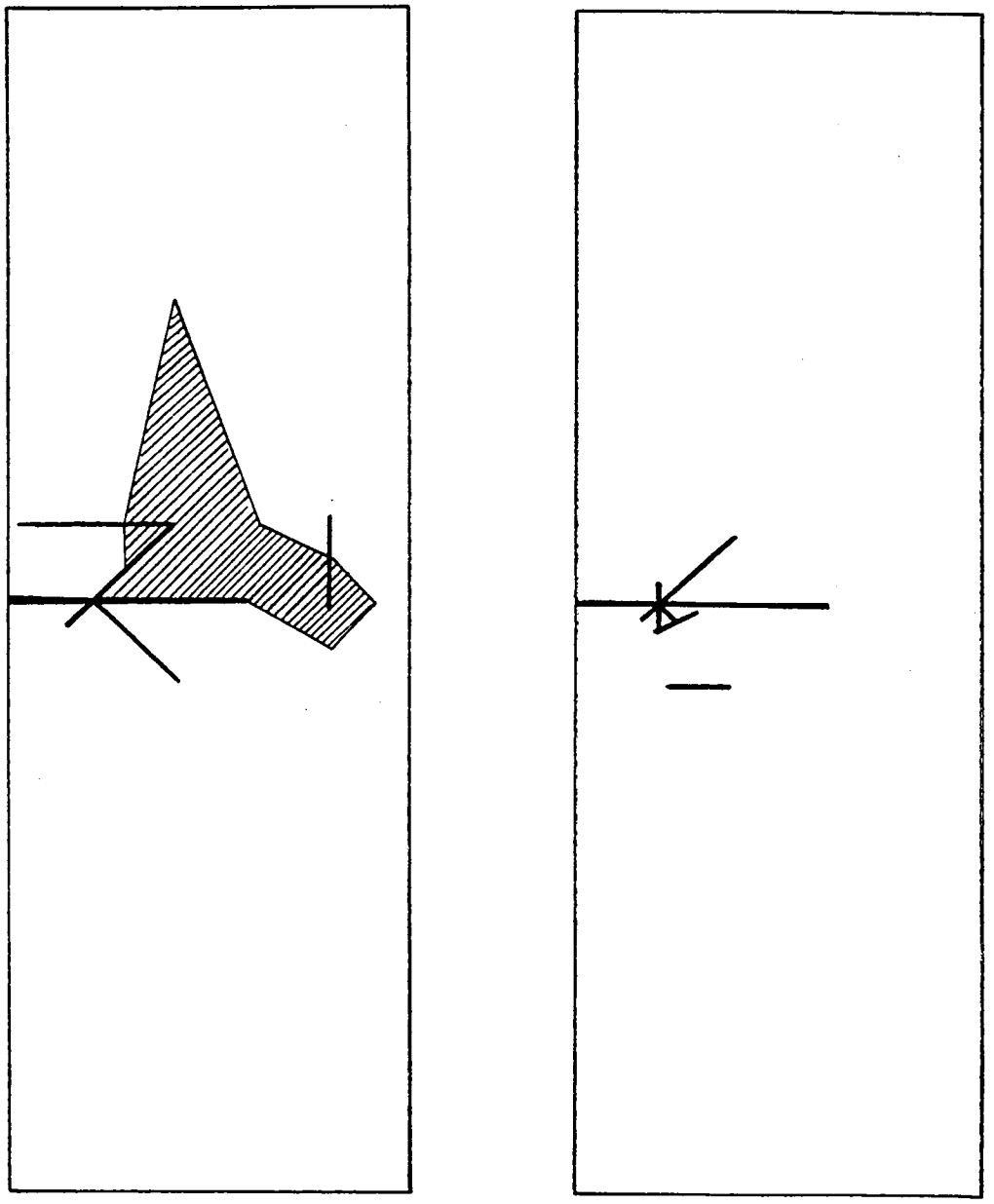

Figure 39 (Continued). Crack/Delamination Growth in a Single-Edge Notched $[\pm 45/0]_s$ Graphite/Epoxy Laminate at an Applied Axial Tensile Stress of 434 MPa (63 ksi).

in predicting crack/damage growth in composite laminates very similar to that which occurs in actual composites.

SECTION 8

CONCLUSIONS AND SUGGESTIONS FOR FUTURE WORK

A new fracture criterion has been developed for the fracture characterization of fiber-reinforced composites. The Griffith energy balance criterion has been modified to include energy absorption due to actual physical failure processes in the form of matrix yielding, matrix cracks, fiber breaks and fiber-matrix interface debonds, all of which are characteristic of the heterogeneous and anisotropic nature of these materials. The integrated micromechanical and macromechanical fracture criterion (IMMFC) proposed here is based on the assumption that microflaws in the form of broken fibers, matrix cracks and debonded fibers that exist in the composite for various reasons strongly influence the fracture process in these materials. Arguing that there is a relation between the size and density of the microflaws and the fracture response of the composite, parameters which are a measure of the size and density of the microflaws are introduced in the development of the IMMFC.

A three-dimensional finite element micromechanics model has been presented to study the influence of these microflaws on the strength, stiffness and fracture toughness of a unidirectional lamina. The model has several advantages over two-dimensional transverse and longitudinal section models [58,59]. Even though the computational costs of using the three-dimensional micromechanics analysis are higher than for two-dimensional micromechanics analyses (the 3-D analysis uses 174 CPU seconds per solution increment on the CDC Cyber 760 computer, compared to 80 CPU seconds per solution when using the 2-D micromechanics analysis), with the rapidly increasing capabilities of digital computers, the

use of three-dimensional models such as in the present analysis appears to be the logical long term approach.

In the present analysis, a local energy release rate in the presence of plasticity has been defined and used as a fracture criterion for the onset and growth of cracks. By including plasticity in the criterion, the analysis is applicable to most of the composite material systems currently in use.

A crack growth simulation technique based on the virtual crack extension method has been developed for use in crack growth studies using a general three-dimensional finite element model. The accuracy of this crack growth technique has been established by applying it to predict the crack propagation in a centrally cracked aluminum plate.

Several conclusions can be drawn from the results of the micromechanics analysis. For example, microcracks from broken fibers and fiber-matrix debonds grow in a self-similar fashion, whereas matrix cracks parallel to fibers are influenced by the presence of these fibers and change direction. This observation may be used to explain the experimentally observed zig-zag path of delamination cracks. The analysis can also be used to verify the double-cantilever beam test, in which a crack is introduced between unidirectional plies and propagated in the fiber direction.

The macromechanics analysis, in which only delamination crack growth is allowed, is useful in studying the amount of delamination associated with different stacking sequences.

In summary, the IMMFC and crack growth simulation techniques developed in the present analysis have been successfully used to predict the onset and growth of cracks/damage in the form of delaminations,

transverse cracks parallel to fibers, and through-the-thickness cracks in a single-edge notched $[\pm 45/0]_s$ graphite/epoxy laminate subjected to inplane tension normal to the notch. Even though the finite element grids used in the present analysis for both the micromechanics and the macromechanics analyses were shown to be adequate, a finer grid than the one used here will result in higher resolution. By considering different sizes and orientations of microflaws, a relation between microflaw parameters and the critical energy release rates eventually can be established.

An extensive experimental study should also be initiated, to further establish the validity of the IMMFC. It should be possible to actually evaluate the material microflaw parameters, by observing and measuring the sizes of microflaws in actual composites. The critical energy release rates corresponding to the measured microflaw parameters could then be used for fracture characterization at the laminate level.

REFERENCES

1. Griffith, A. A., "The Phenomena of Rupture and Flow in Solids," Philosophical Trans. Royal Soc., Vol. A221, 1921, pp. 163-171.

2. Griffith, A. A., "The Theory of Rupture," Proceedings of the First International Congress of Applied Mechanics, Delft, 1924, pp. 55-63.

3. Irwin, G. R., "Fracture Dynamics," Fracturing of Metals, American Society for Metals, 1948, pp. 147-166.

4. Orowan, E., "Energy Criteria of Fracture," Welding Journal, Vol. 34, pp. 157-160, 1955.

5. Irwin, G. R., "Relations of Stresses Near a Crack to the Crack Extension Force," Proceedings of the Ninth International Congress of Applied Mechanics, Vol. VIII, Paper 101 (II), University of Brussels, 1956, p. 245.

6. Irwin, G. R., Kies, J. A. and Smith, H. L., Proceedings of the American Society for Testing and Materials, Vol. 58, 1958, p. 640.

7. Rice, J. R., "A Path-Independent Integral and the Approximate Analysis of Strain Concentration by Notches and Cracks," Journal of Applied Mechanics, Vol. 35, 1968, pp. 379-386.

8. Cherepanov, C. P., "Crack Propagation for Continuous Media," Journal of Applied Mathematics and Mechanics, Vol. 31, 1967, p. 3.

9. Wells, A. A., "Unstable Crack Propagation in Metals: Cleavage and Fast Fracture," Crack Propagation Symposium, Cranfield, England, 1961.

10. Cottrell, A. H., Special Report No. 69, Iron and Steel Institute, 1961, pp. 281.

11. Ke, J. S. and Liu, H. W., "The Measurement of Fracture Toughness of Ductile Materials," Engineering Fracture Mechanics, Vol. 5, 1973, pp. 187-202.

12. Witt, F. G., "Equivalent Energy Procedures for Predicting Gross Plastic Fracture," Proceedings of the Fourth National Symposium on Fracture Mechanics, Carnegie Mellon University, 1970.

13. Heyer, R. H., "Crack Growth Resistance Curves (R-Curves), Literature Review," Fracture Toughness Evaluation by R-Curve Methods, ASTM STP 527, American Society for Testing and Materials, 1973, pp. 3-16.

14. Liebowitz, H. and Eftis, J., "On Nonlinear Effects in Fracture Mechanics," Engineering Fracture Mechanics, Vol. 3, 1971, p. 267.

15. Sih, G. C., "A Special Theory of Crack Propagation," Methods of Analysis and Solutions of Crack Problems (ed. G.C. Sih), Noordhoff International Publishing Co., Vol. 1, 1973.

16. de Koning, A. U., "A Contribution to the Analysis of Quasi-Static Crack Growth in Sheet Material," Fracture, International Congress on Fracture (ICF4), Vol. 3, 1977, pp. 25-31.

17. Shih, C. F., de Lorenzi, H. G. and Andrews, W. R., "Studies on Crack Initiation and Stable Crack Growth," Elastic-Plastic Fracture, ASTM STP 668, 1979, American Society for Testing and Materials, p. 65.

18. Begley, J. A. and Landes, J. D., "The J-integral as a Fracture Criterion," Fracture Toughness, ASTM STP 514, American Society for Testing and Materials, 1972, pp. 1-20.

19. Landes, J. D. and Begley, J. A., "The Effect of Specimen Geometry on J_{IC}," Fracture Toughness, ASTM STP 514, American Society for Testing and Materials, 1972, pp. 24-39.

20. Rice, J. R., Drugan, W. J. and Sham, T. L., "Elastic-Plastic Analysis of Growing Cracks," Fracture Mechanics, ASTM STP 700, American Society for Testing and Materials, 1980, pp. 189-221.

21. Sih, G. C., "Analytical Modeling, Crack Growth Characteristics," Fracture Mechanics (ed. Perrone, et al.), The University Press of Virginia, 1978.

22. Turner, C. E., "Description of Stable and Unstable Crack Growth in the Elastic Plastic Regime in Terms of J_R Resistance Curves," Fracture Mechanics, ASTM STP 677, American Society for Testing and Materials, 1979, pp. 614-628.

23. Turner, C. E., "A J Based Engineering Usage of Fracture Mechanics," Proceedings of the 5th International Congress on Advances in Fracture Research, Vol. 3, Fracture, Cannes, France, March 1981, pp. 1167-1189.

24. Hill, R., "Theory of Mechanical Properties of Fibre-Strengthened Materials: III. Self Consistent Model," Journal of the Mechanics and Physics of Solids, Vol. 13, 1965, pp. 189.

25. Kilchinskii, A. A., "On One Model for Determining Thermoelastic Characteristics of Fiber Reinforced Materials," (in Russian), Prikladnaia Mekhanika, Vol. I, No. 12, 1965, p. 123.

26. Hermans, J. J., "The Elastic Properties of Fiber Reinforced Materials when the Fibers are Aligned," Proceedings of Konigh Nederl. Akad. van Weteschappen Amsterdam, Vol. B70, No. 1, 1967, p. 1.

27. Whitney, J. M. and Riley, M. B., "Elastic Properties of Fiber

Reinforced Composite Materials," Journal of American Institute for Aeronautics and Astronautics, Vol. 4, 1966, p. 1537.

28. Whitney, J. M., "Elastic Moduli of Unidirectional Composites with Anisotropic Filaments," Journal of Composite Materials, Vol. 1, 1967, p. 188.

29. Whitney, J. M., "Geometric Effects of Filament Twist on the Modulus and Strength of Graphite Fiber-Reinforced Composites," Textile Research Journal, Vol. 36, 1966, p. 765.

30. Paul, B., "Prediction of Elastic Constants of Multiphase Materials," Transactions of the Metallurgical Society of AIME, Vol. 218, 1960, p. 36.

31. Hashin, Z. and Rosen, B. W., "The Elastic Moduli of Fiber Reinforced Materials," Journal of Applied Mechanics, Vol. 13, 1964, p. 233.

32. Dow, N. F. and Rosen, B. W., "Evaluation of Filament-Reinforced Composites for Aerospace Structural Applications," NASA CR-207, National Aeronautics and Space Administration, April 1965.

33. Hashin, Z., "On Elastic Behavior of Fiber-Reinforced Materials of Arbitrary Transverse Phase Geometry," Journal of the Mechanics and Physics of Solids, Vol. 13, 1965, p. 119.

34. Hill, R., "Theory of Mathematical Properties of Fiber-Strengthened Materials: I Elastic Behavior," Journal of the Mechanics and Physics of Solids, Vol. 12, 1964, p. 199.

35. Kurshin, L. M. and Fil'shtinskii, "Determination of Reduced Elastic Moduli of an Isotropic Plane Weakened by a Doubly-Periodic Array of Circular Holes," (in Russian), Izv. Akad, NaukSSSR, Mekh. Mash., No. 6, 1961, p. 110.

36. Van Fo Fy, G. A., "On the Equations Connecting the Stresses and Strains in Glass Reinforced Plastics," (in Russian), Prikladnaia Meckhanika, Vol. 1, No. 2, 1965, p. 110.

37. Hermann, L. R. and Pister, K. S., "Composite Properties of Filament-Resin Systems," ASME Paper No. 63 WA-239, presented at the ASME Winter Annual Meeting, Philadelphia, PA, November, 1963.

38. Wilson, H. B., Jr. and Hill, J. L., "Mathematical Studies of Composite Materials," Rohm and Haas Special Report No. 5-50, 1965.

39. Adams, D. F., Doner, D. R. and Thomas, R. L., "Mechanical Behavior of Fiber-Reinforced Composite Materials," Report No. AFML TR 67-96, Wright-Patterson Air Force Base, Ohio, May 1967.

40. Adams, D. F. and Doner, D. R., "Longitudinal Shear Loading of a Unidirectional Composite," Journal of Composite Materials, Vol. 1,

1967, p. 4.

41. Adams, D. F. and Doner, D. R., "Transverse Normal Loading of a Unidirectional Composite," Journal of Composite Materials, Vol. 1, 1967, p. 152.

42. Pickett, G., "Analytical Procedures for Predicting the Mechanical Properties of Fiber Reinforced Composites," Report No. AFML TR 65-220, Part 2, Wright-Patterson Air Force Base, Ohio, 1966.

43. Chen, C. H. and Cheng, S., "Mechanical Properties of Fiber Reinforced Composites," Journal of Composite Materials, Vol. 1, 1967, p. 30.

44. Clausen, W. E. and Leissa, A. W., "Stress and Deflection Analysis of Fibrous Composite Materials Under External Load," Report No. AFML TR 67-15, Wright-Patterson Air Force Base, Ohio, 1967.

45. Jones, R. M., Mechanics of Composite Materials, Scripta Book Company, Washington, D.C., 1975.

46. Ashton, J. E., Halpin, J. C. and Petit, P.H., Primer on Composite Materials: Analysis, Technomic Publishing Co., 1969.

47. Agarwal, B. D. and Broutman, L. J., Analysis and Performance of Fiber Composites, John Wiley & Sons, 1980.

48. Hedgepeth, J. M. and VanDyke, P., "Local Stress Concentrations in Imperfect Filamentary Composite Materials," Journal of Composite Materials, Vol. 1, 1967, pp. 294-309.

49. Goree, J. G. and Gross, R. S., "Stresses in a Three-Dimensional Unidirectional Composite Containing Broken Fibers," Engineering Fracture Mechanics, Vol. 13, 1980, pp. 395-405.

50. Goree, J. G. and Gross, R. S., "Analysis of a Unidirectional Composite Containing Broken Fibers and Matrix Damage," Engineering Fracture Mechanics, Vol. 13, 1979, pp. 563-578.

51. Erdogan, F., "Fracture of Composite Materials, Prospects of Fracture Mechanics," International Conference Proceedings, Delft University of Technology, Netherlands, 1975.

52. Narayaran, T. V. and Erdogan, F., "Penny-Shaped Crack in a Fiber-Reinforced Matrix," International Journal of Solids and Structures, Vol. II, 1975, pp. 1315-1327.

53. Smith, C. W., "Limitations of Fracture Mechanics as Applied to Composites," Publication ASME-AMD V13, ASME Winter Annual Meeting, November 1975, pp. 157-175.

54. Phillips, D. C. and Tetelman, A. S. "The Fracture Toughness of Fibre Composites," Composites, Vol. 3, 1972, p. 216.

55. Cooper, G. A., "Micromechanics Aspects of Fracture and Toughness," Composite Materials, Eds., Broutman, L. J. and Krock, R. H., Vol. 5, Fracture and Fatigue, Ed. Broutman, L. J., Academic Press, New York, 1974.

56. Dharan, C.K.H., "Fracture Mechanics of Composite Materials," Journal of Engineering Materials and Technology, Vol. 100, July 1978, pp. 233-247.

57. Cooper, G. A. and Piggott, M. R., "Cracking and Fracture in Composites," Fracture 77, Volume 1, Waterloo, Canada, June 1977, p. 557.

58. Murphy, D. P. and Adams, D. F., "Energy Absorption Mechanisms During Crack Propagation in Metal Matrix Composites," Report UWME-DR-901-103-1, Department of Mechanical Engineering, University of Wyoming, Laramie, Wyoming, October 1979.

59. Adams, D. F. and Murphy, D. P., "Analysis of Crack Propagation as an Energy Absorption Mechanism in Metal Matrix Composites," Report UWME-DR-101-102-1, Department of Mechanical Engienering, University of Wyoming, Laramie, Wyoming, February 1981.

60. Adams, D. F., "Practical Problems Associated with the Application of the Finite Element Method to Composite Material Micromechanical Analyses," Fibre Science and Technology, Vol. 7, No. 2, April 1974, pp. 111-122.

61. Adams, D. F., "High Performance Composite Materials for Vehicle Construction; An Elastoplastic Analysis of Crack Propagation in a Unidirectional Composite," Report R-1070-PR, The Rand Corporation, Santa Monica, California, March 1973.

62. Repnau, T. and Adams, D. F., "A Finite Element Computer Program for Elastoplastic Analysis of Crack Propagation in a Unidirectional Composite," Report R-1392-PR, The Rand Corporation, Santa Monica, California, October 1973.

63. Adams, D. F., "Elastoplastic Crack Propagation in a Transversely Loaded Unidirectional Composite," Journal of Composite Materials, Vol. 8, No. 1, January 1974, pp. 38-54.

64. Adams, D. F., "A Micromechanical Analysis of Crack Propagation in an Elastoplastic Composite Material," Fibre Science and Technology, Vol. 7, No. 4, October 1974, pp. 237-256.

65. Adams, D. F. and Mahishi, J. M., "Micromechanical Predictions of Crack Propagation and Fracture Energy in a Single-Fiber Boron/Aluminum Model Composite," Report UWME-DR-201-101-1, Department of Mechanical Engineering, University of Wyoming, Laramie, Wyoming, February 1982.

66. Mahishi, J. M. and Adams, D. F., "Micromechanical Predictions of

Crack Initiation, Propagation and Crack Growth Resistance in Boron/Aluminum Composites," Journal of Composite Materials, Vol. 16, No. 6, November 1982, pp. 457-469.

67. Mahishi, J. M. and Adams, D. F., "Fracture Behavior of a Single-Fibre Graphite/Epoxy Model Composite Containing a Broken Fibre or Cracked Matrix," Journal of Materials Science, Vol. 18, No. 2, February 1983, pp. 447-456.

68. Ko, W. L., "Finite Element Microscopic Stress Analysis of Cracked Composite Systems," Journal of Composite Materials, Vol. 12, No. 1, January 1978, pp. 97-115.

69. Gradin, P. and Backlund, J., "Finite Element Analyzing Debonding in an Axisymmetric Bimaterial Body," Numerical Methods in Fracture Mechanics, Eds. Owen, D. R. J., Luxmoore, A. R., Proceedings of the Second International Conference, Swansea, July 1980.

70. Drzal, L. T., Private Communication, October 1973.

71. Mahishi, J. M. and Adams, D. F., "Three-Dimensional Elastoplastic Stress Analysis of Unidirectional Boron/Aluminum Composites Containing Broken Fibers," Report UWME-DR-201-107-1, Department of Mechanical Engineering, University of Wyoming, October 1982.

72. Beaumont, P. W. R. and Anstice, P. D., "A Failure Analysis of Micromechanisms of Fracture of Carbon Fibre and Glass Fibre Composites in Monotonic Loading," Journal of Materials Science, Vol. 15, 1980, pp. 2619-2635.

73. Mandel, J. A., Park, S. C. and Tarazi, S., "Micromechanical Studies of Crack Growth in Fiber Reinforced Materials," Engineering Fracture Mechanics, Vol. 16, No. 5, 1982, pp. 741-754.

74. Bader, M. G., Curtis, P. T. and Chatwal, R. S., "The Micromechanics of Fracture in Fiber-reinforced Thermoplastics," Proceedings of the 1975 International Conference on Composite Materials, Eds. Scala, E., Anderson, E., Toth, I and Noton, B. R., Vol. 2, pp. 191-206.

75. Williams, R. S. and Reifsnider, K. L., "Strain Energy Release Rate Method for Predicting Failure Modes in Composite Materials," Fracture Mechanics, ASTM STP 677, Ed. C. W. Smith, American Society for Testing and Materials, 1979, pp. 629-650.

76. Wells, J. K. and Beaumont, P. W. R., "Fracture Energy Maps for Fiber Composites," Journal of Materials Science, Vol. 17, 1982, pp. 397-405.

77. Hashin, Z., "Analysis of Composite Materials-A Survey," Journal of Applied Mechanics, Vol. 50, September 1983, pp. 481-505.

78. Puppo, A. H. and Evensen, H. A., "Interlaminar Shear in Laminated

Composites Under Generalized Plane Stress," Journal of Composite Materials, Vol. 4, No. 3, April 1970, pp. 204-220.

79. Pipes, R. B. and Pagano, N. J., "Interlaminar Stresses in Composite Laminates Under Uniform Axial Extension," Journal of Composite Materials, Vol. 4, October 1970, pp. 538-548.

80. Raju, I. S. and Crews, J. H., Jr., "Interlaminar Stress Singularities at a Straight Free Edge in Composite Laminates," Computers and Structures, Vol. 14, No. 1-2, 1981, pp. 21-28.

81. Rybicki, E. F. and Schmueser, D. W., "Effect of Stacking Sequence and Lay-Up Angle on Free Edge Stresses Around a Hole in a Laminated Plate Under Tension," Journal of Composite Materials, Vol. 12, July 1978, pp. 300-313.

82. Salamon, N. J., "An Assessment of the Interlaminar Stress Problem in Laminated Composites," Journal of Composite Materials Supplement, Vol. 14, No. 1, 1980, pp. 177-194.

83. Rybicki, E. F., Schmueser, D. W. and Fox, J., "An Energy Release Rate Approach for Stable Crack Growth in the Free-Edge Delamination Problem," Journal of Composite Materials, Vol. 11, October 1977, pp. 470-487.

84. Irwin, G. R., "Fracture," Handbuch der Physik, Vol. V, Springer-Verlag, 1958, p. 551.

85. Rybicki, E. F. and Kanninen, M. F., "A Finite Element Calculation of Stress Intensity Factors by a Modified Crack Closure Integral," Engineering Fracture Mechanics, Vol. 9, 1977, pp. 931-938.

86. Wang, A. S. D. and Crossman, F. W., "Initiation and Growth of Transverse Cracks and Edge Delamination in Composite Laminates, Part 1. An Energy Method," Journal of Composite Materials Supplement, Vol. 14, No. 1, 1980, pp. 71-87.

87. Wang, A. S. D. and Slomiana, M., "Fracture Mechanics of Delamination-Initiation and Growth," Report No. NADC-79056-60, Drexel, University, Philadelphia, PA, January 1982.

88. O'Brien, T. K., "Mixed-Mode Strain Energy Release Rate Effects on Edge Delamination of Composites," NASA TM 84592, National Aeronautics and Space Administration, Langley Research Center, Hampton, Virginia, January 1983.

89. O'Brien, T. K., "Analysis of Local Delaminations and Their Influence on Composite Laminate Behavior," NASA TM 85728, National Aeronautics and Space Administration, Langley Research Center, Hampton, Virginia, January 1984.

90. Whitcomb, J. D., "Strain Energy Release Rate Analysis of Cyclic Delamination Growth in Compressively Loaded Laminates," NASA TM

84598, National Aeronautics and Space Administration, Langley Research Center, Hampton, Virginia, January 1983.

91. Wang, A. S. D., Slomiana, M. and Bucinell, R., "A Three-Dimensional Finite Element Analysis of Delamination Growth in Composite Laminates, I. The Energy Methods and Case-Study Problems," Report No. NADC-84017-60, Drexel University, Philadelphia, PA, September 1983.

92. Chou, P. C., Wang, A. S. D. and Miller, H., "Cumulative Damage Model for Advanced Composite Materials," AFWAL-TR-82-4083, Dyna East Corporation, Wynnewood, PA, September 1982.

93. O'Brien, T. K. and Raju, I. S., "Strain Energy Release Rate Analysis of Delamination Around an Open Hole in Composite Laminates," Proceedings of the 25th AIAA/ASME/ASCE/AHS Structures, Structural Dynamics and Materials Conference, Palm Springs, CA, May 1984.

94. Crossman, F. W., "Analysis of Free-Edge Induced Failure of Composite Laminates," Proceedings of the First USA-USSR Symposium on Fracture of Composite Materials, Riga, USSR, Eds., G. C. Sih and V. P. Tamuzi, Sijthoff and Noordhoff, Publishers, 1979.

95. Wang, A. S. D. and Crossman, F. W., "Fracture Mechanics of Transverse Cracks and Edge Delamination in Graphite/Epoxy Composite Laminates," Report No. AFOSR-TR 83-0452, Drexel University, Philadelphia, PA, March 1982.

96. Crossman, F. W. and Wang, A. S. D., "The Dependence of Transverse Cracking and Delamination on Ply Thickness in Graphite/Epoxy Laminates," Damage in Composite Materials, ASTM STP 775, K. L. Reifsnider, Ed., American Society for Testing and Materials, 1982, pp. 118-139.

97. O'Brien, Johnston, N. J., Morris, D. H. and Simonds, R. A., "A Simple Test for the Interlaminar Fracture Toughness of Composites," SAMPE Journal, July/August 1982, pp. 8-15.

98. O'Brien, T. K., "Characterization of Delamination Onset and Growth in a Composite Laminate," Damage in Composite Materials, ASTM STP 775, K. L. Reifsnider, Ed., American Society for Testing and Materials, 1982, pp. 140-167.

99. Wilkins, D. J., Eisenmann, J. R., Camin, R. A., Margolis, W. S. and Benson, R. A., "Characterizing Delamination Growth in Graphite/Epoxy," Damage in Composite Materials, ASTM STP 775, K. L. Reifsnider, Ed., American Society for Testing and Materials, 1982, pp. 168-183.

100. Wang, S. S., Mandell, J. F. and McGarry, F. J., "Three-Dimensional Solution for a Through-Thickness Crack with Crack Tip Damage in a Cross-Plied Laminate," Fracture Mechanics of Composites, ASTM STP

593, American Society for Testing and Materials, 1975, pp. 61-85.

101. Ramkumar, R. L., "Performance of a Quantitative Study of Instability-Related Delamination Growth," NASA CR 166046, Northrop Corporation, Aircraft Division, Hawthorne, CA, March 1983.

102. Crossman, F. W. and Warren, J., "Initiation and Growth of Transverse Cracks and Edge Delamination in Composite Laminates, Part 2. Experimental Correlation," Journal of Composite Materials Supplement, Vol. 14, No. 1, 1980, pp. 88-108.

103. Konishi, D. Y. and Johnston, W. R., "Fatigue Effects on Delaminations and Strength Degradation in Graphite/Epoxy Laminates," Composite Materials: Testing and Design (Fifth Conference), ASTM STP 674, S. W. Tsai, Ed., American Society for Testing and Materials, 1979, pp. 597-619.

104. Wang, S. S., "Delamination Crack Growth in Unidirectional Fiber-Reinforced Composites under Static and Cyclic Loading," Composite Materials: Testing and Design (Fifth Conference), ASTM STP 674, S. W. Tsai, Ed., American Society for Testing and Materials, 1979, pp. 642-663.

105. Wang, S. S. and Choi, I., "The Mechanics of Delamination in Fiber-Reinforced Composite Materials," Part I-Stress Singularities and Solution Structure," NASA CR 172269, University of Illinois, Urbana, Illinois, November 1983.

106. Wang, S. S., "Fracture Mechanics for Delamination Problems in Composite Materials," Journal of Composite Materials, Vol. 17, May 1983, pp. 210-223.

107. Wang, S. S. and Wang, H. T., "Interlaminar Crack Growth in Fiber Reinforced Composite During Fatigue," Final Report-Part III, NASA CR-165434, Department of Theoretical and Applied Mechanics, University of Illinois, Urbana, Illinois, February 1981.

108. Lekhnitski, S. G., Theory of Elasticity of an Anisotropic Elastic Body, Holden-Day, San Francisco, 1963.

109. Savin, G. N., Stress Concentrations Around Holes, Pergamon Press, New York, 1961.

110. Tirosh, J., "The Mixed Mode Fracture of Unidirectional Fibrous Composites," Engineering Fracture Mechanics, Vol. 13, 1980, pp. 119-127.

111. Heppler, G. R., Frisken, S. and Hansen, J. S., "Stress Intensity Factor Calculation for Designing with Fiber Reinforced Composite Materials," Proceedings of the 24th AIAA/ASME/ASCE/AHS Structures, Structural Dynamics and Materials Conference, Part 1, Lake Tahoe, Nevada, May 1983.

112. Chen, E. P., "A Theory for Laminated Plates with a Through-the-Thickness Crack," Advances in Fracture Research (Fracture 81), Proceedings of the 5th International Conference on Fracture (ICF5), Ed. D. Francois, Vol. 3, Pergamon Press, New York, 1981.

113. Nishioka, T. and Atluri, S. N., "Fracture Analyses of Angle-Ply Laminates," Advances in Fracture Research (Fracture 81), Proceedings of the 5th International Conference on Fracture (ICF5), Ed. D. Francois, Vol. 3, Pergamon Press, New York, 1981.

114. Whitney, J. M. and Nuismer, R. J., "Stress Fracture Criteria for Laminated Composites Containing Stress Concentrations," Journal of Composite Materials, Vol. 8, July 1974, p. 253.

115. Kannien, M. F., Rybicki, E. F. and Brinson, H. F., "A Critical Look at Current Applications of Fracture Mechanics to the Failure of Fiber-Reinforced Composites," Composites, Vol. 8, January 1977, pp. 17-22.

116. Waddoups, M. E., Eisenmann, J. R. and Kaminski, B. E., "Microscopic Fracture Mechanics of Advanced Composite Materials," Journal of Composite Materials, Vol. 5, 1971, p. 466.

117. Bowie, O. L., "Analysis of an Infinite Plate Containing Radial Cracks Originating from the Boundary of an Internal Circular Hole," Journal of Mathematics and Physics, Vol. 35, 1956, p. 60.

118. Cruse, T. A., "Tensile Strength of Notched Composites," Journal of Composite Materials, Vol. 7, 1973, p. 218.

119. Pipes, R. B., Wetherhold, R. C. and Gillespie, Jr., J. W., "Notched Strength of Composite Materials," Journal of Composite Materials, Vol. 13, April 1979, p. 148.

120. Backlund, J., "Fracture Analysis of Notched Composites," Computers and Structures, Vol. 13, 1981, pp. 145-154.

121. Harrison, N. L., "Splitting of Fibre-Reinforced Materials," Fibre Science and Technology, Vol. 6, 1973, p. 25.

122. Sih, G. C. and Chen, E. P., "Cracks in Composites," Mechanics of Fracture, Vol. 6, Martinus Nijhoff, Publishers, The Hague, 1981.

123. Wu, E. M., "Application of Fracture Mechanics to Anisotropic Plates," Journal of Applied Mechanics, Vol. 34, 1967, p. 967.

124. Wu, E. M., "Strength and Fracture of Composites," Composite Materials, Eds. L. J. Broutman and R. H. Krock, Vol. 5, Fracture and Fatigue Ed. L. J. Broutman, Academic Press, New York 1974.

125. Laksminarayana, H. V., Mahishi, J. M. and Aruna, H. M., "On the Behaviour of Cracks in Laminated Composite Panels," Ed. Sih. G. C. and Velluri, S. R., Proceedings of an International Conference on Fracture Mechanics in Engineering Applications, Bangalore, India, Sijthoff and Noordhoff, Publishers, The Netherlands, 1979.

126. Kulkarni, S. V. and Rosen, B. W., "Design Data for Composite Structure Safelife Prediction: Analysis Evaluation," Report TFR/2221, Materials Science Corporation, Bluebell, PA, August 1973.

127. Zweben, C., "On the Strength of Notched Composites," Journal of the Mechanics and Physics of Solids, Vol. 19, 1971, p. 103.

128. Tirosh, J., "The Effect of Plasticity and Crack Blunting on the Stress Distribution in Orthotropic Composite Materials," Journal of Applied Mechanics, Vol. 40, September 1973.

129. Kanninen, M. F., Rybicki, E. F. and Griffith, W. I., "Preliminary Development of a Fundamental Analysis Model for Crack Growth in a Fiber Reinforced Composite Material," Composite Materials: Testing and Design (Fourth Conference), ASTM STP 617, American Society for Testing and Materials, 1977, pp. 53-69.

130. Brinson, H. F. and Yeow, Y. T., "An Experimental Study of the Fracture Behavior of Laminated Graphite/Epoxy Composites," Composite Materials: Testing and Design (Fourth Conference), ASTM STP 617, American Society for Testing and Materials, 1977, pp. 18-38.

131. Gallagher, R. H., "A Review of Finite Element Techniques in Fracture Mechanics," Numerical Methods in Fracture Mechanics, Eds. Luxmoore, A. R. and Owen, D. R. J., Proceedings of the First International Conference, Swansea, January 1978.

132. Anderson, H., "A Finite-Element Representation of Stable Crack Growth," Journal of the Mechanics and Physics of Solids, Vol. 21, 1973, pp. 337-356.

133. Light, M. F. and Luxmoore, A. R., "Application of the Front Solution to Two and Three-Dimensional Elastoplastic Crack Problems," International Journal for Numerical Methods in Engineering, Vol. II, No. 2, 1977.

134. Bleackley, M. H. and Luxmoore, A. R., "An Investigation of Numerical Errors in Finite Element Elastic-Plastic Crack Extension Models," Numerical Methods in Fracture Mechanics, Eds. Luxmoore, A. R. and Owen, D. R. J., Proceedings of the First International Conference, Swansea, January 1978, pp. 508-524.

135. Parks, D. M., "A Stiffness Derivative Finite Element Technique for Determination of Crack Tip Stress Intensity Factors," International Journal of Fracture, Vol. 10, 1974, pp. 487-502.

136. Parks, D. M., "Virtual Crack Extension: a General Finite Element Technique for J-Integral Evaluation," Numerical Methods in Fracture Mechanics, Eds. Luxmoore, A. R. and Owen, D. R. J., Proceedings of the First International Conference, Swansea, January 1978, pp. 464-478.

137. Hellen, T. K., "On the Method of Virtual Crack Extension," International Journal for Numerical Methods in Engineering, Vol. 9, 1975, pp. 187-207.

138. Parks, D. M., "The Virtual Crack Extension Method for Nonlinear Material Behavior," Computer Methods in Applied Mechanics and Engineering, Vol. 12, 1977, pp. 353-364.

139. Younan, M. Y. A., "Fracture Mechanics of Weldments Using Finite Element Analysis," Ph.D. dissertation, University of Tennessee, December 1975.

140. Younan, M. Y. A., Dewey, B. R. and Akin, J. E., "Crack Propagation Analysis for Orthotropic Non-Homogeneous Materials," Engineering Fracture Mechanics, Vol. 16, No. 2, 1982, pp. 189-205.

141. Ingraffea, A., "Nodal Grafting for Crack Propagation Studies," Information Journal for Numerical Methods in Engineering, Vol. II, No. 2, 1977.

142. Barsoum, R. S., "Triangular Quarter-Point Elements as Elastic and Perfectly-Plastic Crack Tip Elements," International Journal for Numerical Methods in Engineering, Vol. II, 1977, pp. 85-98.

143. Shih, C. F., "Relationships between the T-Integral and the Crack Opening Displacement for Stationary and Extending Cracks," Journal of the Mechanics and Physics of Solids, Vol. 29, No. 4, 1981, pp. 305-326.

144. Monib, M. M. and Adams, D. F., "Three-Dimensional Elastoplastic Finite Element Analysis of Laminated Composites," Department Report UWME-DR-102-1, Department of Mechanical Engineering, University of Wyoming, November 1980.

145. Lotsberg, I., "Crack Growth Simulation by Finite Element Method," Numerical Methods in Fracture Mechanics, Eds. Luxmoore, A. R. and Owen, D. R. J., Proceedings of the First International Conference, Swansea, January 1978, pp. 496-507.

146. Hertzberg, R. W., Deformation and Fracture Mechanics of Engineering Materials, Second Edition, John Wiley and Sons, New York, 1983.

147. Adams, D. F., Ramkumar, R. L. and Walrath, D. E., "Analysis of Porous Laminates in the Presence of Ply Drop-Offs and Fastener Holes," Northrop Technical Report NOR 84-113, Northrop Corporation, Hawthorne, CA, May 1984.

148. Richard, R. M. and Blacklock, J. R., "Finite Element Analysis of Inelastic Structures," American Institute of Astronautics and Aeronautics Journal, Vol. 7, No. 3, March 1969, pp. 432-438.

149. Adams, N. J., "Influence of Configuration on R-Curve Shape and G_c When Plane Stress Conditions Prevail," Cracks and Fracture, ASTM STP 601, American Society for Testing and Materials, 1976, pp. 330-345.

150. Kuna, M., "Some Applications of the Finite Element Method to Fracture Mechanics of Elastic and Elastic-Plastic Solids," Numerical Methods in Fracture Mechanics, Eds. Luxmoore, A. R. and Owen, D. R. J., Proceedings of the First International Conference, Swansea, January 1978.

151. Morris, D. H. and Hahn, H. T., "Fracture Resistance Characterization of Graphite/Epoxy Composites," Composite Materials: Testing and Design (Fourth Conference), ASTM STP 617, American Society for Testing and Materials, 1977, pp. 5-17.

152. Hill, R., The Mathematical Theory of Plasticity, Oxford University Press, London, 1950.

153. Langhaar, H. L., Energy Methods in Applied Mechanics, John Wiley and Sons, New York, 1962.

154. Cook, R. D., Concepts and Applications of Finite Element Analysis, John Wiley and Sons, New York, 1974.

APPENDIX A

THREE-DIMENSIONAL, ELASTOPLASTIC, GENERALLY ORTHOTROPIC FINITE ELEMENT ANALYSIS

The theory of the three-dimensional, elastoplastic, generally orthotropic finite element analysis developed by Monib and Adams [144] for the analysis of composite laminates is summarized here.

The unidirectional composite lamina is assumed to be homogeneous and transversely isotropic. The three principal material axes are assumed as follows: the 1-axis, in the direction of the reinforcing fibers, the 2-axis, normal to the fibers but in the plane of the lamina, and the 3-axis, normal to the plane of the lamina (see Figure 2a of Section 3). The 2-3 plane is the plane of transverse isotropy.

A quadratic yield condition similar to Hill's yield criterion [152] is chosen in the form

$$2f(\sigma_{ij}) = F(\sigma_2 - \sigma_3)^2 + G(\sigma_3 - \sigma_1)^2 + H(\sigma_1 - \sigma_2)^2 \qquad (A.1)$$

$$+ 2L\,\tau_{23}^2 + 2M\,\tau_{31}^2 + 2N\,\tau_{12}^2 = 1$$

where F, G, H, L, M, and N are parameters characteristic of the current state of anisotropy. These parameters of anisotropy are allowed to vary with changes in temperature and/or moisture content. It can be shown [152] that

$$\frac{1}{(\sigma_1^y)^2} = G + H \ , \quad 2F = \frac{1}{(\sigma_2^y)^2} + \frac{1}{(\sigma_3^y)^2} - \frac{1}{(\sigma_1^y)^2}$$

$$\frac{1}{(\sigma_2^y)^2} = H + F \ , \quad 2G = \frac{1}{(\sigma_3^y)^2} + \frac{1}{(\sigma_1^y)^2} - \frac{1}{(\sigma_2^y)^2} \tag{A.2}$$

$$\frac{1}{(\sigma_3^y)^2} = F + G \ , \quad 2H = \frac{1}{(\sigma_1^y)^2} + \frac{1}{(\sigma_2^y)^2} - \frac{1}{(\sigma_3^y)^2}$$

where σ_1^y, σ_2^y, and σ_3^y are the tensile yield stresses in the 1, 2, and 3 directions of anisotropy. Also, if τ_{23}^y, τ_{31}^y and τ_{12}^y are the yield stresses in shear with respect to the principal axes of anisotropy, then

$$2L = \frac{1}{(\tau_{23}^y)^2} \ , \quad 2M = \frac{1}{(\tau_{31}^y)^2} \ , \quad 2N = \frac{1}{(\tau_{12}^y)^2} \tag{A.3}$$

The functional dependence of the parameters of anisotropy on temperature and moisture follows from Eqs. (A.2) and (A.3) when the yield stresses are expressed as functions of temperature and moisture content.

The obvious association, implied by the term 'work-hardening,' between the work used to produce plastic flow and the hardening created, suggests the hypothesis that the degree of hardening is a function only of the total plastic work, and is otherwise independent of the strain path. The external work dW per unit volume done on the element during an infinitesimal increment of strain $d\epsilon_{ij}$, with the continued loading of an element of the material is

$$dW = \sigma_{ij} d\epsilon_{ij} \tag{A.4}$$

A part of this work

$$dW_e = \sigma_{ij} d\varepsilon^e_{ij} \tag{A.5}$$

represents recoverable elastic energy; the remainder is the plastic work per unit volume, i.e.,

$$dW_p = dW - dW_e = \sigma_{ij}(d\varepsilon_{ij} - d\varepsilon^e_{ij}) = \sigma_{ij} d\varepsilon^p_{ij} \tag{A.6}$$

where $d\varepsilon^p_{ij} = d\varepsilon_{ij} - d\varepsilon^e_{ij}$ is termed the plastic strain increment. The term dW_p is necessarily positive since plastic distortion is an irreversible process, and the plastic work is then

$$W_p = \int \sigma_{ij} d\varepsilon^p_{ij} \tag{A.7}$$

In order for plastic work to be performed, the state of stress must be on the yield surface, i.e., the stress state must also satisfy the condition given by Eq. (A.1). To enforce this constraint, the Lagrange multiplier $d\lambda$ is used [153]. Then

$$\frac{\partial}{\partial \sigma_{ij}} [\sigma_{ij} d\varepsilon^p_{ij} - f(\sigma_{ij}) d\lambda] = 0 \tag{A.8}$$

which gives

$$d\varepsilon^p_{ij} = \frac{\partial f}{\partial \sigma_{ij}} d\lambda \tag{A.9}$$

With the use of Eq. (A.1), a set of equations for the plastic strain increments can then be written as follows:

$$d\varepsilon_{ij}^{p} = \sigma_{ij}^{*} d\lambda, \quad i = j \tag{A.10}$$

$$d\gamma_{ij}^{p} = 2\tau_{ij}^{*} d\lambda, \quad i \neq j \tag{A.11}$$

where

$$\sigma_1^* = [H(\sigma_1 - \sigma_2) + G(\sigma_1 - \sigma_3)]/(F + G + H)$$

$$\sigma_2^* = [F(\sigma_2 - \sigma_3) + H(\sigma_2 - \sigma_1)]/(F + G + H)$$

$$\sigma_3^* = [G(\sigma_3 - \sigma_1) + F(\sigma_3 - \sigma_2)]/(F + G + H)$$

$$\tau_{23}^* = L\tau_{23}/(F + G + H) \tag{A.12}$$

$$\tau_{31}^* = M\tau_{31}/(F + G + H)$$

$$\tau_{12}^* = N\tau_{12}/(F + G + H)$$

Separating the strains into elastic and plastic components gives

$$d\varepsilon_1 = S_{11}d\sigma_1 + S_{12}d\sigma_2 + S_{13}d\sigma_3 + d\varepsilon_1^p$$

$$d\varepsilon_2 = S_{21}d\sigma_1 + S_{22}d\sigma_2 + S_{23}d\sigma_3 + d\varepsilon_2^p \tag{A.13}$$

$$d\varepsilon_3 = S_{31}d\sigma_1 + S_{32}d\sigma_2 + S_{33}d\sigma_3 + d\varepsilon_3^p$$

and for the shear components

$$d\gamma_{23} = S_{44}d\tau_{23} + d\gamma_{23}^p$$

$$d\gamma_{31} = S_{55}d\tau_{31} + d\gamma_{31}^p \tag{A.14}$$

$$d\gamma_{12} = S_{66}d\tau_{12} + d\gamma_{12}^p$$

where the S_{ij} are the coefficients of the elastic compliance matrix $[S^e]$ in

$$\{d\varepsilon\} = [S^e]\{d\sigma\} \tag{A.15}$$

The inverse of Eq. (A.15) is

$$\{d\sigma\} = [C^e]\{d\varepsilon\} \tag{A.16}$$

where $[C^e]$ is the elastic stiffness matrix. If X_o, Y_o, etc., are the initial yield stresses, then according to the assumption of isotropic hardening above, $X = hX_o$, $Y = hY_o$, etc., where h is a parameter increasing monotonically from unity that expresses the amount of hardening. The anisotropic parameters must then decrease in accordance with Eq. (A.2) as $F = F_o/h^2$, etc. The manner in which h varies with strain can be explained by analogy with the isotropic theory due to von Mises. Let

$$\begin{aligned}\bar{\sigma}^2 &= \left[\frac{3}{2}\frac{h^2}{F+G+H}\right] \\ &= \frac{3}{2}\left[\frac{F(\sigma_2-\sigma_3)^2 + G(\sigma_3-\sigma_1)^2 + H(\sigma_1-\sigma_2)^2}{F+G+H}\right. \\ &\quad \left. + \frac{2L\tau_{23}^2 + 2M\tau_{31}^2 + 2N\tau_{12}^2}{F+G+H}\right]\end{aligned} \tag{A.17}$$

be a nondimensional measure of the equivalent stress $\bar{\sigma}$. By analogy with the von Mises criterion for isotropic materials, Hill [152] suggested that if there is a functional relation between $\bar{\sigma}$ and the work W (this is yet to be demonstrated by experiment), there must be one between $\bar{\sigma}$ and the effective (or equivalent) strain, $\int d\bar{\varepsilon}$, as defined by

$$d\bar{\varepsilon} = \left[\frac{2}{3}(F + G + H)\right]^{\frac{1}{2}} \left[\frac{F(Gd\varepsilon_2 - Hd\varepsilon_3)^2 + G(Hd\varepsilon_3 - Fd\varepsilon_1)^2 + H(Fd\varepsilon_1 - Gd\varepsilon_2)^2}{(FG + GH + HF)^2}\right.$$

$$\left. + \frac{2(d\gamma_{23})^2}{L} + \frac{2(d\gamma_{31})^2}{M} + \frac{2(d\gamma_{12})^2}{N}\right]^{\frac{1}{2}} \tag{A.18}$$

where $d\varepsilon_{ij}$ and $d\gamma_{ij}$ are given by Eqs. (A.13) and (A.14). This is the analogue of the equivalent stress-equivalent strain curve for isotropic materials, the area under which is equal to the work per unit volume. Accordingly,

$$dW_p = \bar{\sigma}(d\bar{\varepsilon} - d\bar{\varepsilon}^e) = \bar{\sigma}d\bar{\varepsilon}^p \tag{A.19}$$

But, from Eq. (A.5)

$$dW_p = \sigma_1 d\varepsilon_1^p + \ldots + \tau_{23} d\gamma_{23}^p + \ldots \tag{A.20}$$

Substituting for $d\varepsilon_{ij}^p$ and $d\gamma_{ij}^p$ from Eq. (A.10) into Eq. (A.20) yields

$$dW_p = \frac{2}{3}\bar{\sigma}^2 \, d\lambda \tag{A.21}$$

If an effective stress-effective plastic strain curve is then constructed, the slope of such a curve at any point will be

$$H' = \frac{d\bar{\sigma}}{d\bar{\varepsilon}^p} \tag{A.22}$$

from which

$$d\bar{\varepsilon}^p = \frac{d\bar{\sigma}}{H'} \tag{A.23}$$

Now, substituting for $d\bar{\varepsilon}^p$ in Eq. (A.19), and equating the result to Eq. (A.21) since both are equal to the plastic work per unit volume dW_p,

$$\frac{\bar{\sigma}}{H'} d\bar{\sigma} = \frac{2}{3} \bar{\sigma}^2 d\lambda = dW_p \tag{A.24}$$

Rearranging

$$\frac{2}{3} \bar{\sigma} d\bar{\sigma} = \frac{4}{9} \bar{\sigma}^2 H' d\lambda \tag{A.25}$$

The left-hand side of Eq. (A.25) is recognized as the differential of Eq. (A.17), defining $\bar{\sigma}$. Thus,

$$\begin{aligned} \frac{2}{3} \bar{\sigma} d\bar{\sigma} = \frac{1}{F + G + H} \Big\{ & [-G(\sigma_3 - \sigma_1)d\sigma_1 + H(\sigma_1 - \sigma_2)d\sigma_1] \\ & + [F(\sigma_2 - \sigma_3)d\sigma_2 - H(\sigma_1 - \sigma_2)d\sigma_2] \\ & + [-F(\sigma_2 - \sigma_3)d\sigma_3 - G(\sigma_3 - \sigma_1)d\sigma_3] \\ & + 2L\tau_{23}d\tau_{23} + 2M\tau_{31}d\tau_{31} + \tau 2N\tau_{12}d\tau_{12} \Big\} \end{aligned} \tag{A.26}$$

With the use of the definitions of Eq. (A.12), Eq. (A.26) can be re-written as

$$\begin{aligned} \frac{2}{3} \bar{\sigma} d\bar{\sigma} = & \sigma_1^* d\sigma_1 + \sigma_2^* d\sigma_2 + \sigma_3^* d\sigma_3 \\ & + 2\tau_{23}^* d\tau_{23} + 2\tau_{31}^* d\tau_{31} + 2\tau_{12}^* d\tau_{12} \end{aligned} \tag{A.27}$$

To arrive at a relation between stress and strain, Eqs. (A.13) and (A.14) must be inverted. Rewriting these equations in matrix form,

$$\{d\varepsilon\} = [S^e]\{d\sigma\} + \{d\varepsilon^p\} \tag{A.28}$$

Thus,

$$[S^e]^{-1}\{d\varepsilon\} = [S^e]^{-1}[S^e]\{d\sigma\} + [S^e]^{-1}\{d\varepsilon^p\} \tag{A.29}$$

But $[S^e]^{-1} = [C^e]$. Also, because of the symmetry of $[S^e]$,

$$[S^e]^{-1}[S^e] = [I] \tag{A.30}$$

where [I] is the identity matrix. Hence, the above expression becomes

$$[C^e]\{d\varepsilon\} = \{d\sigma\} + [C^e]\{d\varepsilon^p\} \tag{A.31}$$

or

$$\{d\sigma\} = [C^e]\{d\varepsilon\} - [C^e]\{d\varepsilon^p\} \tag{A.32}$$

Substituting from Eq. (A.10) for $d\varepsilon^p$,

$$\left\{\frac{d\sigma_{ii}}{d\tau_{ij}}\right\} = [C^e_{ij}]\left\{\frac{d\varepsilon_{ii}}{d\gamma_{ij}}\right\} - d\lambda[C^e_{ij}]\left\{\frac{\sigma^*_{ii}}{2\tau^*_{ij}}\right\} \tag{A.33}$$

or

$$\{d\sigma_{ij}\} = [C^e_{ij}]\{d\varepsilon_{ij}\} - d\lambda\{A\} \tag{A.34}$$

where, for an orthotropic material, i.e., a material with three planes of symmetry,

$$\{A\} \equiv \begin{Bmatrix} C_{11}\sigma_1^* + C_{12}\sigma_2^* + C_{13}\sigma_3^* \\ C_{12}\sigma_1^* + C_{22}\sigma_2^* + C_{23}\sigma_3^* \\ C_{13}\sigma_1^* + C_{23}\sigma_2^* + C_{33}\sigma_3^* \\ 2C_{44}\tau_{23}^* \\ 2C_{55}\tau_{31}^* \\ 2C_{66}\tau_{12}^* \end{Bmatrix} \tag{A.35}$$

Equating Eqs. (A.25) and (A.27) yields

$$\frac{4}{9}\bar{\sigma}^2 H' d\lambda = \sigma_1^* d\sigma_1 + \sigma_2^* d\sigma_2 + \sigma_3^* d\sigma_3 + 2\tau_{23}^* d\tau_{23} + 2\tau_{31}^* d\tau_{31} + 2\tau_{12}^* d\tau_{12} \tag{A.36}$$

Now, substituting for $d\sigma$ in Eq. (A.36) from Eq. (A.34), and solving for $d\lambda$

$$d\lambda = \frac{A_1 d\varepsilon_1 + A_2 d\varepsilon_2 + A_3 d\varepsilon_3 + A_4 d\gamma_{23} + A_5 d\gamma_{31} + A_6 d\gamma_{12}}{B} \tag{A.37}$$

where $A_i (i = 1, \ldots, 6)$ are elements of $\{A\}$, and

$$B = \frac{4}{9}\bar{\sigma}^2 H' + A_1\sigma_1^* + A_2\sigma_2^* + A_3\sigma_3^* + 2A_4\tau_{23}^* + 2A_5\tau_{31}^* + 2A_6\tau_{12}^* \tag{A.38}$$

Finally, substituting for $d\lambda$ from Eq. (A.37) into Eq. (A.38) yields the desired form for the stress-strain relation, viz,

$$\{d\sigma\} = [C^P]\{d\varepsilon\} \tag{A.39}$$

where

$$[C^P] = \begin{bmatrix} C_{11} - \frac{A_1^2}{B} & C_{12} - \frac{A_1A_2}{B} & C_{13} - \frac{A_1A_3}{B} & -\frac{A_1A_4}{B} & -\frac{A_1A_5}{B} & -\frac{A_1A_6}{B} \\ & C_{22} - \frac{A_2^2}{B} & C_{23} - \frac{A_2A_3}{B} & -\frac{A_2A_4}{B} & -\frac{A_2A_5}{B} & -\frac{A_2A_6}{B} \\ & & C_{33} - \frac{A_3^2}{B} & -\frac{A_3A_4}{B} & -\frac{A_3A_5}{B} & -\frac{A_3A_6}{B} \\ & & & C_{44} - \frac{A_4^2}{B} & -\frac{A_4A_5}{B} & -\frac{A_4A_6}{B} \\ & \text{Symmetric} & & & C_{55} - \frac{A_5^2}{B} & -\frac{A_5A_6}{B} \\ & & & & & C_{66} - \frac{A_6^2}{B} \end{bmatrix} \tag{A.40}$$

is the plastic stiffness matrix.

For the 20-node quadratic isoparametric brick element, the element local coordinates and node numbers used in the present formulation are as shown in Figure A.1.

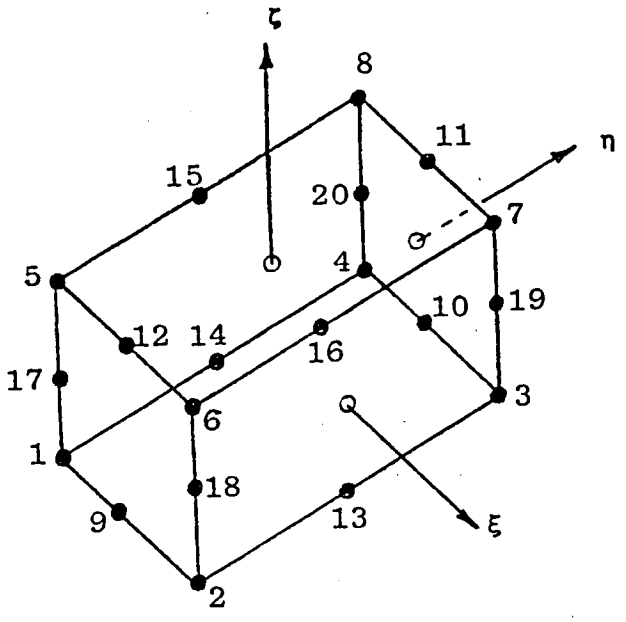

Figure A.1. Node Point Numbering System for the 20-Node Quadratic Isoparametric Brick Element.

The shape functions are:

For the corner nodes

$$N_i = \frac{1}{8} (1 + \xi_o) (1 + \eta_o) (1 + \zeta_o) (\xi_o + \eta_o + \zeta_o - 2) \qquad (A.41)$$

$$i = 1\text{-}8$$

For the midside nodes

$$N_i = \frac{1}{4}(1-\zeta^2)(1+\eta_o)(1+\zeta_o) \qquad i = 9\text{-}12$$

$$N_i = \frac{1}{4}(1-\eta^2)(1+\xi_o)(1+\zeta_o) \qquad i = 13\text{-}16 \qquad \text{(A.42)}$$

$$N_i = \frac{1}{4}(1-\zeta^2)(1+\xi_o)(1+\eta_o) \qquad i = 17\text{-}20$$

where

$$\xi_o = \xi\xi_i \quad , \quad \eta_o = \eta\eta_i \quad , \quad \text{and} \quad \zeta_o = \zeta\zeta_i$$

The relation between derivatives in the local and global coordinate systems is given by the chain rule of differentiation as

$$\begin{Bmatrix} (\quad),_\xi \\ (\quad),_\eta \\ (\quad),_\zeta \end{Bmatrix} = \begin{bmatrix} x,_\xi & y,_\xi & z,_\xi \\ x,_\eta & y,_\eta & z,_\eta \\ x,_\zeta & y,_\zeta & z,_\zeta \end{bmatrix} \begin{Bmatrix} (\quad),_x \\ (\quad),_y \\ (\quad),_z \end{Bmatrix} = [J] \begin{Bmatrix} (\quad),_x \\ (\quad),_y \\ (\quad),_z \end{Bmatrix} \qquad \text{(A.43)}$$

where commas denote partial differentiation and [J] is the tranformation Jacobian matrix, which can be given as

$$[J] = \begin{bmatrix} \partial N_1/\partial\xi & \cdots\cdots & \partial N_{20}/\partial\xi \\ \partial N_1/\partial\eta & \cdots\cdots & \partial N_{20}/\partial\eta \\ \partial N_1/\partial\zeta & \cdots\cdots & \partial N_{20}/\partial\zeta \end{bmatrix} \begin{bmatrix} x_1 & y_1 & z_1 \\ x_2 & y_2 & z_2 \\ \vdots & \vdots & \vdots \\ x_{20} & y_{20} & z_{20} \end{bmatrix} \qquad \text{(A.44)}$$

The strains at a point within an element can be written in terms of element nodal displacements as

$$\{\varepsilon\} = [B]\{\delta\} \tag{A.45}$$

where $\{\delta\}^T = [u, v, w, u_2, v_2, w_2 \cdots u_{20}, v_{20}, w_{20}]$ is the displacement vector.

The element stiffness matrix is given by

$$[K] = \int_{Vol} [B]^T[\bar{C}][B]\, d(Vol) \tag{A.46}$$

The $\bar{C}$ coefficients in the generally orthotropic stiffness matrix in Eq.(A.46) are listed below:

$$\begin{aligned}
\bar{C}_{11} &= U_1 + U_2 \cos(2\theta) + U_3 \cos(4\theta) \\
\bar{C}_{12} &= U_4 + U_3 \cos(4\theta) \\
\bar{C}_{13} &= C_{13}\cos^2\theta + C_{23}\sin^2\theta \\
\bar{C}_{14} &= \bar{C}_{15} = 0 \\
\bar{C}_{16} &= \tfrac{1}{2} U_2 \sin(2\theta) - U_3 \sin(4\theta) \\
\bar{C}_{22} &= U_1 = U_2 \cos(2\theta) + U_3 \cos(4\theta) \\
\bar{U}_{23} &= C_{13}\sin^2\theta + C_{23}\cos^2\theta \\
\bar{C}_{24} &= \bar{C}_{25} = 0 \\
\bar{C}_{26} &= \tfrac{1}{2} U_2 \sin 2\theta + U_3 \sin(4\theta) \\
\bar{C}_{33} &= C_{33} \\
\bar{C}_{34} &= \bar{C}_{35} = 0 \\
\bar{C}_{36} &= C_{13}\sin\theta\cos\theta - C_{23}\sin\theta\cos\theta \\
\bar{C}_{44} &= C_{44}\cos^2\theta + C_{55}\sin^2\theta \\
\bar{C}_{45} &= C_{44}\sin\theta\cos\theta + C_{55}\sin\theta\cos\theta
\end{aligned} \tag{A.47}$$

$$\bar{C}_{46} = 0$$

$$\bar{C}_{55} = C_{44}\sin^2\theta + C_{55}\cos^2\theta$$

$$\bar{C}_{56} = 0$$

$$\bar{C}_{66} = U_5 = U_3 \cos(4\theta)$$

where

$$U_1 = 1/8\ (3C_{11} + 3C_{12} + 4C_{66})$$

$$U_2 = 1/2\ (C_{11} - C_{22})$$

$$U_3 = 1/8\ (C_{11} + C_{22} - 2C_{12} - 4C_{66})$$

$$U_5 = 1/8\ (C_{11} + C_{22} - 2C_{12} + 4C_{66})$$

$$C_{11} = (1 - \nu_{23}\,\nu_{22})\ VE_{11}$$

$$C_{22} = (1 - \nu_{31}\,\nu_{13})\ VE_{22}$$

$$C_{33} = (1 - \nu_{12}\,\nu_{21})\ VE_{33} \qquad \text{(A.48)}$$

$$C_{12} = (\nu_{21} + \nu_{23}\,\nu_{31})\ VE_{11} = (\nu_{12} + \nu_{13}\,\nu_{32})\ VE_{22}$$

$$C_{13} = (\nu_{31} + \nu_{21}\,\nu_{32})\ VE_{11} = (\nu_{13} + \nu_{23}\,\nu_{12})\ VE_{33}$$

$$C_{23} = (\nu_{32} + \nu_{12}\,\nu_{31})\ VE_{22} = (\nu_{23} + \nu_{21}\,\nu_{13})\ VE_{33}$$

$$C_{44} = G_{23}$$

$$C_{55} = G_{31}$$

$$C_{66} = G_{12}$$

and

$$V = (1 - \nu_{12}\nu_{21} - \nu_{23}\nu_{32} - \nu_{13}\nu_{31} - \nu_{12}\nu_{23}\nu_{31})^{-1} \qquad \text{(A.49)}$$

The Richard-Blacklock three-parameter model [148] has been used to represent the nonlinear stress-strain response of the material. The model is in the form:

$$\sigma = E\varepsilon/[1 + |E\varepsilon/\sigma_o|^n]^{1/n} \qquad \text{(A.50)}$$

where σ_o and n are two independent parameters, and E is the initial slope of the stress-strain curve. Since the shape of an effective stress-effective strain curve is similar to a tensile stress-strain curve, a similar equation for the effective stress-effective strain can be written as

$$\bar{\sigma} = \bar{E}\,\bar{\varepsilon}/[1 + |\bar{E}\,\bar{\varepsilon}/\bar{\sigma}_o|^n]^{1/n} \tag{A.51}$$

where $\bar{\sigma}$ is the effective stress and $\bar{\varepsilon}$ is the effective strain, as defined by Eqs. (A.17) and (A.18), respectively. The two independent parameters $\bar{\sigma}_o$ and n, together with the third parameter $\bar{E}$, which is the initial slope of the curve, are selected to best fit the experimental data.

The tangent modulus H' of the effective stress-effective plastic strain curve is related to $\bar{E}$ as [154]

$$H' = \frac{\bar{E}\,\bar{E}_T}{\bar{E}-\bar{E}_T} \tag{A.52}$$

where $\bar{E}_T$ is found by differentiating Eq. (A.51) with respect to $\bar{\varepsilon}$. The resulting equation is

$$\bar{E}_T = \bar{E}/[1 + |\bar{E}\,\bar{\varepsilon}/\bar{\sigma}_o|^n]^{\frac{1+n}{n}} \tag{A.53}$$

Since the material properties depend on temperature in the case of metal matrix composites and on both temperature and moisture in the case

of polymetric matrix composites, the material properties are represented by a second order polynomial of the form

$$P(T,M) = C_1T^2 + C_2M^2 + C_3TM + C_4T + C_5M + C_6 \qquad (A.54)$$

where P is the functional material property of interest, T is temperature, M is moisture content, and C_1 through C_6 are regression coefficients for that property. The parameters in Eq. (A.51), viz $\bar{E}$, $\bar{\sigma}_o$ and n, which can also vary with temperature and moisture, are thus also expressed in the same polynomial form of Eq. (A.54).

APPENDIX B

Crack Growth Simulation Technique

The crack growth simulation in a three-dimensional elastoplastic finite element analysis, as developed in Section 4, is further explained here. Implementation of this crack growth simulation technique in the actual finite element computer code is also discussed.

The technique uses the critical strain energy release rate (fracture toughness) of the material as the criterion for the onset and growth of a crack. That is, at any stage of loading, if the computed strain energy release rate for a virtual crack extension Δa exceeds the fracture toughness of the material, the original crack is assumed to have extended by an amount Δa.

The strain energy release rate in the presence of plasticity, I, is computed using the rate of change of compliance method. It must be noted that the symbol I is used to denote strain energy release rate in the present analysis, to distinguish it from the symbol G which is generally used to represent the strain energy release rate in linear elastic fracture mechanics.

Making use of the observations made in Section 4 relative to the stiffness derivative method for both fixed load and fixed grip conditions, that any small extension of the crack in a finite element model affects only the relatively few elements near the crack tip, the strain energy release rate in the present analysis is computed in terms of local compliance changes.

The organization of the three-dimensional, elastoplastic, generally orthotropic finite element analysis computer code (WYO3D) with crack

propagation capability, as developed for use in the present analysis, is shown in Figure B.1.

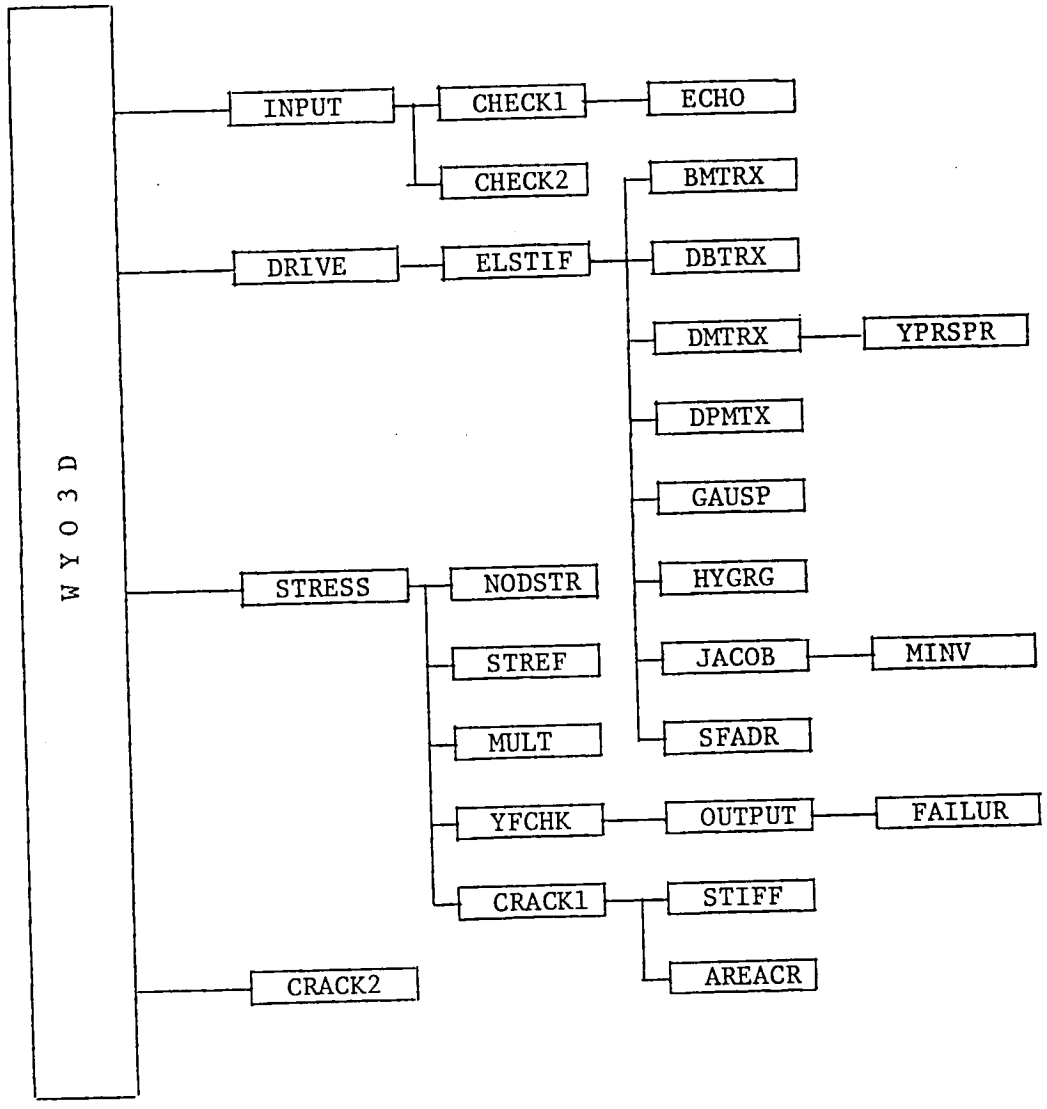

Figure B.1. Block Diagram of the WYO3D Computer Code

The bulk of the input data regarding the model geometry, material properties, and loading conditions are read into the INPUT subroutine following the general format given in Reference [144]. For crack propagation, the following additional variables should be read as input:

NPCR: Crack Propagation Flag. It must be equal to 1 for crack propagation analysis.

NNCT: Number of Nodes near a Crack Tip.

NNCTN: Node Number of Crack Tip Nodes.

NELCN: Elements surrounding a crack tip node as shown in Figure B.2.

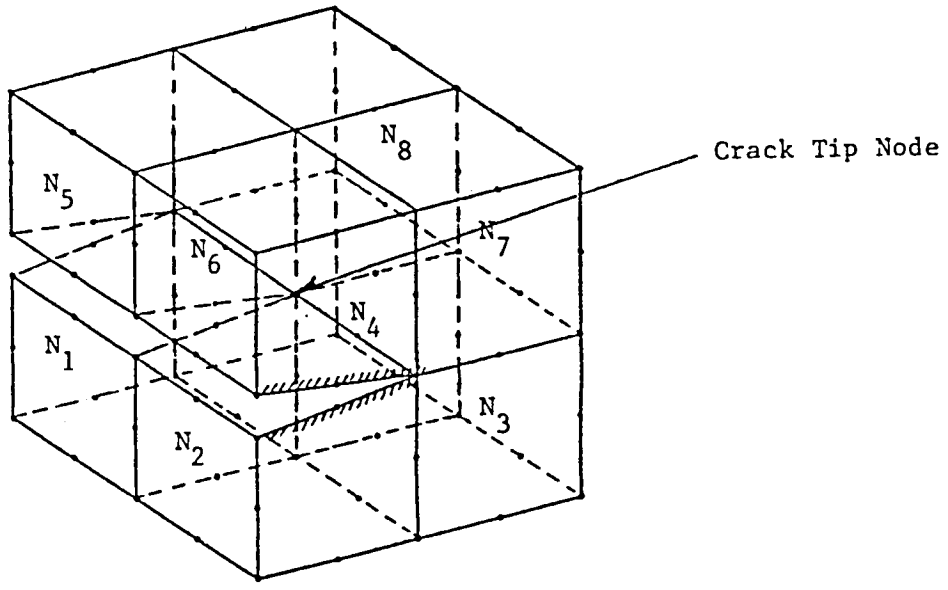

Figure B.2. Numbering Order of Elements Near a Crack Tip Node

The step by step procedure adapted for crack growth simulation in the computer code is as follows:

Step 1: During the first load increment, the total stiffness coefficients (used for computing the strain energy release rates) at all crack tip node points in all nine modes of crack extension (refer to Figures 5, 6, and 7) are evaluated in subroutines STRESS, CRACK, and STIFF, as explained in Section 4 using a two-dimensional example. The stiffness coefficients K are then stored in an array for later use.

Step 2: The three incremental force components F_X, F_Y, and F_Z at all crack tip nodes are also stored in an array (this is done in subroutine CRACK1). In all of the subsequent load increments, the incremental force components F_X, F_Y, F_Z at the crack tip nodes are computed and added to the previous incremental values to obtain total force components (in CRACK1).

Step 3: In subsequent load increments, the crack is virtually extended to the next nearest grid points in all possible directions (in both opening and shearing modes) and the reduced stiffness coefficients $\bar{K}$ are evaluated as explained in the two-dimensional example in Section 4. It must be noted that there may not be two values of $\bar{K}$ for each mode, depending on which set of elements were used to compute $\bar{K}$ (e.g., Elements 1 and 2, or 3 and 4 in Figure 9).

Step 4: The strain energy release rates I are calculated in all nine modes of crack extension using the expressions given in Eq. (29). (Equation 29 gives I values for Modes M_{ZI}, M_{ZII}, and M_{ZIII}. For Modes M_{XI}, M_{XII}, M_{XIII}, M_{YI}, M_{YII}, and M_{YIII}, similar expressions can be derived by cylically changing the subscripts.) In an actual computation, there are two values of I for each mode, corresponding to two values of the reduced stiffness coefficients. The higher of the two computed strain energy release rates is taken as the strain energy release rate in that particular mode.

Step 5: In subroutine CRACK2 the computed values of the strain energy release rates are compared with the critical energy release rates (the fracture toughness values for the nine modes of fracture, which are read as material properties in subroutine INPUT). If the computed strain energy release rate is higher than the critical strain energy release rate, the crack tip node point is split into two node points. A new node number is then assigned to one of the nodes and the element connectivity matrix is updated to include new nodes. Reaction forces are than applied to the old and the new node points. The crack propagation flag (NPCR) is set equal to 2, to check for any further crack growth due to reaction forces in the same load increment. If there are no further crack extensions, the NPCR is set back to 1 and loading is resumed.

1. Report No.	2. Government Accession No.	3. Recipient's Catalog No.
NASA CR-172598		

4. Title and Subtitle	5. Report Date
Delamination Micromechanics Analysis	May 1985
	6. Performing Organization Code

7. Author(s)	8. Performing Organization Report No.
Donald F. Adams Jayant M. Mahishi	UWME-DR-401-108-1
	10. Work Unit No.

9. Performing Organization Name and Address	11. Contract or Grant No.
Composite Materials Research Group University of Wyoming Laramie, Wyoming 82071	NAG-1-454
	13. Type of Report and Period Covered Technical Report March 1984-December 1984

12. Sponsoring Agency Name and Address	14. Sponsoring Agency Code
National Aeronautics and Space Administration Washington, D.C. 20546	

15. Supplementary Notes

Langley Technical Monitor:
Dr. John H. Crews, Jr. M/S 188E

16. Abstract

A three-dimensional finite element analysis has been developed that includes elastoplastic, orthotropic material response, and fracture initiation and propagation. Energy absorption due to physical failure processes characteristic of the heterogeneous and anisotropic nature of composite materials is modeled. A local energy release rate in the presence of plasticity has been defined and used as a criterion to predict the onset and growth of cracks in both micro-mechanics and macromechanics analyses. This crack growth simulation technique is based upon a virtual crack extension method.

The accuracy of the technique has been established by applying it to predict crack propagation in a centrally notched aluminum plate. A three-dimensional finite element micromechanics model is used to study the effects of broken fibers, cracked matrix and fiber-matrix debond on the fracture toughness of the unidirectional composite. The energy release rates at the onset of unstable crack growth in the micromechanics analyses are used as critical energy release rates in the macromechanics analysis. This integrated micro-mechanical and macromechanical fracture criterion has been shown to be very effective in predicting the onset and growth of cracks in general multilayered composite laminates by applying the criterion to a single-edge notched $[\pm 45/0]_s$ graphite/epoxy laminate subjected to inplane tension normal to the notch.

17. Key Words (Suggested by Author(s))	18. Distribution Statement
Composite Materials Finite Element Analysis Micromechanics Laminate Analysis Fracture Mechanics	Unclassified, Unlimited Subject Category 24

19. Security Classif. (of this report)	20. Security Classif. (of this page)	21. No. of Pages	22. Price*
Unclassified	Unclassified	152	A08

* For sale by the National Technical Information Service, Springfield, Virginia 22161